Acknowledgements

There are a couple of people who have, in one way or another, made it possible for me to write this thesis. I thank some of these people below.

Dr. Marco Caldin, Director of the "San Marco" Private Veterinary Clinic of Padua, who have made possible this work giving us the financial and instrumental resources available.

My advisor Prof. Francesco Mascarello for trusting in me and in my project.
Prof. Gianfranco Gabai, for his help during these years.

The reviewers of this thesis for their comments and corrections which indeed helped me in improving my thesis. Prof. Mathias Prokop, MD, Professor and Chairman of Radiology, University Medical Centre of Utrecht, and Prof. Paul Simoens, DVM, Chairman of the Department of Morphology, Faculty of Veterinary Medicine, Ghent University, Chairman of the Subcommittee on Angiology of the International Committee of Veterinary Gross Anatomical Nomenclature.

Prof. Mathias Prokop, for giving me twice the opportunity to work for few months with him and his group. He has been a continuous source of inspiration and has made his best to guide and encourage me even when his time became scarce.

The anesthesiology team of the "San Marco" Private Veterinary Clinic of Padua, dr. Gloria Bianchini, dr. Linda Di Martino, dr. Irene Mascella, dr. Cristiano Stefanello, that every day guarantee the patient' safety and comfort, and contribute to the quality of my work.

Other colleagues, clinicians and pathologists of the "San Marco" Private Veterinary Clinic of Padua, have also given support to the development of this thesis, by discussing relevant topics with me during these years. I thank particularly dr. Edoardo Carlo Rolla, excellent surgeon, for creating an ideal working atmosphere in a multi-disciplinary environment.
Dr. Enrica Rossetti, PhD, outstanding pathologist and friend deserves a special mention. She was and continues to be an important source of encouragement for me. I will never forget her smile.

My husband, my partner in life and work, who is a great source of strength all through my life.

Giovanna Bertolini

Summary

Aim. The aim of the present doctoral thesis was to evaluate the use of multidetector row computed tomography as new non invasive method in the assessment of *in vivo* abdominal vascular anatomy in dogs. Normal anatomy of abdominal vessels, their variants, and the congenital anomalies were assessed.

Background. Conventional and helical computed tomography have been used for cross-sectional anatomy of the abdomen and liver vascular descriptions in dogs. We first described the use of multidetector-row computed tomography in small animals. Multidetector row computed tomography represents a breakthrough in computed tomography technology, providing a substantial gain in performance in comparison to previous technologies. Multidetector row can provide volumetric original data sets. With proper workstations, these data can be viewed in volume-rendered mode, creating excellent three-dimensional maps of the vessels.

Methods. This thesis included 1437 dogs underwent multidetector row computed tomography of the abdomen for clinical purposes. Twenty of these dogs presenting no abnormal findings in the abdomen were used for describing the normal vascular anatomy. Variants and vascular anomalies were recorded. Abdominal multidetector row protocols have been adapted to the clinical circumstances, and included non-angiographic and angiographic studies. Images were evaluated and processed initially on two-dimensional multiplanar images to visualize the vascular structures from all points of view.

Transverse views were always reviewed together with sagittal and dorsal views. To enhance depiction of normal anatomy, anatomical variants, and pathologies, three-dimensional images were created on a free-standing workstation, each time with emphasis on the selected vessel or vascular system.

Results. The most immediate issue of the present study was that multidetector row computed tomography allows detailed *in vivo* imaging of the abdominal vasculature in dog. Normal vasculature, variants, and anomalies can be easily recognized. Over the course of this study, we identified various arterial and venous congenital anomalies, viz. arterioportal fistulas, arteriovenous fistula, dislocated lumbar artery, dislocated caudal vena cava, “double caudal vena cava”, congenital interruption the caudal vena cava and/or the portal vein, azygous continuation of the caudal vena cava, and various portosystemic connections. These included portoazygos shunts (from right gastric, left gastric, and splenic veins to the azygos vein) and portocaval shunts (from right gastric, left gastric veins to the caudal vena cava pre-hepatic, hepatic, and post-hepatic segments, and from left or right portal branch to the hepatic segment of the caudal vena cava). Some of these anomalies have been not previously reported in veterinary literature.

Conclusions. Multidetector row computed tomography can be an useful tool for educational support, providing accurate mapping of individual venous and arterial anatomy and variations. Post processed volume rendered images from living animals can be used instead of specimens. Knowledge of individual variations is of clinical importance for pre-operative imaging of the abdomen. Morever, multidetector row examinations can provide additional detailed information in patients with radiographic or ultrasonography patterns of abdominal vascular disorders.

Sommario

Scopo del lavoro. Lo scopo di questa tesi di dottorato e' di valutare l'utilizzo della tomografia computerizzata multidetettore come metodo non invasivo per lo studio *in vivo* della anatomia vascolare dell'addome nel cane. Sono state studiate l'anatomia normale, le sue varianti e le anomalie vascolari di origine congenita.

Premessa. La tomografia assiale computerizzata e la tomografia spirale sono state impiegate per la descrizione della anatomia tomografica dell'addome e per la descrizione della vascolarizzazione epatica del cane. Noi per la prima volta abbiamo descritto l'impiego della tomografia computerizzata multidetettore nei piccoli animali. La tomografia computerizzata multidettore e' una evoluzione tecnologica importante nel campo della tomografia, che ha portato notevoli progressi e nuove possibili applicazioni, rispetto alle precedenti tecnologie. La tomografia computerizzata multidetettore puo' fornire dati volumetrici del paziente in esame. Questi dati, elaborati in apposite workstation, possono essere visualizzati in modelli tridimensionali, che consentono la creazione di mappe vascolari ad elevato dettaglio.

Metodi. Questo studio e' stato eseguito su 1437 cani sottoposti ad esame tomografico dell'addome per diverse ragioni cliniche. Venti di questi cani, che non avevano segni riferibili a patologie dell'addome, sono stati utilizzati per la descrizione della anatomia vascolare normale. Sono state registrate le varianti e le anomalie vascolari. I protocolli per l'esame dell'addome sono stati adattati alle esigenze cliniche ed includono sia esami angiografici che non-angiografici. Le immagini sono state valutate inizialmente in

modalità bidimensionale multiplanare, per visualizzare le strutture vascolari secondo diversi piani. La vista trasversa e' stata sempre valutata insieme a quella sagittale e dorsale ed ogni altro piano obliquo utile alla interpretazione del corso del vaso. Per meglio visualizzare la anatomia normale, le varianti e le anomalie, sono state create delle mappe tridimensionali utilizzando una apposita workstation, di volta in volta enfatizzando la struttura vascolare in esame.

Risultati. Il primo importante risultato che emerge da questo studio e' che la tomografia computerizzata multidetettore permette la dettagliata visualizzazione i*n vivo* della vascolarizzazione addominale del cane. La vascolarizzazione normale e le sue varianti individuali possono essere riconosciute con facilità. Nel corso di questo studio abbiamo identificato e descritto varie anomalie congenite del sistema arterioso e venoso dell'addome, in particolare fistole arterovenose, arteroportali, dislocazione delle arterie lombari, dislocazione della vena cava caudale, la c.d. vena cava doppia, l'interruzione congenita della vena cava e/o della vena porta, la continuazione della vena cava nella vena azygos, oltre a varie connessioni anomale tra il sistema portale e la circolazione sistemica. Tra queste ultime, gli shunt portoazygos (tra le vene gastrica destra, sinistra o la vena splenica e la vena azygos) and gli shunt portocavali (tra le vene gastrica destra, sinistra ed i segmenti pre-epatico, epatico o post-epatico della vena cava caudale, oppure tra la branche portali sinistra e destra ed il tratto epatico della vena cava caudale). Alcune di queste anomalie non erano mai state descritte prima in medicina veterinaria.

Conclusioni. La tomografia computerizzata multidetettore può essere un importante strumento per la didattica, perché in grado di fornire dettagliate mappe dell'anatomia normale e delle sue varianti individuali. I modelli volumetrici che si ottengono

processando dati ottenuti su animali vivi, possono sostituire i modelli artificiali o ottenuti tramite casting vascolare. La conoscenza dell'anatomia normale e delle varianti individuali e' di grande rilevanza clinica in caso di pazienti da sottoporre a procedure interventistiche o chirurgie addominali. Inoltre, la tomografia computerizzata multidetettore può fornire informazioni più dettagliate in quei pazienti che abbiano evidenza radiografica o ecografica di una patologia vascolare addominale.

CHAPTER 1

COMPUTED TOMOGRAPHY

1.1 COMPUTED TOMOGRAPHY BASIC PRINCIPLES

Computed tomography (CT) was introduced in the early 1970s and was the first non-invasive radiological method allowing the generation of tomographic images of the human body without superimposition of adjacent structures. CT was probably the first tomographic technique combining computer calculation power with medical imaging, thus starting the era of digital imaging. Computed tomography is based on X-ray densitometry and uses the same basic physics as conventional radiography. As a collimated high-kilovolt X-ray beam penetrates the patient's body, fractions of the original beam are absorbed while others pass through. The absorption of X-rays within the body is directly proportional to the linear attenuation coefficient of the different tissues, nearly corresponding to their electron density. The attenuation data of each volume element of the patient obtained from thousands of different projection angles are calculated from a computer using a mathematical process (HOUNSFIELD 1973). Each volume element or voxel is displayed on the monitor as picture element or pixel in shades of gray in a two-dimensional digital image matrix. Each pixel represents then the surface element of the correspondent volume element within the patient.

The computer assigns to each pixel a CT number or Hounsfield Units (HU) that represent the mean value of the attenuation values within the voxel. The Hounsfield Units of tissues are related to the attenuation of water, that is 0 HU. On this assumption, the Hounsfield Unit scale has about 2000 gray levels, ranging from + 1000 for compact bone to – 1000 for air, from white to black (CITTADINI G. 2002, PASSARIELLO R. 2005).

The human eye can only differentiate 20-50 different levels of gray, depending on the ambient light of the reading room. If all the grays (at least 2000) within the image would be represented, the operator could not distinguish the different tissues, due to the lack of contrast resolution. To maximize the perception of the differences, images can be digitally processed to meet a variety of visualization requirements. The operator can then open a "window" more or less wide (window width) along the Hounsfield scale, including only a small number of gray levels (window level) (Fig.1).

The attenuation values of various normal and pathologic tissues have been described in humans as well as in veterinary medicine (DROST et al. 2004, ISIOKA et al. 2005, BERTOLINI et al. 2006a, BERTOLINI et al. 2008, TAEYMANS et al. 2008). It is important to know that CT numbers may vary little with the change depending on the type of scanner, the scanning algorithm, the contrast medium etc. (BERRY 2002, KALENDER 2005) There are several reports suggesting different window settings in small animals and their effects on diagnostic certainty for CT characteristics associated with different conditions (TROMBLEE et al. 2007, AURIEMMA et al. 2007, CARDOSO et al. 2007, RIVERO et al. 2008).

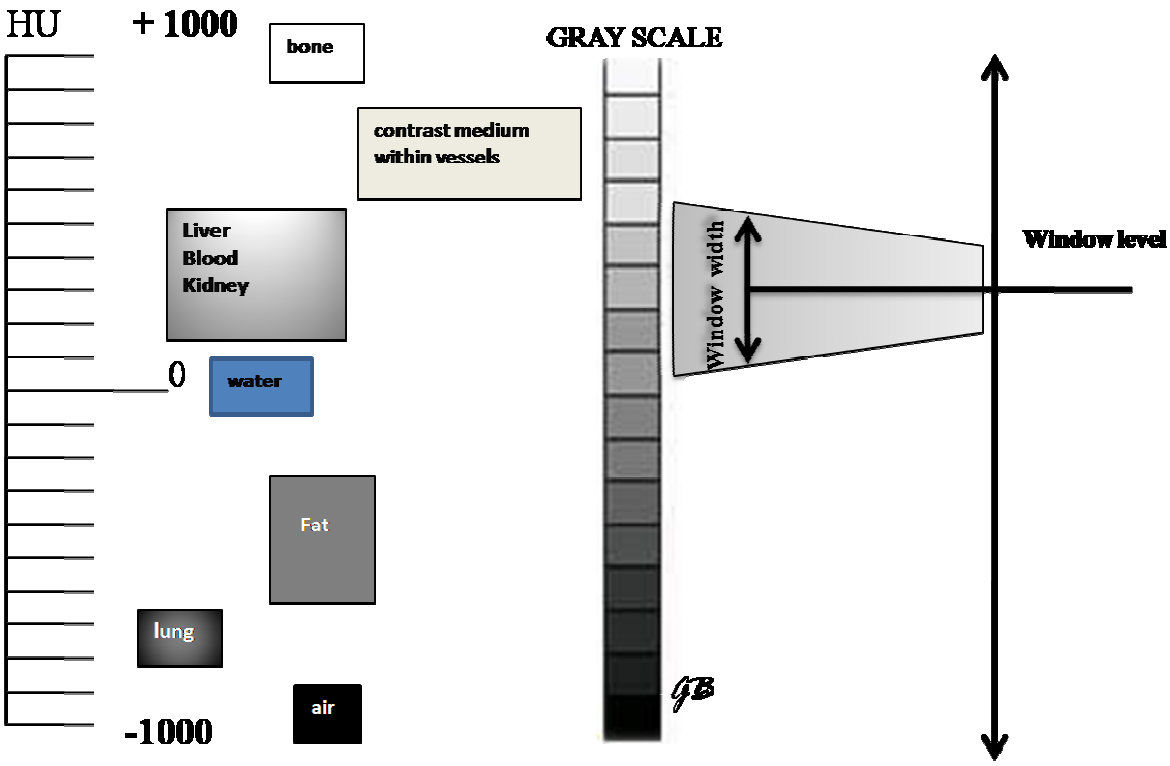

Fig. 1. Hounsfield scale. Values of water (0 HU), bone (+1000), and air (-1000) are reported. Bone, calcifications, and contrast media within the vessels have high density value and appear white, hyperdense or hyperattenuating. Fat is generally negative in value or hypodense or hypoattenuating, but less than lung tissue containing air. Most soft tissues have positive low-density values. Optimization of window settings is crucial to visualize their characteristics.

1.2 COMPUTED TOMOGRAPHY TECHNOLOGY

Components of a computed tomography scanner are the X-ray tube generating the high-power X-ray beam, and the receiving system formed by detectors. The tube-detector system is placed into a ring called *gantry* (Fig. 2). The overall performance of a CT

system depends on several key components. These include the X-ray source; a high-powered generator, detector, and detector electronics; data transmission systems, and the computer system for image reconstruction and manipulation. Modern CT systems generally use solid-state detectors. Each detector element consists of a radiation-sensitive solid-state material (such as cadmium tungstate, gadolinium-oxide, or gadolinium oxisulfide), which converts the absorbed X-rays into visible light (PASSARIELLO 2005, FLOHR et al. 2005).

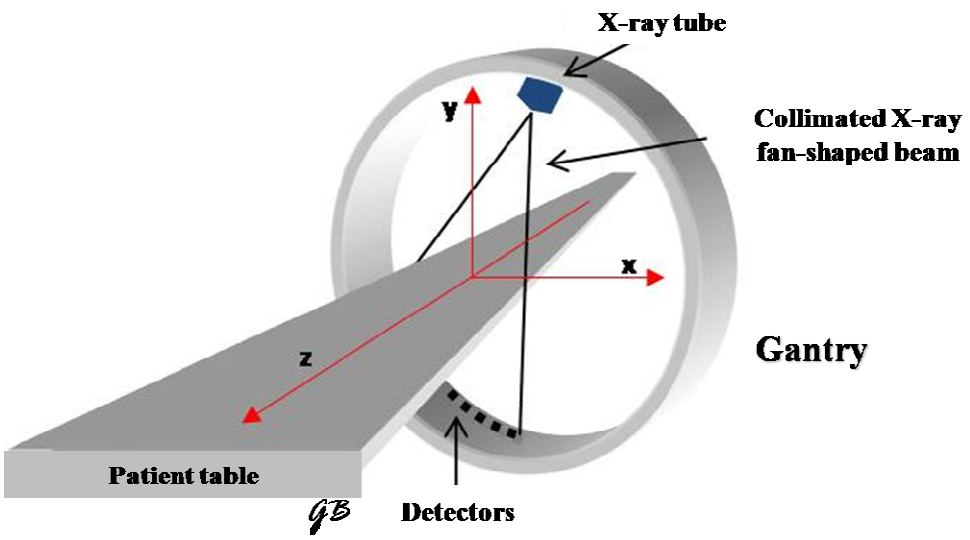

Fig. 2. Schematic representation of a computed tomography system. X-y is the transverse or axial plane, that crosses the patient body. Z is the longitudinal plane, along the patient body.

Since the 1970s four different generations of scanners have been developed. The third and fourth generations are still in use in veterinary practice (OLERTH and SHARF 2007). The third generation uses a wide fan-shaped beam falling in a larger array containing many detectors. The fourth generation scanner has a stationary ring of

detectors, while the tube alone rotates around the patient. The patient table doesn't move during the scan. These generations of scanners are penalized from electrical cables that don't allow one-way rotations around the patient. The tube-detector array system moves then in a rotate-rotate (clockwise-anticlockwise directions) mode around the patient (Fig. 3a). The examination volume has to be covered by subsequent transverse scans in a "step and shot" mode. Time to relocate the cables and other technical factors make these scanners prone to artifacts from patient movement, miscalibration or failure of one or more detectors (KALENDER et al. 1990, KALENDER et al. 1994, WANG and VANNIER 1994, PROKOP 2006).

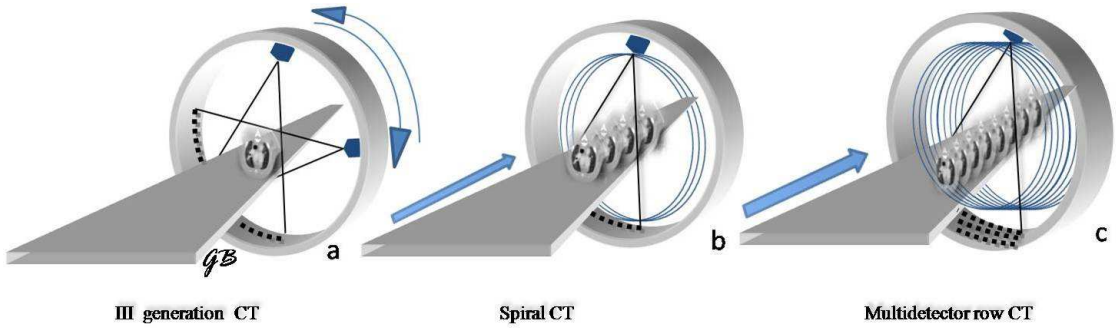

Fig. 3. Schematic representation of various CT systems.

a) III generation scanner. Arrows indicate the rotate-rotate modality of tube-detectors system. The patient table doesn't move during the scans.

b) Spiral or helical CT. The tube-detectors system moves in a one-way continuous rotation within the gantry. The rotation time is generally 1 sec. Most recent helical CT scanners can reach rotation times of 0.7 sec The arrow means that the table moves during the scans.

c) Multidetector row CT scanner (MDCT). The tube-detectors system rotates fast within the gantry. Most recent MDCT scanners have thousands of detectors with isotropic resolution. The rotation time is 0.5 – 0.27 sec. depending on the type of scanner. The table moves fast during the scans.

The continuous one-way rotation of the tube-detector system around the patient only became possible with the invention of the slip-ring techniques in the late 1980s, which eliminated the need to rewind the gantry after each rotation and enabled continuous data acquisition during subsequent rotations. In early 1990s the helical or spiral CT was then introduced (CRAWFORD and KING 1990). With the spiral CT, the patient is scanned with a rotating tube-detector system while the table transports the patient through the gantry, along the longitudinal direction *z*. The tube-detector system takes then an helical or spiral path around the patient, while the detectors collect the data (Fig. 3b).

The transverse plane *x-y* actually consists of a slice of the volume in exam with a third dimension in the longitudinal direction *z*, corresponding in the spiral CT to the slice thickness (Fig. 4). Ideally, volume data should be isotropic in nature, meaning that each voxel should be of equal dimensions in all three spatial axes (*x-y-z*), allowing the image to be displayed in arbitrarily oriented imaging planes (isotropic resolution). With spiral CT the ideal isotropic resolution can only be achieved for very limited scan ranges (KALENDER 1995). For most clinical applications, spiral CT is unable to fulfill this prerequisites of spatial resolution. If a large scan range (thorax and/or abdomen) has to be covered, a thick collimated slice width must be used to complete the scan in a certain timeframe to avoid motion artifacts (generally in a single breath-hold). A thick collimation results in a considerable mismatch between the transverse resolution (*x-y plane*) and the longitudinal resolution (*z*) (FLOHR et al. 2005).

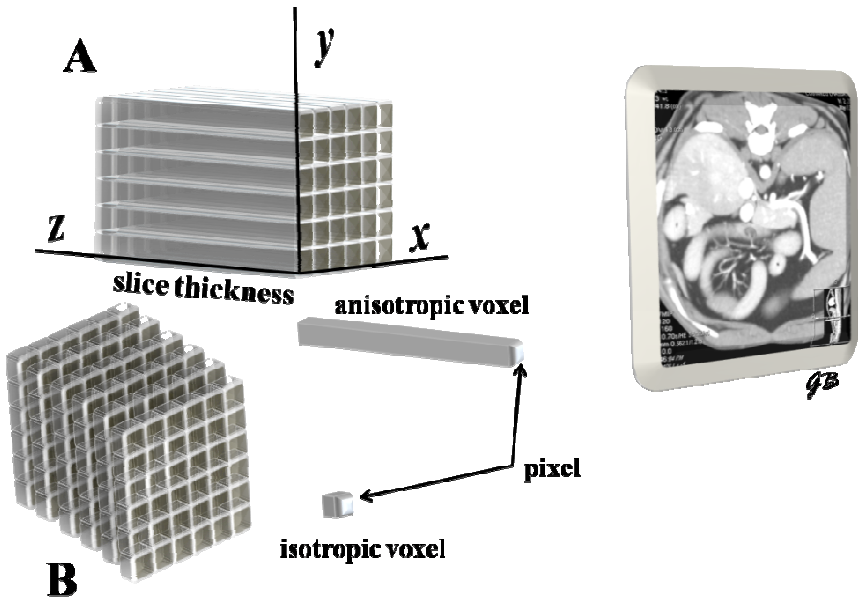

Fig. 4. Schematic representation of a the same volume examined with spiral CT (A) or MDCT (B). The volume in exam is composed of thousands volume elements (voxels). The image on the screen (on the right) is a matrix of two-dimensional picture elements (pixels). The computer assigned a CT number (Hounsfield Unit) to each pixel, that is in fact the mean attenuation value of each point within the corresponding voxel. The corresponding level of gray of a pixel is the sum of the gray levels within that voxel. The smaller the voxel (or thinner the slice), the higher the spatial resolution of the study. **A.** In spiral CT planes x-y and z are unequal. The anisotropic voxel results in a considerable mismatch between the transverse resolution (*x-y plane*) and the longitudinal resolution (*z*). **B.** In MDCT the volume is acquired as thousand of isotropic voxels, with equal resolution in all three directions.

To achieve more substantial volume coverage with improved longitudinal resolution, the simultaneous acquisition of more than one slice at a time and a reduction of the gantry rotation time are necessary (Fig. 3c). In 1998, all major CT manufacturers introduced the 4-detector arrays multidetector row (MDCT) or multi-slice CT (MSCT) systems, which

typically offered simultaneous acquisition of 4 slices at a rotation time of down to 0.5 s. The simultaneous acquisition of several detector sections resulted not only in an increase in speed but also in an extension of the scan range. Systems with 8-, 10-, 16-detector arrays and more have become available over the past few years. Scanners with 32-,40-, 64- or more detector rows are now available. MDCT has transformed CT from a transaxial cross-sectional technique into a truly three-dimensional imaging modality (PROKOP 2003). From 16-MDCT scanners onwards the detector element has now equal dimensions in *x*-*y* and *z* direction, making it possible to routinely acquire substantial anatomic volumes with isotropic sub-millimeter spatial resolution. In humans, MDCT is now an established imaging modality that has almost completely replaced single slice CT technology (PROKOP 2005). Volumetric imaging affects the type of examinations we perform with CT, how we scan the patients, and how we review the data. This extended high quality scan range is particularly valuable for large oncological staging scans of the body, and for trauma. However, the most dramatic impact is in the area of computed tomography angiography. The greatly increased longitudinal (*z*-axis) resolution allows arbitrary cross-sectional planes visualization from the data volume and excellent three-dimensional displays. With MDCT systems, we scan the volume of interest (eg, the abdomen or the entire body), and we display that volume not as sections but as a true volume (FISHMAN 2001).

1.3 COMPUTED TOMOGRAPHY ANGIOGRAPHY

In humans, multidetector row computed tomography angiography (MDCT-A) is now widely considered to be equal if not superior to catheter digital subtraction angiography (DSA) in terms of diagnostic accuracy for many types of examinations. MDCT-A offers certain information about anatomy and vascular pathology that simply cannot be obtained with DSA (MARTIN et al. 2003, SAKAMOTO et al. 2006). Computed tomography angiography has been described in veterinary medicine using spiral CT, (FRANK et al. 2003, ZWINGERBERGEN and SCHWARZ 2004, ZWINGERBERGEN et al. 2005a, ZWINGERBERGEN et al. 2005b, CACERES et al. 2006, ECHANDI et al. 2007) and using a multidector row CT scanner (BERTOLINI et al. 2006b). CT angiography requires the use of contrast medium, generally an iodinate medium, injected intravenously at a certain flow rate. The success of CT angiography depends on a number of critical steps, including properly timed delivery of contrast medium, correct timing of data acquisition, and selection of proper scanning parameters. Several concepts of contrast medium injection that were conceived empirically for use in spiral CT angiography are no longer applicable with faster scan times. (FLEISCHMANN 2005) Optimizing the contrast protocol is crucial and requires knowledge of the physiological and pharmacokinetic principles of arterial enhancement (JOHNSON and FISHMAN 2006). In fact, the contrast effect varies depending on technical factors including the iodine dose, concentration, volume, injection speed, and iodine delivery rate as well as patient related factors such as body size, age, and cardiac output (TATEISHI et al. 2008, KISHIMOTO et al. 2008). In patients with a normal cardiac output, the peak arterial contrast

enhancement is achieved shortly after the termination of a contrast medium injection. The time interval for an intravenously injected bolus of contrast medium to appear in the arterial territory of interest is generally referred to as the contrast medium transit time (FLEISCHMANN 2005). The contrast medium transit time can vary substantially between patients. The contrast medium transit time can be determined by either using a test bolus injection or using automated bolus-triggering techniques. The test bolus method uses the injection of a small amount of contrast medium and multiple low dose scans performed over the region of interest until the contrast is visualized in the selected vessel. This gives value of time to peak enhancement in that vessel, then determining the scan delay for that patient. With bolus-triggering technique the test bolus injection is unnecessary. Multiple images are obtained over the region of interest during the contrast medium injection. The scan will be initiated when the density within the vessel exceeds a predetermined Hounsfield unit value or when a visual threshold is reached (HITTMEIR and FLEISCHMANN 2001, FLEISHMANN 2003, HAMMERSTINGL and VOGL 2005).

The discrepancy of the contrast medium transit time reported from various authors in abdominal CT angiography in veterinary medicine reflects the significant variation in the population of dogs included in the study (different body sizes and clinical conditions), the different scanner technology, and the contrast medium injection parameters used (flow rate, injection duration etc.).

1.4 COMPUTED TOMOGRAPHY POST-PROCESSING TECHNIQUES

The data sets obtained on multidetector CT, from 16-64-row onwards, may result in 1000-5000 images per examination. The large size of these data makes impractical to extract all information by using just standard two-dimensional planes, and makes clear the importance of volume imaging and three-dimensional image display (FISHMAN et al. 2006).

With proper workstations, the post-contrast data sets from CT-angiography can be viewed in three-dimensional, volume-rendered mode. Volume rendering is a generic term that simply refers to a three-dimensional (3D) volume reconstruction method that allows every voxel in the volume data to contribute to the reconstructed image. Image rendering types depends on the computer algorithm that the workstation uses to process the data set and generate an image (FLOHR et al. 2005).

There is almost an unlimited number of ways to reconstruct and view MDCT data sets, and no unique correct way to do it. The preferences frequently change and evolve as radiologists gain experience with volumetric imaging. Nowadays, a freestanding workstation has become an essential tool for interpreting cases using post-processing techniques. This also allows consultation and reviewing findings with referring physicians or surgeons. This system has been recently reported for enhancing veterinary students' understanding and interest in anatomy offering them a quality veterinary medical education as well (YAMADA et al. 2007). Optimal image quality first depend on

the CT angiography technique performed and the quality of the original data. The image post-processing may seem deceptively simple, but understanding of the basic concepts is necessary to reliably generate high-quality work (LELL et al. 2006, FISHMANN et al. 2006). In-depth discussion of the various rendering techniques is not a focus of this thesis. The information presented here is restricted to data essential for understanding the post-processing techniques that have been used in this work.

Multiplanar reformatted reconstruction

Multiplanar reformatted reconstruction (MPR) is a two-dimensional technique (2D) that can simultaneously display multiple views of the same volume, in sagittal, dorsal, transverse or any oblique plane. The quality of multiplanar reconstructions is directly related to the image slice thickness. When isotropic voxels ($x=y=z$) are used the quality of a reconstructed image in any plane is virtually identical to the original axial image.

Maximum Intensity Projection

Maximum Intensity projection (MIP) is created using a computer algorithm that evaluates each voxel along a line from the viewer's eye through the image and selects the voxel with the maximum intensity as the value of the corresponding display pixel. It is the most widely used three-dimensional (3D) technique for visualization of blood vessels for CT angiography. When other high-density structures such as bone, enhancing organs, or calcifications are present and overlying the blood vessels, these structures will be averaged with the vessels and obscure them. Therefore, bone elimination techniques are essential for processing vascular MIP images.

Volume Rendering

In contrast to a MIP image that takes only the highest density value for a given ray, with Volume Rendering (VR) no information is lost or discarded, and every voxel contributes to the final image. The resulting images therefore contain more information and are potentially much more clinically useful. The image is generated by assigning each voxel in the examined volume an opacity value (from 0% to 100%, total transparency to total opacity) based on its Hounsfield unit. Color can be applied to enhance the discrimination between the tissues. This can be done by preselected tools or changing parameters until the desired effect is achieved. A great strength of volume rendering is its interactivity. This means that the image can be rotated and viewed from any angle. Volumes can be manipulated in many different ways to demonstrate the desired anatomy.

CHAPTER 2

DEVELOPMENTAL ANATOMY OF THE ABDOMINAL VESSELS

2.1 DEVELOPMENT OF VASCULAR SYSTEM

A full understanding of the vascular development is important not only for normal radiological or surgical anatomy systematization, but also because for understanding vascular variations and anomalies, as well as the role of angiogenesis in several pathological conditions. For this, a brief description of embryonic and developmental anatomy of the abdominal vessels is described here.

The vascular system is one of the first organs to function during vertebrate development, and the creation of a precisely patterned, seamless network of blood vessels is absolutely essential for embryonic survival. The circulatory system is composed of vascular, hematopoietic, and cardiac components, each formed in a stepwise pattern from discrete regions of mesoderm (McGRATH et al. 2003). Blood vessels are formed via two processes during development, i.e. vasculogenesis and angiogenesis. After the developing embryo has formed a primary vascular plexus by a process termed vasculogenesis, further blood vessels are generated by both sprouting and non-sprouting angiogenesis, which finally are progressively pruned and readily reshaped by local environmental perturbations. In general, major blood vessels and capillaries form during development by vasculogenesis, while the vasculature of organs is created by angiogenesis. Angiogenic vascular sprouts emerge from the longitudinal trunk axial vessels (the dorsal aorta and cardinal veins) in spatially and temporally distinct steps. In addition, angiogenesis can occur throughout the life of the organism, but vasculogenesis is restricted to embryonic development (RISAU and FLAMME 1995, RISAU 1997). As vessels begin to be remodeled into a functioning circulation, they need to undergo

localized proliferation and regression, as well as programmed branching and migration into different regions of the body. They need to be specified into different caliber and types of vessels, including division into arteries, veins, and lymphatics, with their separate subdivisions into large vessels, venules, arterioles, capillaries, etc. Circulatory flow dynamics certainly play an important role in helping to determine the pattern of interconnections between the primary network and secondary sprouts, and to ascertain the final arterial or venous identity of the vessels in the functional network (ISOGAI 2003). Nevertheless, other data suggest that molecular differences between arterial and venous endothelial cells are apparent well before the onset of circulation, because numerous different genes and molecular players, such as the vascular endothelial-specific growth factor (VEGF) and the angiopoietin/Tie receptors or other signaling pathways have some specific vascular role, such as Ephrin/Eph receptor and Delta/Notch (WEINSTEIN 1999, YANCOPULOS et al. 2000, LAWSON et al. 2001). These molecules, together with some specific anti-angiogenetic factors such as angiostatin, endostatin, and antithrombin, seem to play an important role in the destabilization of vessels and vascular regression. One of the key players in regulating the extent of angiogenesis and vessel growth along with these molecules, is the oxygen level in a given tissue as well. (ROSSANT and HOWARD 2002, ISOGAI et al. 2003).

The gross vascular anatomy of the developing embryo is similar amongst the various mammals. It is typically conserved in its basic plan with some species-specific variations, responsible for the particular characteristics of the various anatomical patterns in the adult animals.

2.2 ARTERIES

Paired ventral and dorsal aortae develop in the embryo. In their cranial parts, the ventral and dorsal aortae are initially connected by a series of up to six aortic arches. Some aortic arches regress early, others become carotids, subclavian arteries, the arch of the aorta (i.e., the left IV aortic arch), and pulmonary arteries. Each dorsal aorta gives off ventral branches, the vitelline arteries, supplying the yolk sack, and the umbilical arteries that supplies blood to the allantoid (Fig. 5A). Caudal to the aortic arches, the paired dorsal aortae merge finally to form a single descending aorta, the caudal continuation of the aortic arch, as found in adult animals (BARONE 1993a).

The descending aorta gives off dorsal, lateral, and ventral intersegmental arteries, from which originate the parietal and visceral collaterals of the aorta. The dorsal arteries are paired and symmetrical in the embryo, and most of them maintain this pattern also in the adult. They supply blood to the ribs, spine, thoracic and abdominal wall, and form the parietal collaterals of the aorta in the adult. Most paired lateral arteries degenerate, while other enlarge, and provide blood to the adrenal glands, kidneys, and gonads. The ventral intersegmental arteries become unpaired and develop into the major vessels of the gastrointestinal tract, viz. the celiac artery and the mesenteric arteries (BARONE 993a,b).

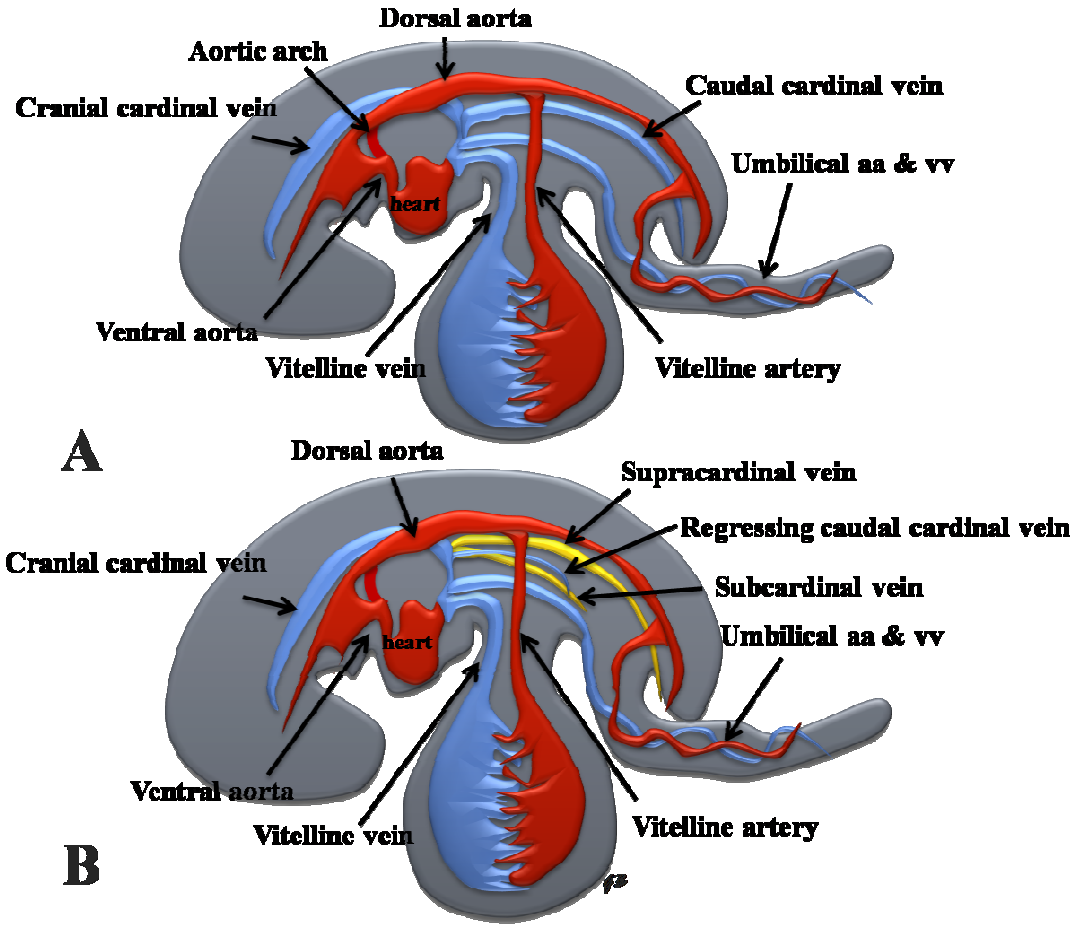

Fig. 5. Schematic drawing of the paired vascular channels in the embryo. **A**. the left lateral schematization shows the dorsal and ventral aorta, the IV and VI left aortic arch, vitelline veins which drain the yolk sac, umbilical veins which drain the allantois, and cranial and caudal cardinal veins which drain the embryo. **B.** each caudal cardinal vein regresses together with the regression of the mesonephroi and gives rise to supracardinal and subcardinal veins.

2.3 VEINS

The development of the venous system has been widely described in domestic animals, but several items are still controversial (HUNTINGTON and McCLURE 1920,

MCCLURE and BUTLER 1925, RIECK and REIS 1953, REIS and TEPE 1956, REIS and ESENTHER 1959). There are a few inconsistencies among the different studies, particularly regarding the origin of the caudal part of the caudal/inferior vena cava, in animals as well as in humans (MACCHI et al. 2003, CORNILLIE et al. 2008a,b). At least five different theories concerning the origin and development of the embryonic veins which are involved in the construction of this segment of the caudal vena cava have been described. Each of these theories is named according to the original embryonic vein which is considered as the precursor of the caudal part of the caudal vena cava (CORNILLIE and SIMOENS 2005). The supracardinal model is the most commonly accepted theory, and both the official Nomina Embryologica (NE 1983) and Nomina Embryologica Veterinaria (NEV 2006) are still based upon this model. This theory seems to be substantiated from several clinical studies on vascular variations and congenital anomalies in domestic animals as well as in humans (HUNT et al. 1998, HOFSTAETTER et al. 2000, MINNITI et al. 2002, FASOULIOTIS et al. 2002, GUIMARÃES FILHO et al. 2008).

Common features of the different theories about embryonic vein development in both humans and domestic animals are:

- the venous system begins its development in the earliest stages of intrauterine life, being symmetrical in its origin and asymmetrical in its final anatomical structure
- three paired symmetrical venous pathways are situated longitudinally in the embryo: the cardinal, covering the entire length of the embryo, and the vitelline, and umbilical veins

- each caudal cardinal vein regresses together with the regression of the mesonephroi and gives rise to supracardinal and subcardinal veins (Fig. 5B)
- the subcardinal veins take over the main venous drainage after the caudal cardinal regression
- when the left venous channels regress the blood flow is diverted to the right side of the body
- the caudal vena cava, azygos vein, ductus venosus, and portal vein develop by selective anastomosis, persistence, and degeneration of components of the above-mentioned embryologic vessels.

According to the supracardinal model, the cranial part of the right supracardinal vein develops into the azygos vein; its middle part degenerates and the caudal part gives origin to the pre-renal segment of the caudal vena cava (point of disagreement amongst different theories). From the right subcardinal vein arises the pre-hepatic segment of the caudal vena cava; it anastomoses with the cranial part of vitelline venous system (which forms the hepatic segments of caudal vena cava). Anastomoses between the right supracardinal and subcardinal vessels give origin to the renal segment of the caudal vena cava (point of disagreement amongst different theories). The vitelline veins produce the portal system, the hepatic sinusoids, and the hepatocardiac channels that will become the hepatic and post-hepatic segment of the caudal vena cava. The left umbilical vein anastomoses with the left branch of the portal vein, forming the ductus venosus (Fig. 6 A-D).

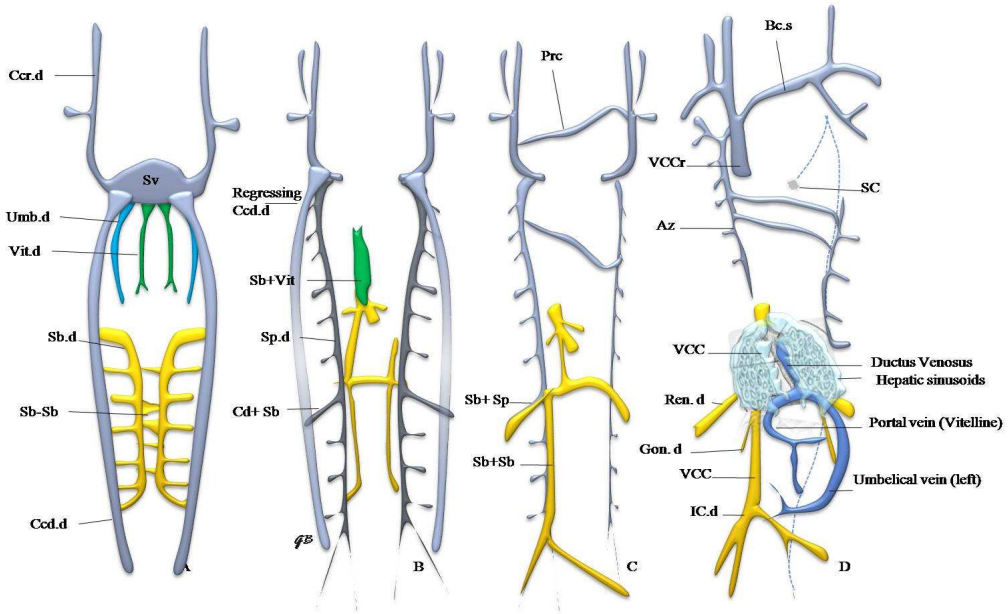

Fig. 6 A-C. Schematic drawing of the caudal vena cava, azygos vein, ductus venosus, and portal vein development by selective anastomosis, persistence, and degeneration of components of the embryologic vessels, according to the supracardinal model. Az, vena azygos; Bc.s vena brachiocephalica sinistra; Cd.d, vena cardinalis caudalis dextra; Cd+Sb, caudal cardinal-subcardinal anastomosis; Gon.d, vena gonadalis dextra; ICd, vena iliaca communis dextra; Prc, anastomosis precardinalis; Ren.d, vena renalis dextra; Sb.d, vena subcardinalis dextra; Sb-Sb, anastomosis subcardinalis; Sb+Sp, anastomosis subsupracardinalis; Sb+Vit, anastomosis subcardinalis-vitellina; SC, sinus coronarius; SV, sinus venosus; Umb.d, vena umbelicalis dextra; VCCr, vena cava cranialis; VCC, vena cava caudalis; Vit.d, vena vitellina dextra. **D.** Venous system at birth.

The ductus venosus is a fetal channel through which oxygenated blood can pass directly from the left umbilical vein to the left hepatic vein, thereby enter the systemic circulation, bypassing the hepatic sinusoids. At birth, stretching of the umbilical arteries results in arterial constriction and reduced fetal blood flow to the placenta. Reduced venous return through the left umbilical vein and ductus venosus allows this to gradually close in 3-6 days (TISDALL et al. 1997, BURTON and WHITE 1999).

CHAPTER 3

MATERIAL & METHODS

3.1 EQUIPMENT

The equipment used in the present study has been installed at the “San Marco” Private Veterinary Clinic of Padua since 2003, and includes: a multidetector computed 16-row (MDCT) system (Lightspeed 16, GE Healthcare, Milwaukee, WI, USA), an injector system for the contrast medium (Envision CT Injector System, Medrad, Indianola, PA), a workstation for post-processing (Advantage Workstation 4.1, GE Healthcare, Milwaukee, WI), and an anaesthesiology unit (Fabius Tiro, Dräger Medical AG & Co. KGaA, Lübeck, Germany) (Fig. 7). Contrast medium used in this study is a water-soluble, low-osmolar, non-ionic, dimeric, hexa-iodinated medium (Visipaque® 320, GE Healthcare, Milwaukee, WI, USA).

3.2 ANIMALS

From January 2006 to November 2008, 1437 dogs underwent enhanced abdominal MDCT examination at the “San Marco Veterinary Clinic” of Padua, for several clinical purposes. Twenty of these dogs (10 males, 10 females, ranging in weight from 3 to 46 kg, and from 24 to 60 months old) presenting no abnormal findings in the abdomen were used for describing the normal vascular anatomy. Owners of all dogs included in the study provided informed consent.

3.3 ANESTHESIA PROTOCOL

The following paragraphs summarize the anesthesia protocol for dogs undergoing MDCT examination:

- Food and water is withheld from dogs overnight prior to performing MDCT procedures
- Premedication with methadone (0.2 mg/kg, IM) and acepromazine (0.01 mg/kg IM combined in the same syringe), about 30-minutes before the induction of the anesthesia
- A large-bore intravenous (14-18 Gauge) line placed in the right or left cephalic vein
- Administration of Ringer's Acetate solution at a rate of 10 mL/kg/h IV throughout the anesthetic period
- Induction with fentanyl (0.003 mg/kg, IV, over 60 sec) followed by midazolam (0.2 mg/kg, IV, over 60 sec), and propofol at a rate of approximately 4 mg/kg/minute
- Intubation with an appropriate orotracheal tube
- Maintenance with 3% sevoflurane delivered in 100% oxygen (flow rate, 3 L/min) through a semi closed circle anesthetic system, to rapidly achieve the end-expired partial pressure of sevoflurane of 1.8-2.0%, then adjusted on the basis of clinical assessments of anesthetic depth

- Use of intermittent positive pressure ventilation (IPPV), with an electronically controlled piston-driven ventilator, to maintain the end-tidal partial pressure of carbon dioxide (Petco2) between 38 and 42 mm Hg
- Parameters continuously monitored include end-tidal sevoflurane concentration (FeSEVO) and Petco2, lead-II- electrocardiogram ECG, the oxygen saturation (Spo_2), non-invasive arterial blood pressure and rectal body temperature.
-

Fig. 7. Equipment used for the study. **1.** Anesthesiology unit. **2.** CT console and post-processing workstation. **3.** MDCT 16-row scanner.

3.4 MDCT PROTOCOLS

Abdominal MDCT protocols are adapted to the clinical circumstances, and include non-angiographic and angiographic studies, that essentially differ in scan timing. The non-angiographic studies are routinely performed for abdominal MDCT examinations, with a fixed scan-delay method that can give a mix of vascular and organ enhancement. The angiographic studies use an individualized scan delay per patient, to achieve and maintain optimal vascular enhancement throughout the scan.

The two protocols have several common points summarized in the following paragraphs:

- patients are in dorsal recumbency on the CT examination table, head first, with extended limbs
- cranio-caudal scanning direction
- contrast-enhanced scans were performed from the diaphragm to the symphysis pubis
- Images are acquired as a volume data set during a single brief apnea
- Iodixanol 320 I/ml is injected in a cephalic vein at 37°C temperature, dose 2 ml/Kg, and rate of injection 2-5 ml/sec
- Scanning parameters: helical modality, 0.7 s/rotation, standard algorithm, 120 kVp, 160-200 mAs, 1.2 mm slice thickness, and pitch 0.562:1

For non-angiographic studies, a standard delay of about 15 sec. (5-25 sec) is usually used so as to best outline either the vasculature or to image the abdominal parenchymal organs.

For MDCT angiography a bolus tracking technique is used, allowing the scan delay individualization per patient. The time-to-peak vessel enhancement is determined using Smart Prep bolus-tracking software technique (GE, Healthcare, Milwaukee, WI). The selected vessel is the descending aorta, at the dome of the diaphragm. This is also the starting point of the area of scanning, then the delay for the table to move and the scanning to begin is minimized. A region of interest (ROI) is manually placed on the section of the descending aorta. As the injection of contrast is begun, the scanner obtains multiple images across the region of interest, and measures the change in aortic enhancement over time. We have predetermined that the scan starts when the contrast density in the aorta exceeds the threshold of 30 HU (Hounsfield Units) above baseline (Fig. 8). There is an additional instrumental delay taking approximately 2 sec.

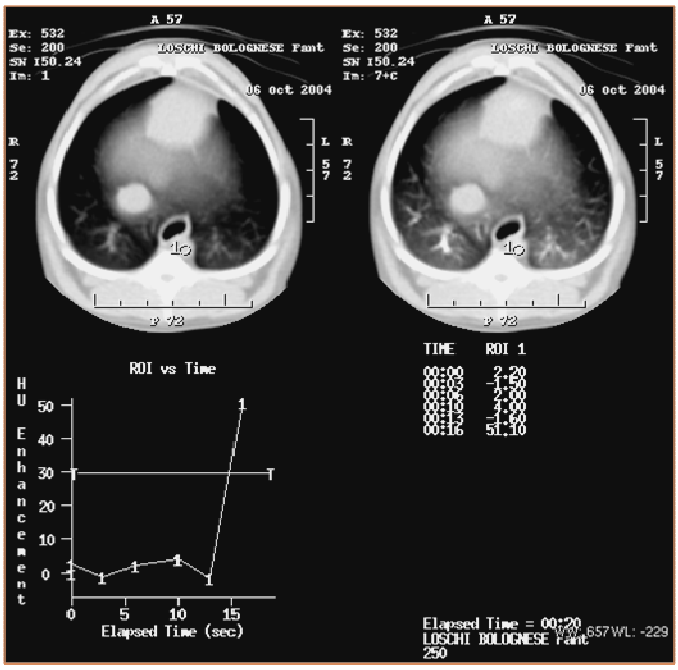

Fig. 8. The image shows the bolus tracking software technique, with 30 Hounsfield Units as the threshold to timing the arterial phase.

3.5 POST-PROCESSING TECHNIQUES

All reconstructed images with an original resolution of 512x512 are automatically transferred to a freestanding workstation for post-processing. Selected images of angiographic studies are retro-reconstructed with 50% overlap (every 0.625 mm) by the scanner software and then sent to the workstation. The data set are processed with the multiplanar reformatting (MPR), maximum Intensity Projection (MIP), and volume rendering (VR) software techniques.

MDCT images are evaluated and processed initially on MPR to visualize the vascular structures from all points of view. Transverse views are always reviewed together with sagittal and dorsal views. To follow the course of vessels during the real-time evaluation, every arbitrary plane is interactively chosen in a fourth oblique view (Fig. 9).

To enhance depiction of normal anatomy, anatomical variants, and pathologies, MIP and VR images are created, each time with emphasis on the selected vessel or vascular system. Manual and automated segmentation techniques are both used for each time outline the anatomy to be saved or discarded in the final images, or just to discard the background.

Maximum Intensity projection is interactively created from the portion of the data set of interest, mainly to visualize thin vessels or vessels within the parenchyma.

Volume rendering is the algorithm chosen in this study to create vascular maps as it maintain spatial relationships and depth, allowing the three-dimensional anatomic representation of the structures.

3.6 IMAGE ANALYSIS

The assessment of the abdominal vasculature and its variants is based on textbooks of anatomy of the dog: BARONE R. Anatomia comparata dei mammiferi domestici. Vol. 5: Angiologia and the Miller's Anatomy of the Dog (H. E.Evans ed.), and the following selected references: ABIDU-FIGUEIREDO et al. 2005, CHRISTENSEN 1952, COTMOIS 1987, ENGE and FLATMARK 1972, GOMETZ et al. 1973, HUNTINGTON and McCLURE 1920, PAYNE et al. 1970, REIS R.H. AND TEPE 1956, ROSENBLUM et al 1997, SCHMIDT et al. 1980, SCHMIDT and SUTER 1980, SINGH et al. 1982, TEIXEIRA et al. 2007, SHIVELY 1978, VITUMS 1959, , URSˇICˇ et al. 2007.

The nomenclature for description of the anatomical structures and their variants is based on the Angiology and Splanchnology sections of the Illustrated Veterinary Anatomical Nomenclature (SIMOENS and DE VOS 2007a), the Nomina Anatomica Veterinaria (NAV 2005), Nomina Embryologica Veterinaria (NEV 2006). Figures and figure legends mention the Latin terms of vessels. A bilingual Latin-English list of terms is reported at the end of the thesis.

The terms describing the computed tomography protocols are based on "Standardized Nomenclature and Description of CT Scanning Techniques" (KALRA 2006). Imaging planes terminology is based on the Veterinary CT/MR Society Letter (1996), and on "Advanced imaging concepts: A pictorial glossary of CT and MRI technology" (TIDWELL 1999).

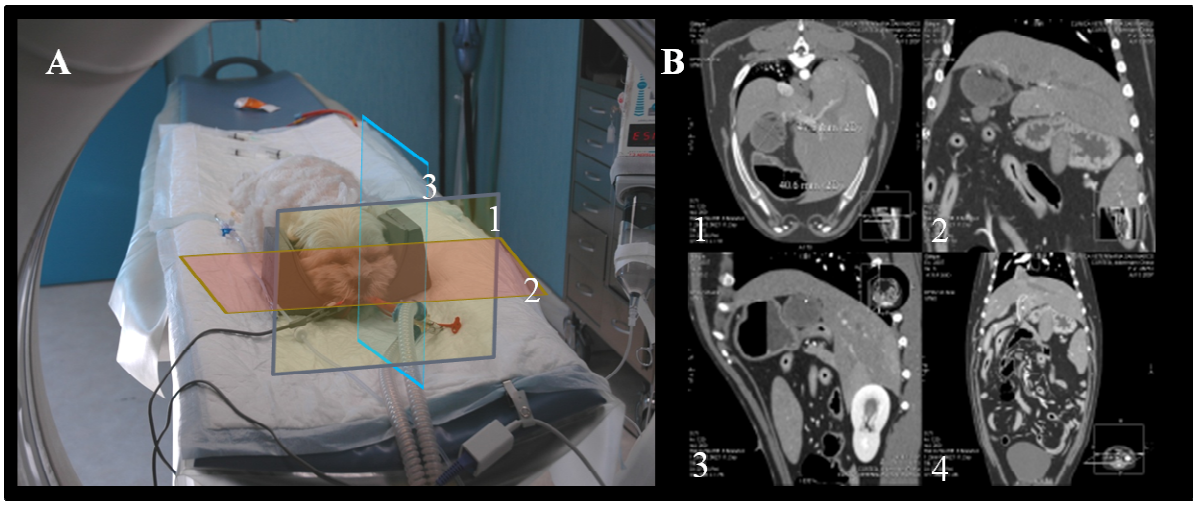

Fig. 9. Image planes in animals. **A.** Either for sternal or dorsal recumbency, the planes are named as follows: 1. Transverse plane (axial in humans) 2. Dorsal plane (coronal in humans) 3. Sagittal plane (sagittal in humans as well). **B.** The resulting images in multiplanar (MPR) mode of visualization are: 1.Transverse 2. Oblique 3. Sagittal 4. Dorsal.

Note that “dorsal view” refers to the CT plane of section and not to the anatomic view. According to the image orientation guidelines, the left side of patient is on the right of the reader and viceversa, in two-dimensional images. Three-dimensional images are generally oriented in space just to better visualize the structures of interest.

CHAPTER 4

RESULTS *(part I)*

This is a pictorial section of normal vascular abdominal anatomy as demonstrated by multidetector row computed tomography. Images of the abdominal vessels and their major branches are here represented and accompanied with brief descriptions of the anatomy. The images of this section include two-dimensional (2D) Multiplanar Reformatted (MPR) images, and three-dimensional (3D) Maximum Intensity Projection (MIP) or Volume Rendering (VR) images, obtained from post-processing of either angiographic or non-angiographic clinical studies.

4.1 ANATOMY OF THE ABDOMINAL VESSELS

In the adult dog there are three unpaired abdominal vascular systems, viz. the aorta, the caudal vena cava, and the portal vein, and their pertaining unpaired tributaries. In normal adult animals, there are no active connections between the caval and porta venous systems, except for the ductus venosus which is an intrahepatic channel between the left umbilical vein and the left branch of the portal vein in the fetus, but closes shortly after birth.

The aorta is the more dorsal vessel. It courses just ventral to the spine, to the left side. The caudal vena cava courses ventral to the aorta, to the right side. The portal vein is ventral to the caudal vena cava, on the right side as well.

4.2 AORTA AND ITS BRANCHES

The descending aorta (*Aorta descendens*) is the caudal continuation of the aortic arch (*Arcus aortae*). It is divided in two segments, viz. the intrathoracic aorta (*Aorta thoracica*), that extends to the aortic hiatus (*Hiatus aorticus*), and the abdominal aorta (*Aorta abdominalis*). In consequence of the large branches which it gives off at the level of the penultimate or last lumbar vertebra (i.e the left and right *A. iliaca externa*), the abdominal aorta diminishes considerably in size, and after giving of the left and right *A. iliaca interna* it continues into the median sacral artery (*A. sacralis mediana*) (Fig. 10).

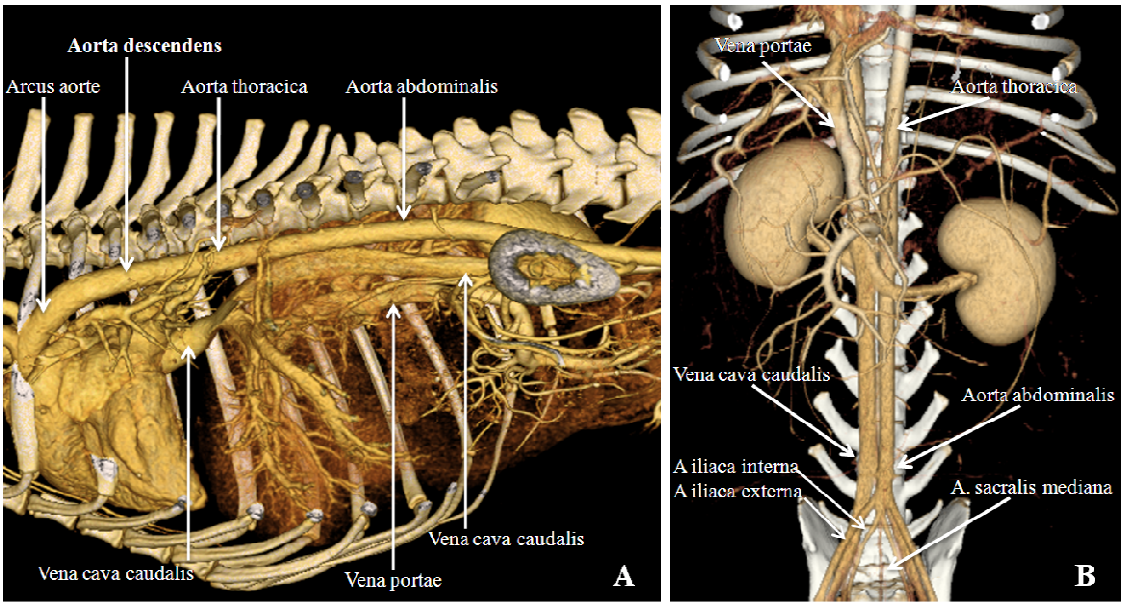

Fig. 10. A. Sagittal contrast enhanced volume rendered (VR) image in an adult dog. Ribs of the left side have been partially removed, as well as part of the left kidney. The aorta courses ventral the vertebral column, dorsal the caudal vena cava and the portal vein. **B**. Contrast enhanced VR image in a dog, ventral aspect. Both kidneys are visible.

The abdominal aorta begins at the aortic hiatus of the diaphragm and courses ventral to the vertebral column, giving off branches to supply the stomach, kidneys, intestines, gonads, and other organs through extensive arterial networks.

The branches of the abdominal aorta may be divided into three sets: parietal, visceral, and terminal branches (Fig. 11).

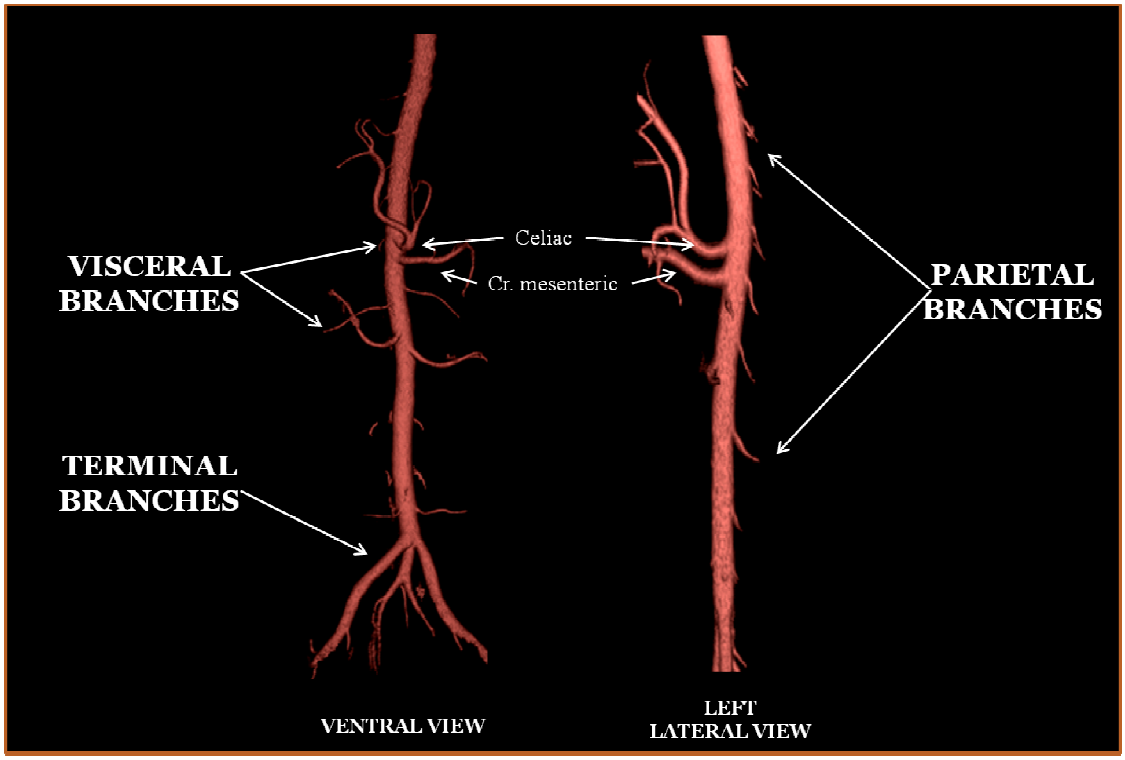

Fig. 11. Volume rendered images of the *Aorta abdominalis* and its major parietal, visceral, and terminal branches.

4.2.1 PARIETAL BRANCHES

The parietal branches of the aorta develop from the fetal dorsal intersegmental arteries. From the abdominal aorta arise the paired and symmetrical phrenic and abdominal

arteries (*A. phrenica caudalis, A. abdominalis cranialis*), the lumbar arteries (*Aa. lumbales*), and the deep circumflex iliac arteries (*A. circumflexa ilium profunda*) (Fig. 12-17).

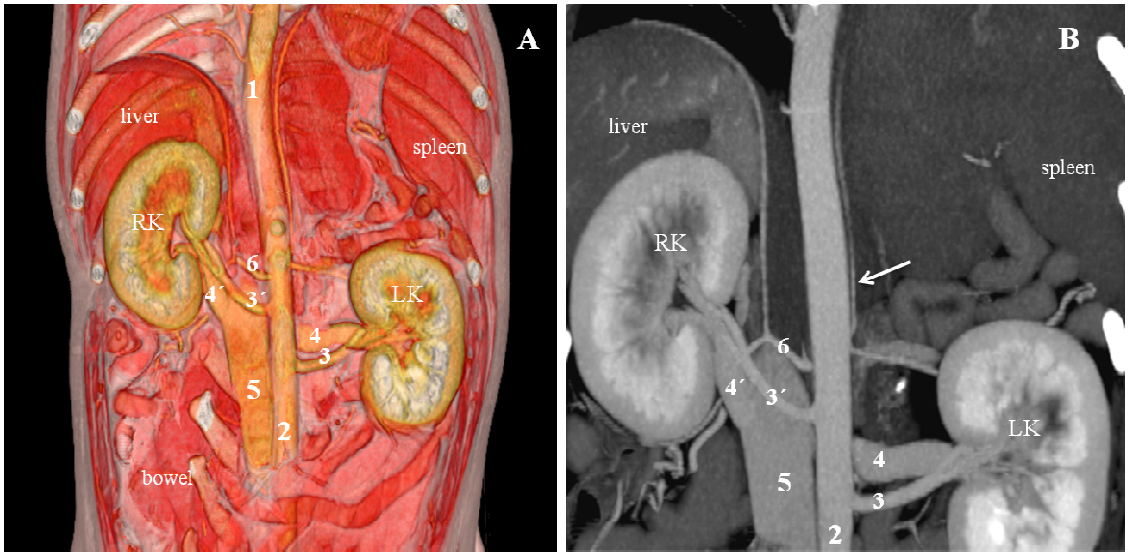

Fig. 12. The descending aorta and its branches. **A.** Volume rendered image of the abdomen, ventral aspect. **B.** Maximum Intensity Projection image, dorsal view. RK, right kidney, LK, left kidney. From the cranial abdominal artery arises a branch that courses cranially into the lumbar part of the diaphragm, *A. phrenica caudalis*. This dog had two small branches to the diaphragm, arising from the cranial abdominal artery on the right side, and one vessel on the left side from the abdominal aorta, just cranially to the cranial abdominal artery (arrow in B). 1. *Aorta thoracica*. 2. *Aorta abdominalis*. 3. *A. renalis sinistra.* 3'. *A. renalis dextra*. 4. *V. renalis sinistra.* 4'. *V. renalis dextra*. 5. *Vena cava caudalis*. 6. *A. abdominalis cranialis*.

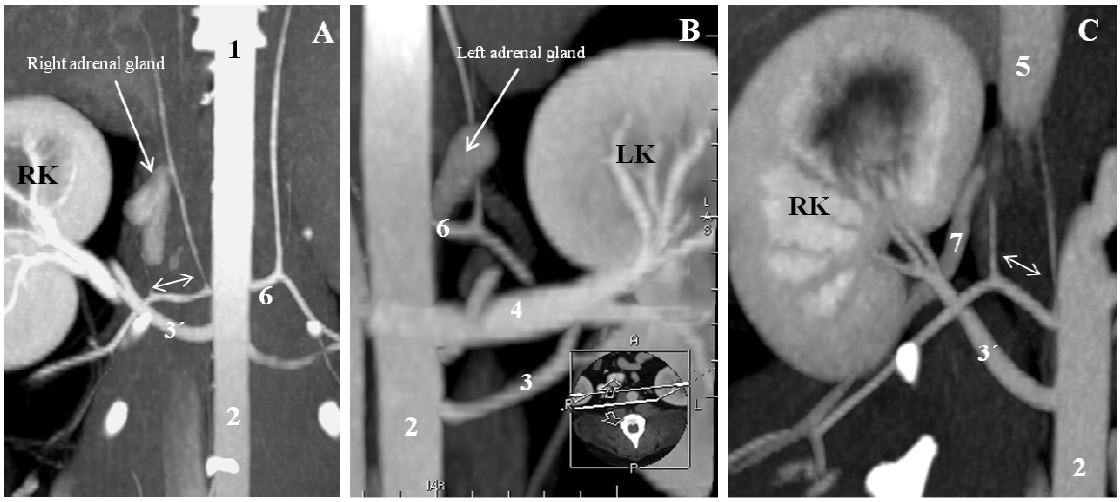

Fig. 13. Maximum Intensity Projection images of three different dogs. RK: right kidney. LK: left kidney. 1. *Aorta thoracica*. 2. *Aorta abdominalis*. 3. *A. renalis sinistra*. 3'. *A. renalis dextra* (A, C). 4. *V. renalis sinistra* (B). 5. *V. cava caudalis*. 6. *A. abdominalis cranialis*, giving rise to caudal phrenic branches (double-headed arrow) (A, C).

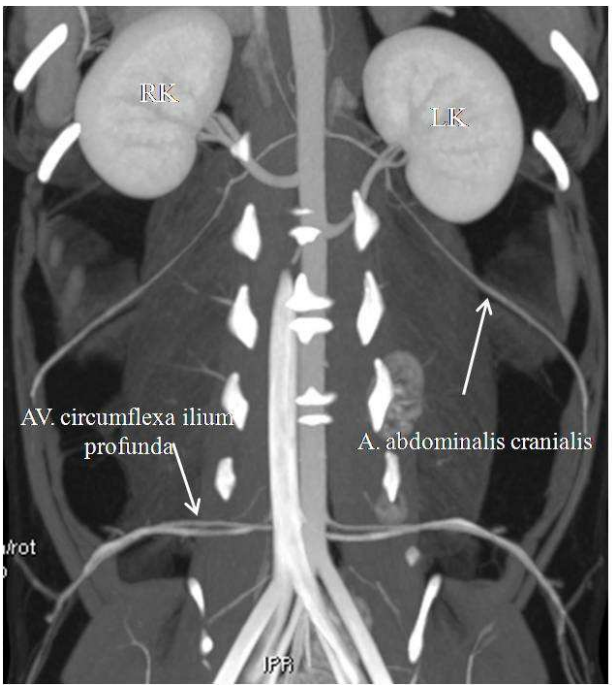

Fig. 14. Maximum Intensity Projection of the abdomen in a dog. RK: right kidney. LK: left kidney.

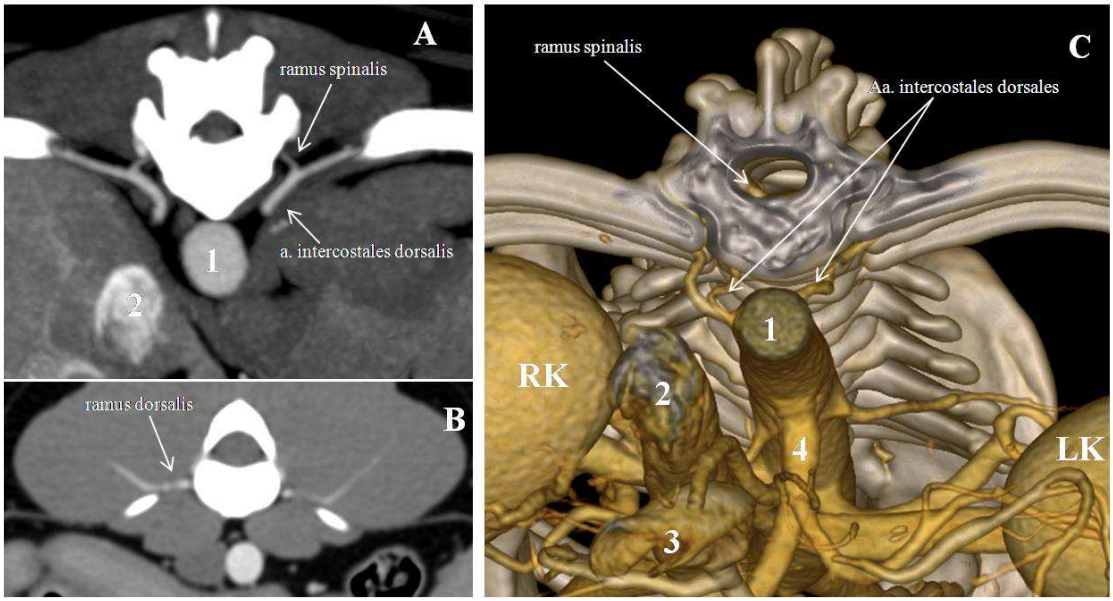

Fig. 15. A, B. Transverse Maximum Intensity Projection (MIP) images of the thoracic aorta and its parietal branches (*Aa. intercostales dorsales*). The *Ramus spinalis* enters the spinal canal through the intervertebral foramen. **B.** *Ramus dorsalis*, that courses dorsally to the epaxial muscles. **C.** Volume Rendering (VR) of the abdomen, in an oblique-frontal view, showing the thoracic aorta and some of parietal and visceral branches. 1. *Aorta thoracica*. 2. *Vena cava caudalis*. 3. *Vena portae*. 4. *A. coeliaca*. RK: right kidney. LK : left kidney.

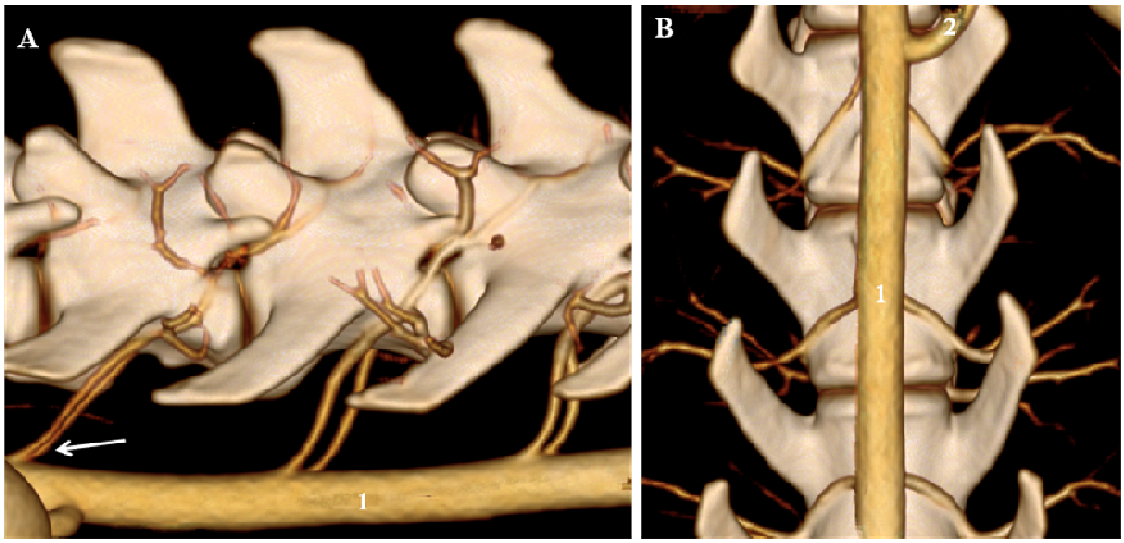

Fig. 16. Lumbar segment of the *Aorta descendens*. A: left view. B: ventral view. 1: *Aorta abdominalis*, intra-abdominal segment of the descending aorta; the *Aa. lumbales* are paired vessels that arise from the abdominal aorta and are often initially fused (arrow). 2. *A. renalis sinistra* (B).

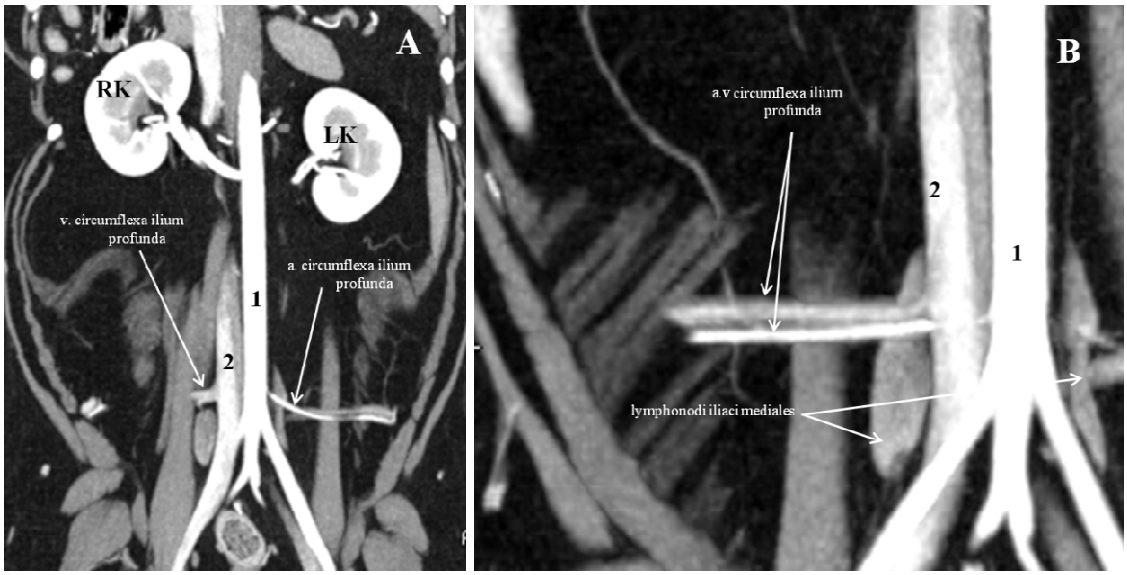

Fig. 17. A. Maximum Intensity Projection dorsal view of the abdomen in a dog. 1. *Aorta abdominalis* 2. *Vena cava caudalis*, pre-renal segment of the caudal vena cava. **B.** Close view of the same image showing right deep circumflex iliac artery and vein.

4.2.2 VISCERAL BRANCHES

The visceral branches of the abdominal aorta include unpaired vessels, viz. the celiac artery (*A. coeliaca*), the cranial and caudal mesenteric arteries (*A. mesenterica cranialis et caudalis*), and paired vessels, i.e. the renal arteries (*A. renalis sinistra et dextra)*, adrenal arteries (*A. adrenalis sinistra et dextra*), and the gonadal arteries (*A. testicularis*, *A. ovarica*).

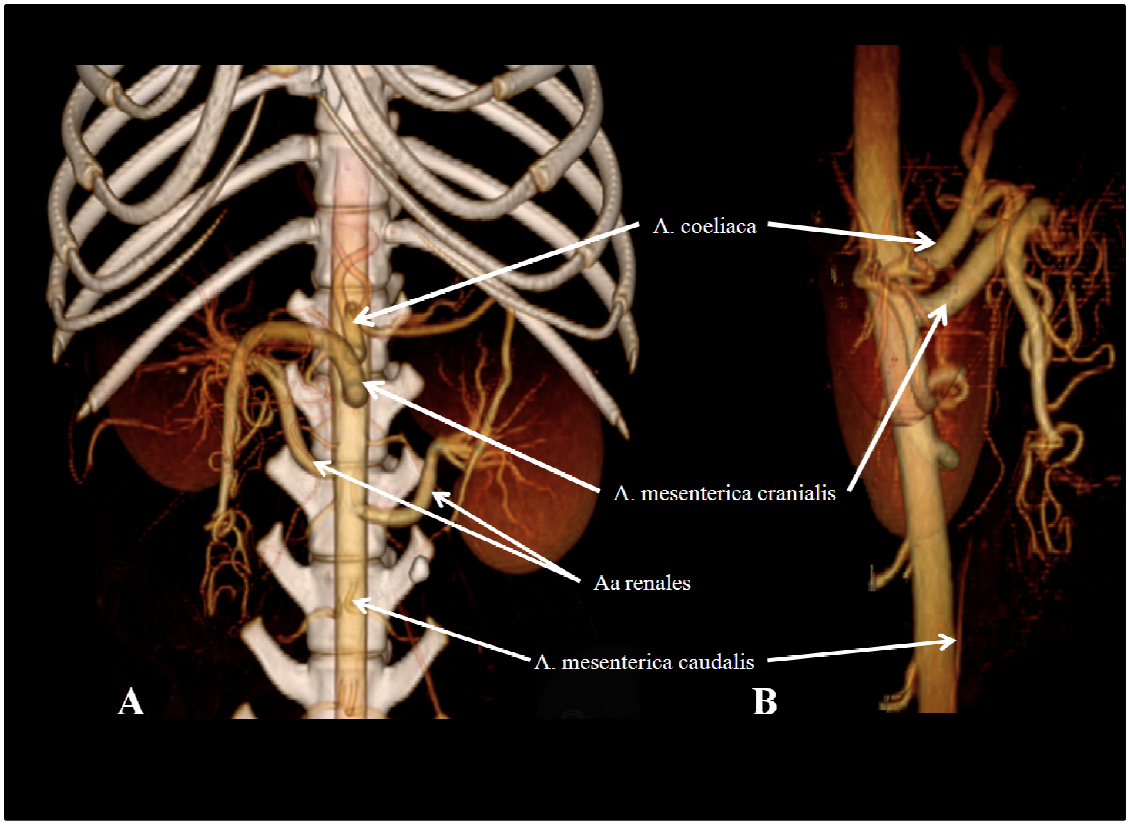

Fig. 18. Volume Rendering of major visceral branches in a dog. A. Ventral aspect. B. Right lateral aspect.

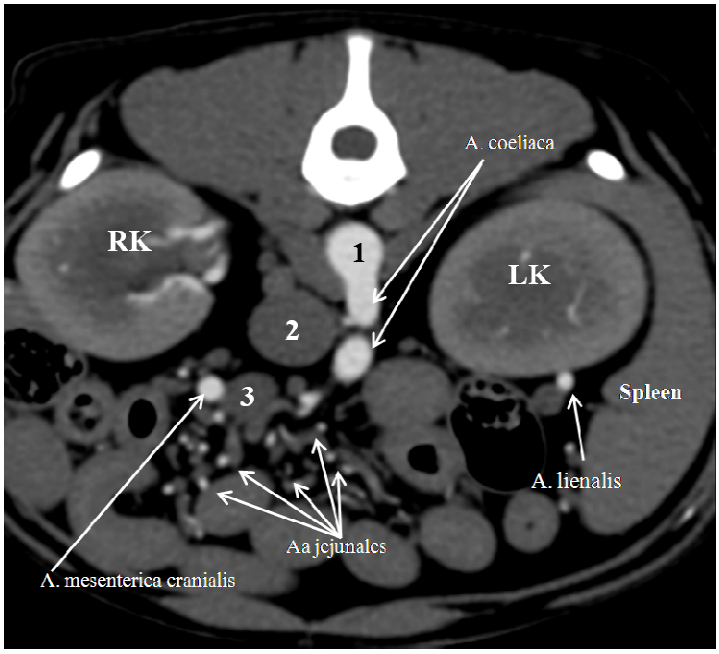

Fig. 19. 2D transverse image of the abdomen in a dog at the level of the first lumbar vertebra. Arterial phase. 1. *Aorta abdominalis*. 2. *V. cava caudalis*, non-enhanced. 3. *V. mesenterica cranialis*, non-enhanced. RK: right kidney, LK: left kidney.

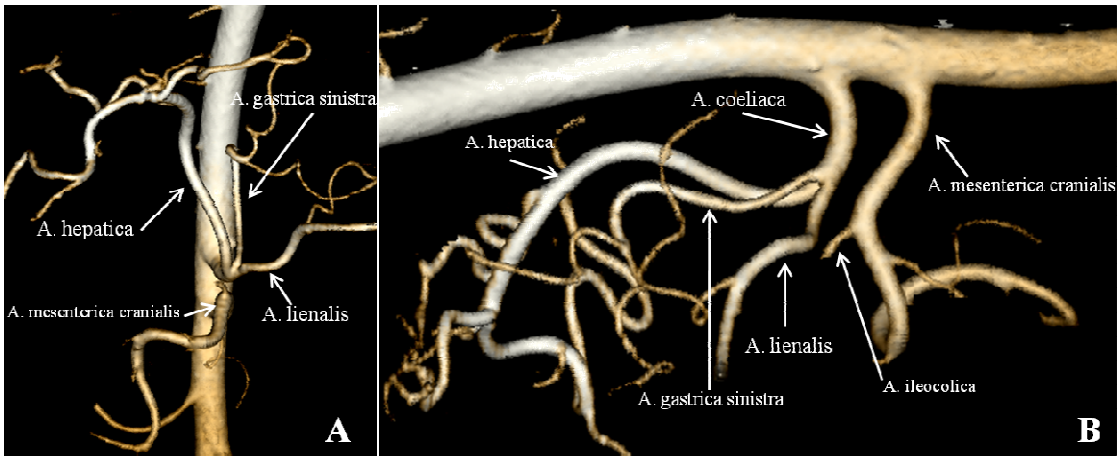

Fig. 20. Volume Rendering of the celiac and cranial mesenteric arteries. A. Ventral view. B. Left lateral view.

Celiac artery - The celiac artery (*A. coeliaca*) is an unpaired artery that emerges from the ventral surface of the abdominal aorta at the level of the first lumbar vertebra. It gives off at least three branches, i.e. the hepatic artery (*A. hepatica*), the left gastric artery (*A.*

gastrica sinistra), and the splenic artery (*A. lienalis*). It ends by trifurcating or can give off the hepatic artery and a gastro-splenic trunk. The gastrosplenic trunk subsequently divides to form the left gastric artery and the splenic artery (Fig. 18-21).

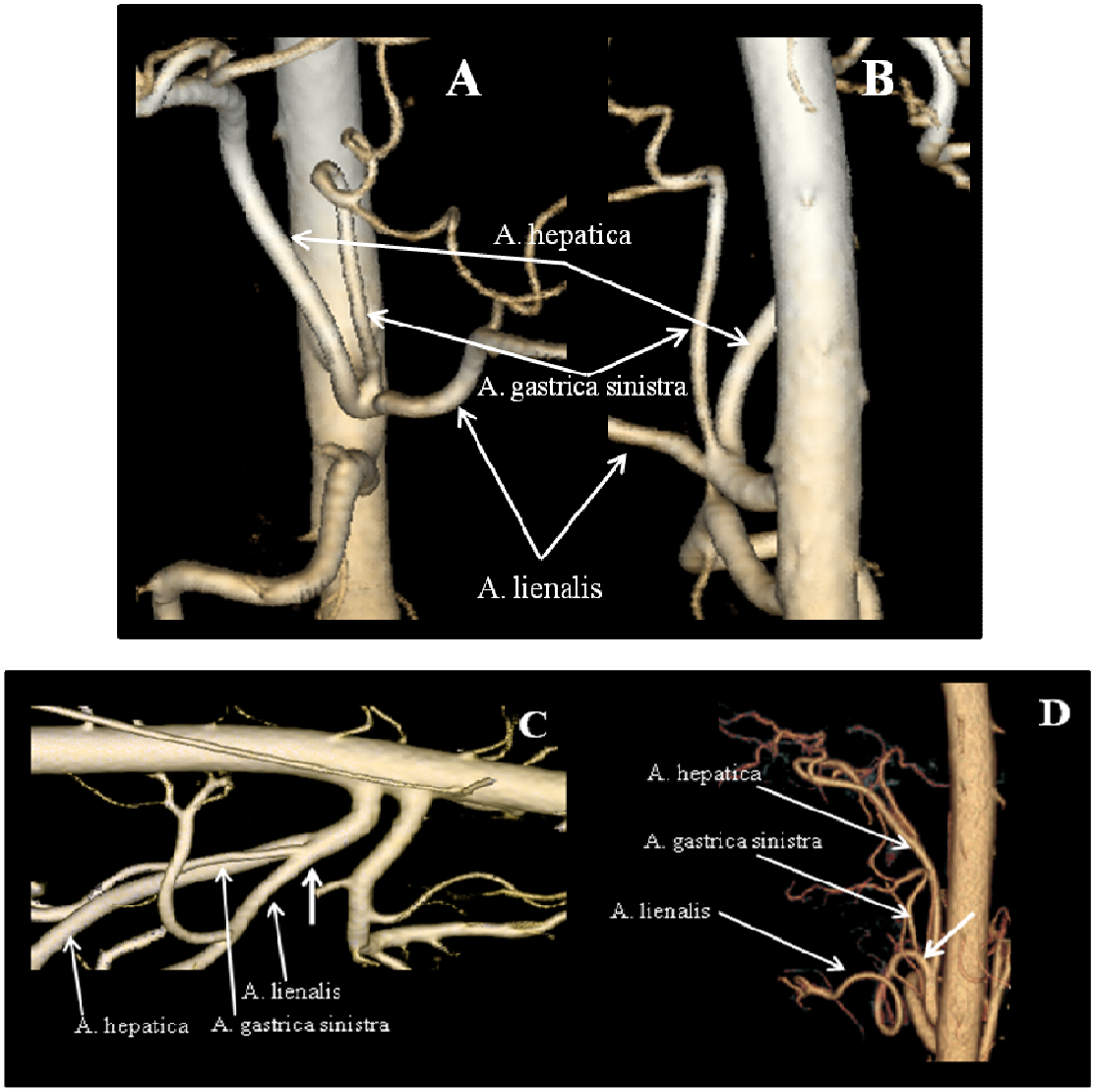

Fig. 21. *A. coeliaca*, and its branches. A,B. The celiac artery ends by trifurcating into the *A. hepatica*, *A. lienalis*, and *A. gastrica sinistra*.

Hepatic artery - In its extrahepatic course the hepatic artery runs cranioventrally to the right side next to the portal vein. It gives off a variable number of branches, three to five, which enter the portal area of the liver and accompany the hepatic branches of the portal vein. The number and course of the branches of the hepatic artery, as well as the regions supplied by them vary among individuals (Fig. 19-23).

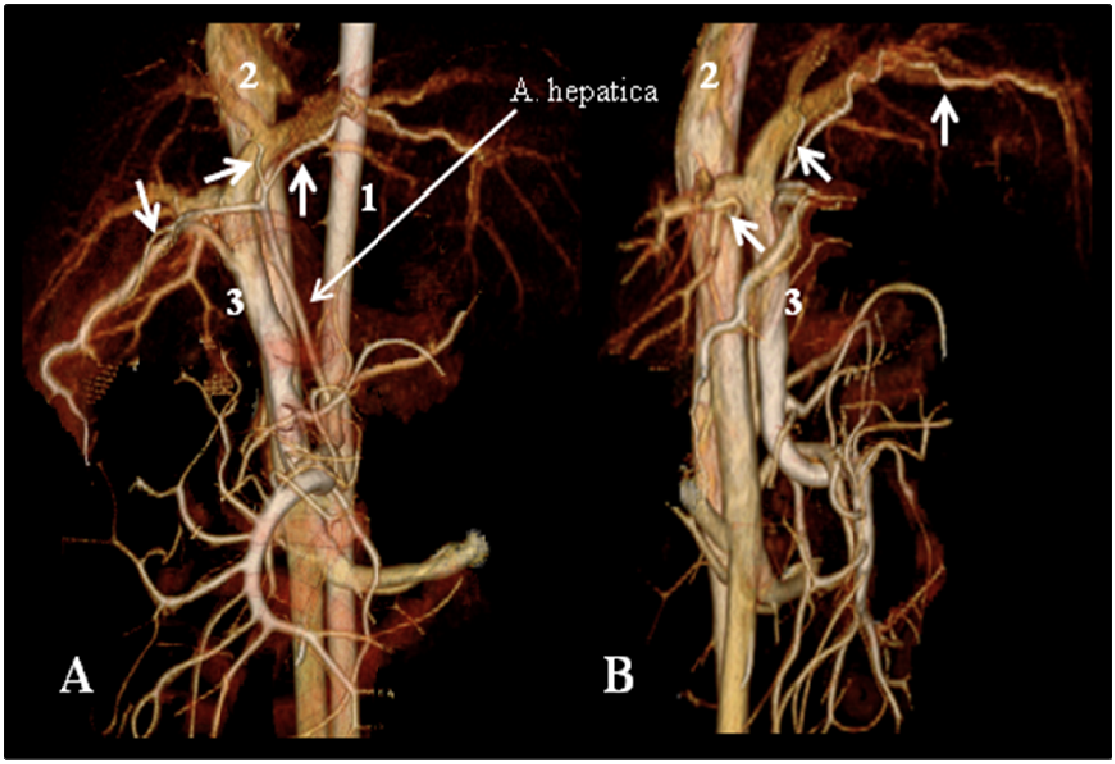

Fig. 22. Volume Rendered images. A: ventral view, B: right lateral view. *A. hepatica*, hepatic artery and is relationships with other abdominal vessels. 1. *A. abdominalis*. 2. *Vena cava caudalis*, hepatic segment. 3. *Vena porta*. The extra-hepatic segment of the hepatic artery courses close to the portal vein to the liver. Small arterial branches arise from the hepatic artery and enter the liver together with the portal branches. At least three branches of the hepatic artery enter the liver (*ramus dexter lateralis, ramus dexter medialis, ramus sinister*) (arrows).

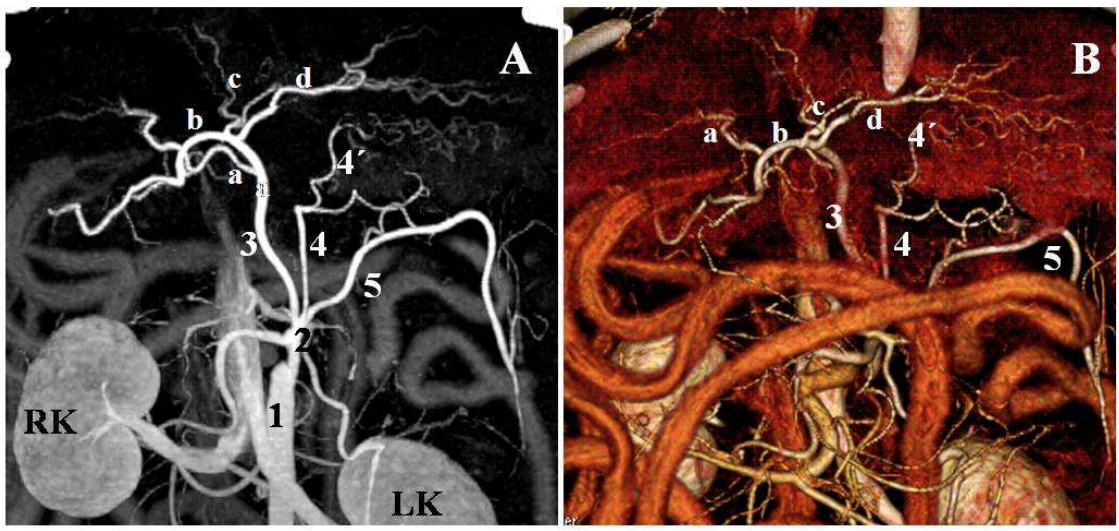

Fig. 23. A. Maximum Intensity Projection image of the hepatic artery. **B.** Volume Rendered image, ventral view. 1. *Aorta abdominalis*. 2. *A. coeliaca*. 3. *A. hepatica*, extra-hepatic segment. 4. *A. gastrica sinistra*. 4'. *Ramus esophageus* 5. *A. lienalis*. The intrahepatic branches of the hepatic arteries are visible: **a.** *Ramus dexter medialis* **b.** *Ramus dexter lateralis* **c.** *Ramus sinister medialis* **d.** *Ramus sinister lateralis*.

Mesenteric arteries – The cranial mesenteric artery (*A. mesenterica cranialis*) is the largest visceral branch of the abdominal aorta. It arises from the ventral surface of the aorta directly caudal to the celiac artery. It gives off several branches for the pancreas and the small and large intestine. The caudal mesenteric artery (*A. mesenterica caudalis*) is a thin vessel that originates from the ventral surface of the abdominal aorta (approximately at the same level of the deep circumflex iliac arteries) and supplies the terminal portion of the intestine (Fig. 18-21, 24, 25).

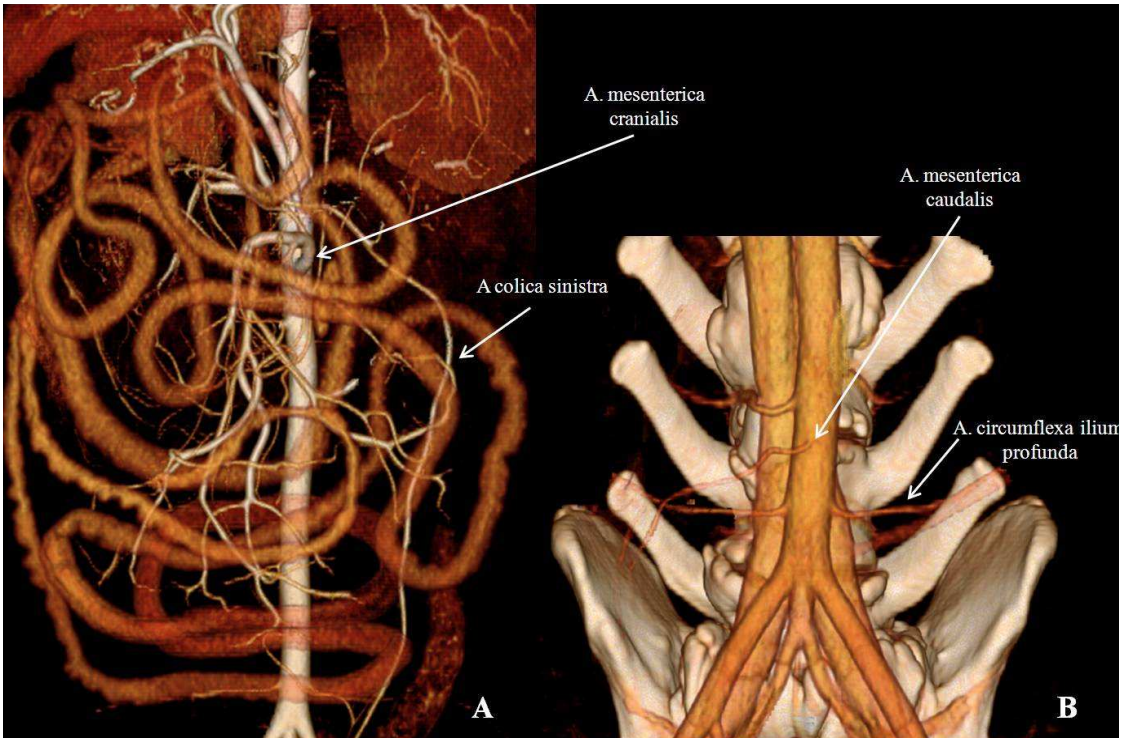

Fig. **24**. **A, B.** Volume rendered images of the cranial and caudal mesenteric arteries, supplying the small and large bowel.

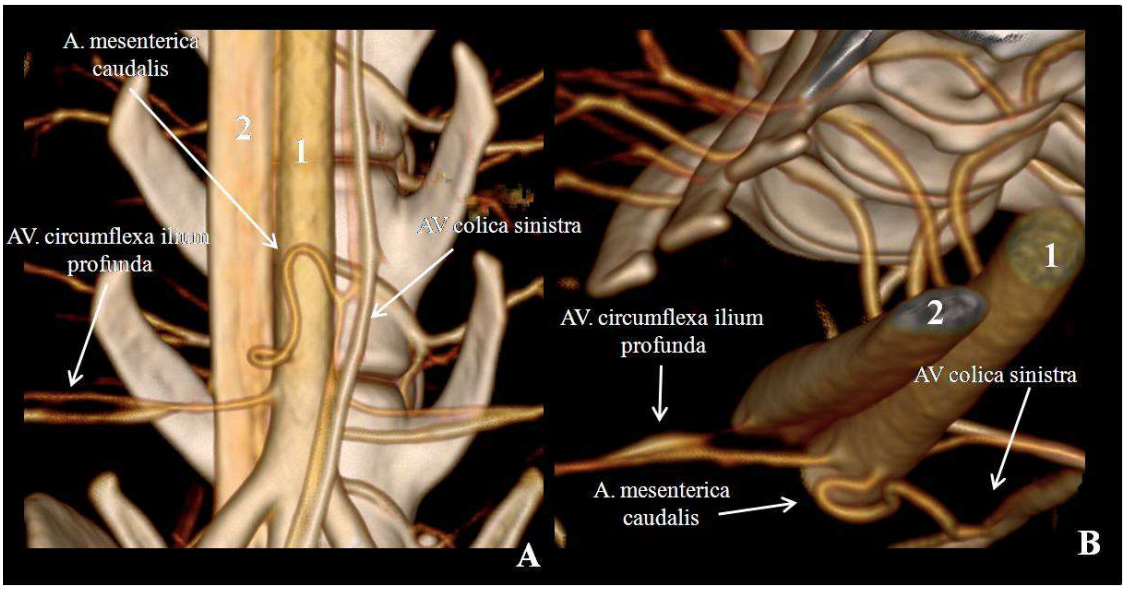

Fig. 25. Volume rendered images of the caudal mesenteric artery. A. ventral view. B. frontal-oblique view. The *A. mesenterica caudalis* commonly arises from the ventral surface of the aorta. It goes initially to the right and then curves in cranial direction, before turning back caudally and giving off the left colic artery.

Renal arteries – The renal arteries (*Aa. renales*) are paired lateral visceral branches of the abdominal aorta. The patterns of renal vessels are extremely variable. Commonly, a single renal artery bifurcates into dorsal and ventral branches which supply the cranial and caudal portion of the kidney. A double renal artery was frequently noted either on one or both sides. In the renal hilus, each renal artery branch gives off interlobar end arteries, which continue into the kidney and form the arcuate, interlobular arteries, and the glomerular afferent arterioles (Fig. 12, 13 26-30).

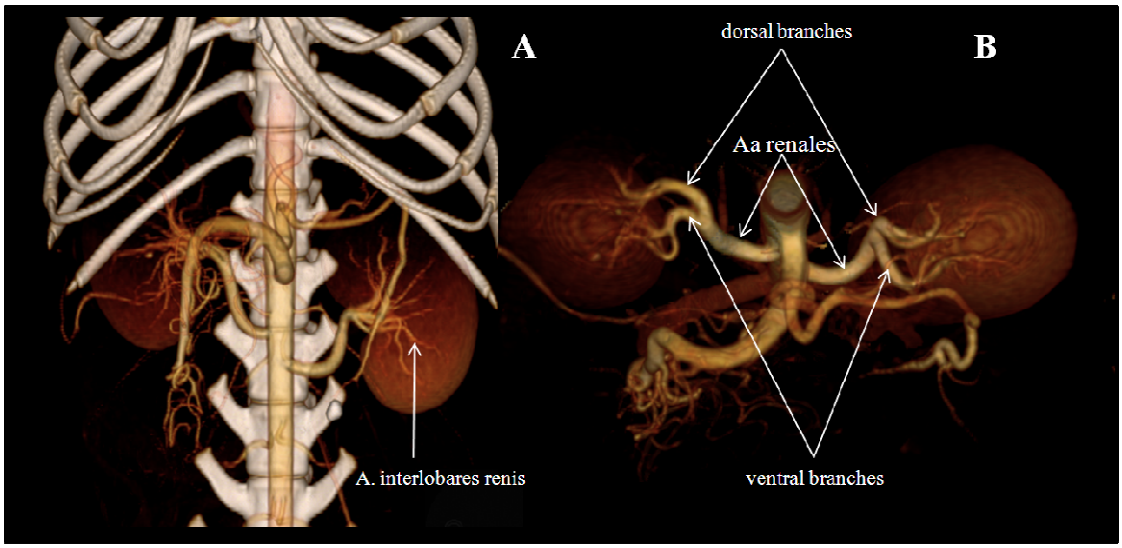

Fig. 26. Volume rendered images of renal arteries and their branches in a dog. **A.** ventral view. **B.** Cranial view.

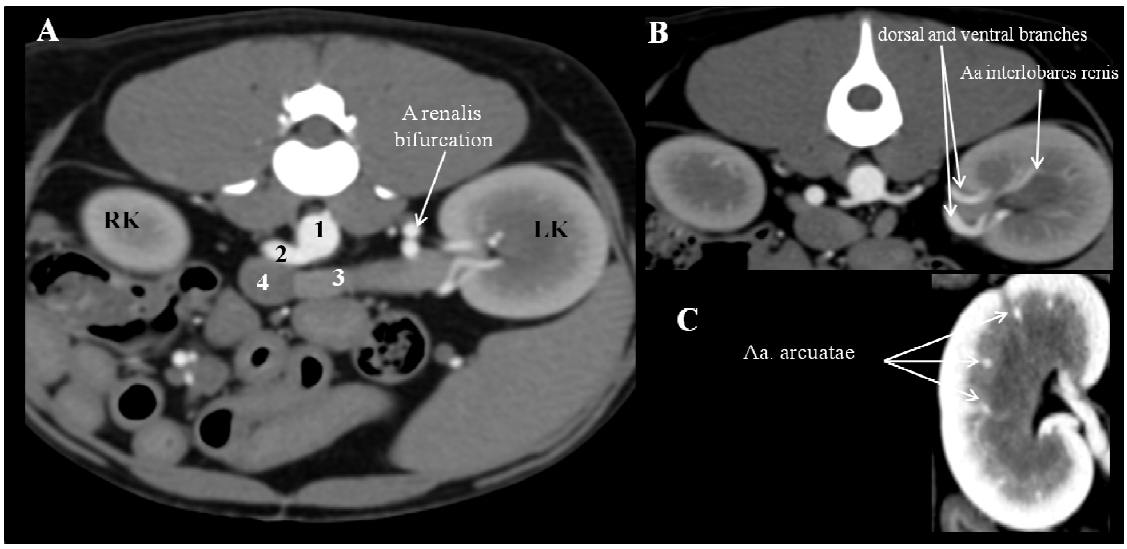

Fig. 27. 2D transverse views of the renal arteries in a dog. Arterial phase. RK: right kidney. LK: left kidney. 1. *Aorta abdominalis*. 2. *A. renalis dextra*. **A.** The left renal artery bifurcates proximal to the kidney. **B.** Dorsal and ventral branches of the left renal artery are visible. *Aa. interlobares renis*, interlobar renal arteries. **C.** Higher magnification of the left kidney. *Aa. arcuatae*, arcuate arteries (arrows).

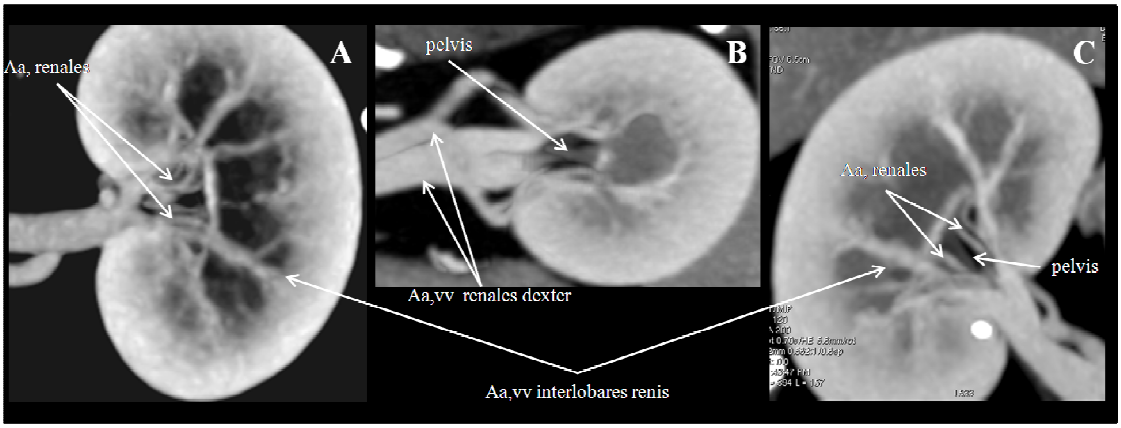

Fig. 28. Maximum Intensity Projection images of renal vessels. **A**. Dorsal reformatted image of the right kidney in a dog. **B.** Oblique reformatted view of the right kidney in a dog. **C**. Dorsal reformatted image of the left kidney in a dog.

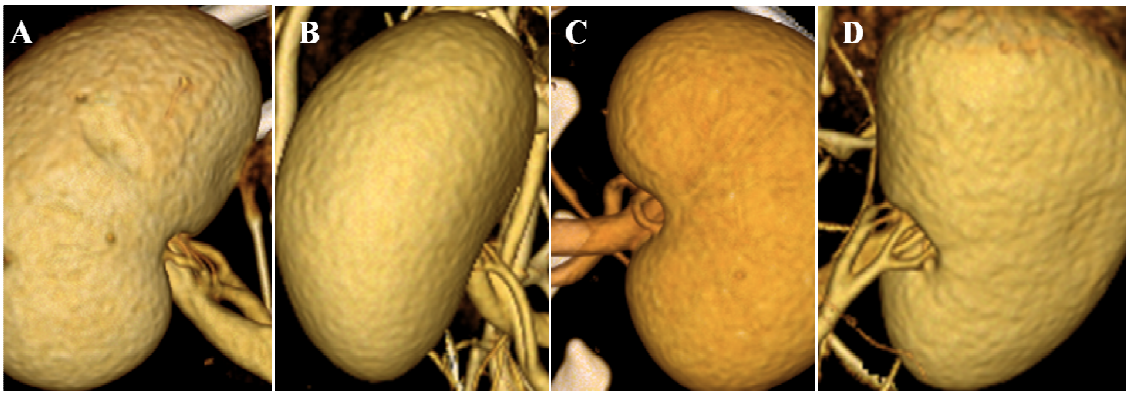

Fig. 29. Volume rendered images of kidneys showing different patterns of renal vessels. **A.** Ventral view of a right kidney. **B**. Dorsal view of a left kidney. **C.** Ventral view of a left kidney. **D.** Dorsal view of a right kidney.

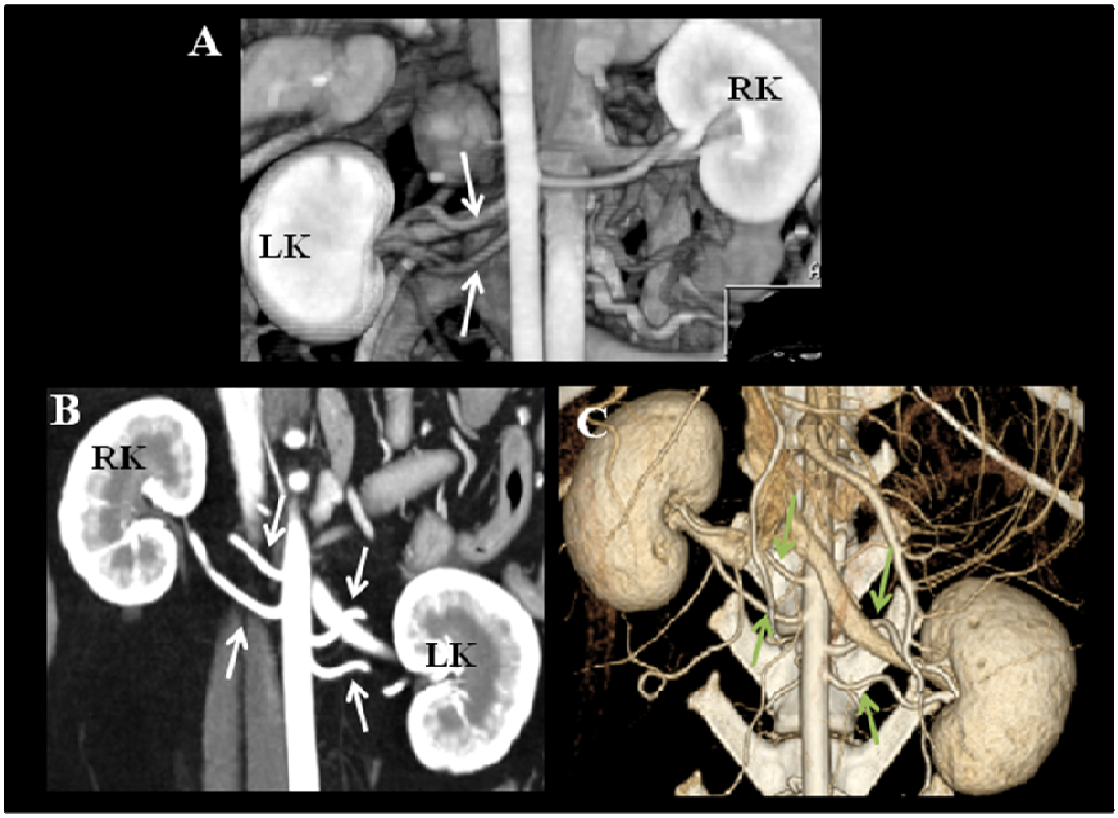

Fig. 30. **A**. Volume Rendering of the renal vessels in a dog. Posterior view. There are two renal arteries on the left side, and one right renal artery (arrows). **B.** Maximum Intensity projection image of another dog. Double renal arteries are present on both sides (arrows). **C.** Volume rendering of the same dog. Double renal arteries are present on both the left and the right side (arrows). RK: right kidney, LK: left kidney.

4.2.3 TERMINAL BRANCHES

At the level of the penultimate or last lumbar vertebra the abdominal aorta gives off the left and right external iliac arteries (*Aa. iliacae externae*) for the pelvic limbs, whereafter it decreases much in size and soon gives off the internal iliac arteries (*Aa. iliacae internae*) and ends by diminishing rapidly in size, continuing into the median sacral artery, *A. sacralis mediana* (Fig. 9, 31)**.**

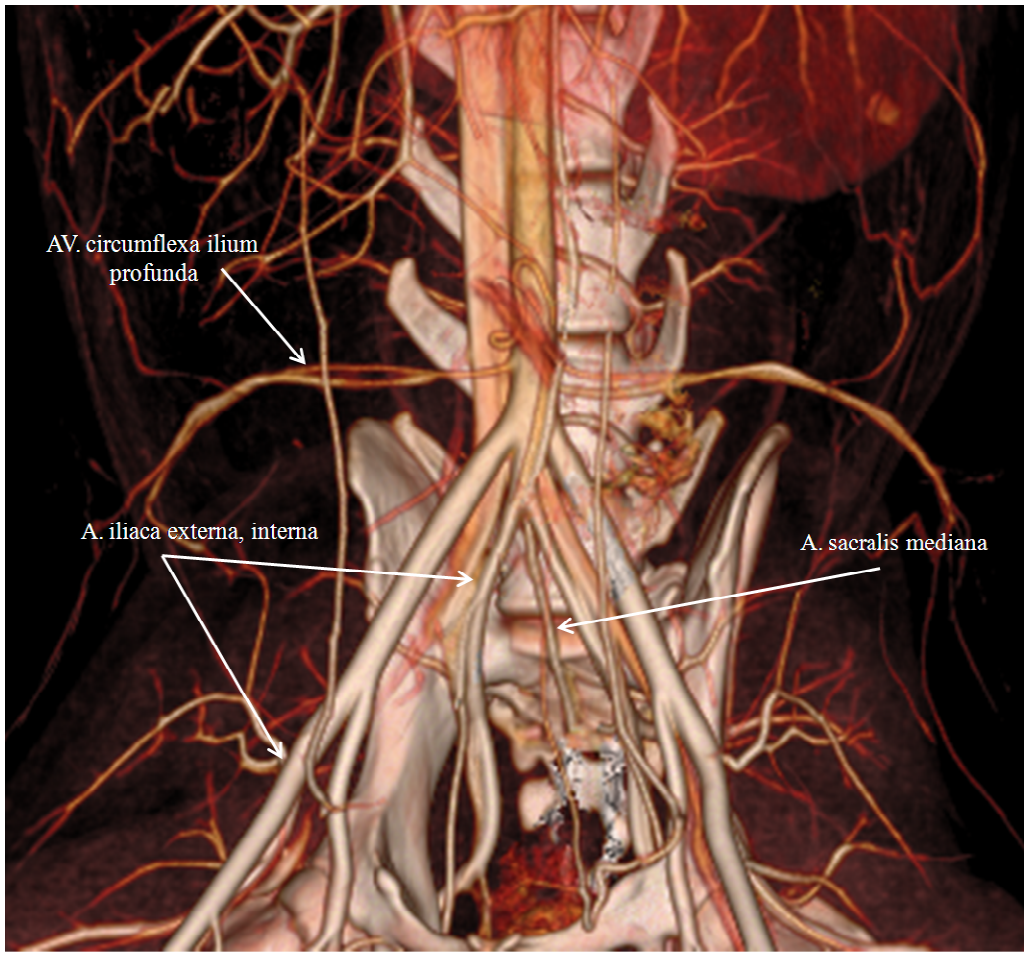

Fig. 31. Terminal branches of the abdominal aorta and branches of the abdominal wall.

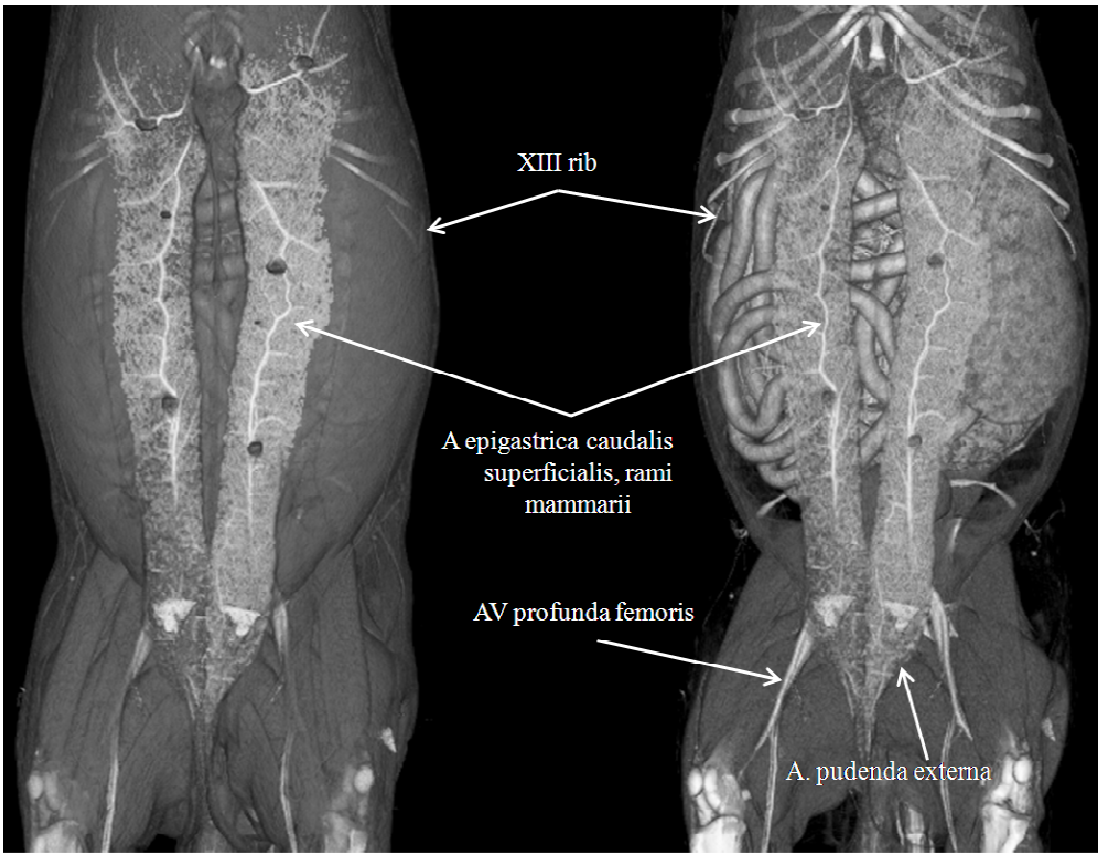

Fig. 32. Superficial vessels of the abdomen in a female dog.

4.3 CAUDAL VENA CAVA AND ITS TRIBUTARIES

The caudal vena cava (*V. cava caudalis*) begins about at the penultimate lumbar vertebra or more cranially by the convergence of the left and right common iliac veins (*V. iliaca communis*). It is the largest vessel of the abdomen. On the basis of its embryologic origin, the caudal vena cava can be customarily divided into four segments, pre-renal, renal, pre-hepatic, hepatic segment (Fig. 33).

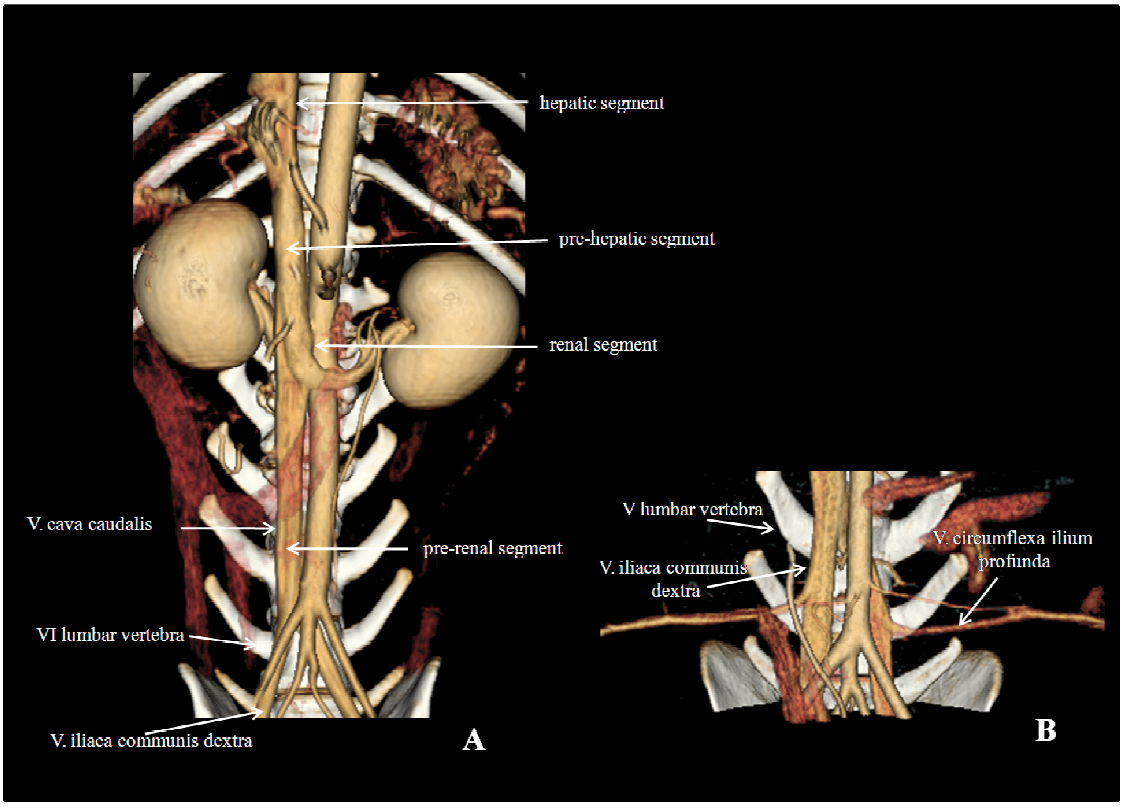

Fig. 33. **A.** Volume Rendering (VR) of the aorta and caudal vena cava in a dog, ventral aspect. **B.** VR image in another dog. The common iliac veins fuse at the level of the fifth lumbar vertebra. The *Vv. circumflexae ilium profundae*, are tributaries of the common iliac veins rather than from the caudal vena cava.

V. circumflexa ilium profunda, the deep circumflex iliac vein is the first tributary of the caudal vena cava. When the caudal vena begins cranial to the sixth lumbar vertebra, the deep circumflex iliac vein can discharge into the corresponding common iliac vein (Fig. 14, 17, 25, 31).

Vv. lumbales, lumbar veins, are segmental vessels that accompany the corresponding arteries (Fig. 34).

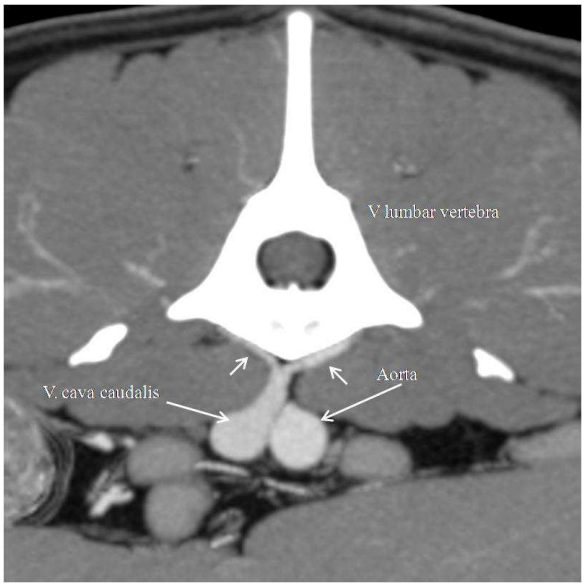

Fig. 34. Maximum Intensity projection transverse view at the level of the fifth lumbar vertebra. Note the *Vv. lumbales*, lumbar veins (arrows) draining into the pre-renal segment of the *v. cava caudalis*.

Renal Vein – The renal veins (*Vv. renales*) are paired tributaries of the caudal vena cava. Within the kidney the arcuate and interlobular veins accompany the corresponding arteries (Fig. 28,29)**.** The left renal vein receives the left gonadal vein (*v. testicularis sinistra* or *v. ovarica sinistra),* accompanying the corresponding arteries (Fig. 35). The contralateral gonadal veins join directly the caudal vena cava.

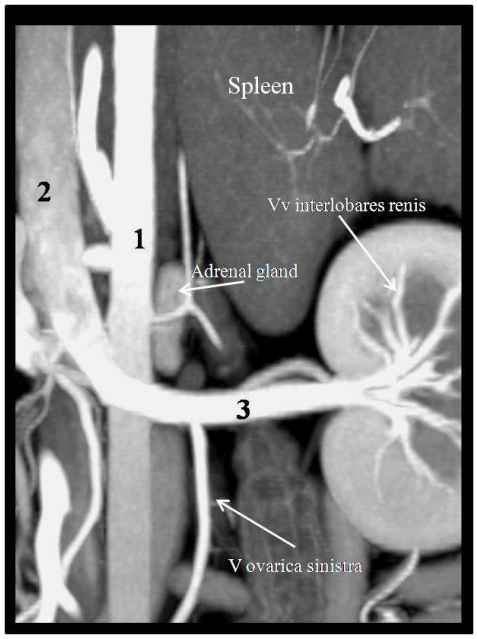

Fig. 35. Maximum Intensity Projection image in a female dog. 1. *Aorta abdominalis* 2. *V. cava caudalis* 3. *V. renalis sinistra*, receiving the left ovaric vein (*v. ovarica sinistra*).

Hepatic veins – The v*v. hepaticae* are situated within the liver parenchyma and join the caudal vena cava (hepatic segment) along its lateral and ventral surface. The major hepatic veins include the *v. hepatica dextra* for the right liver lobes, *v. hepatica media*, draining the quadrate lobe of the liver, and *v. hepatica sinistra* for the left part of the liver. Each hepatic vein receives numerous tributaries.

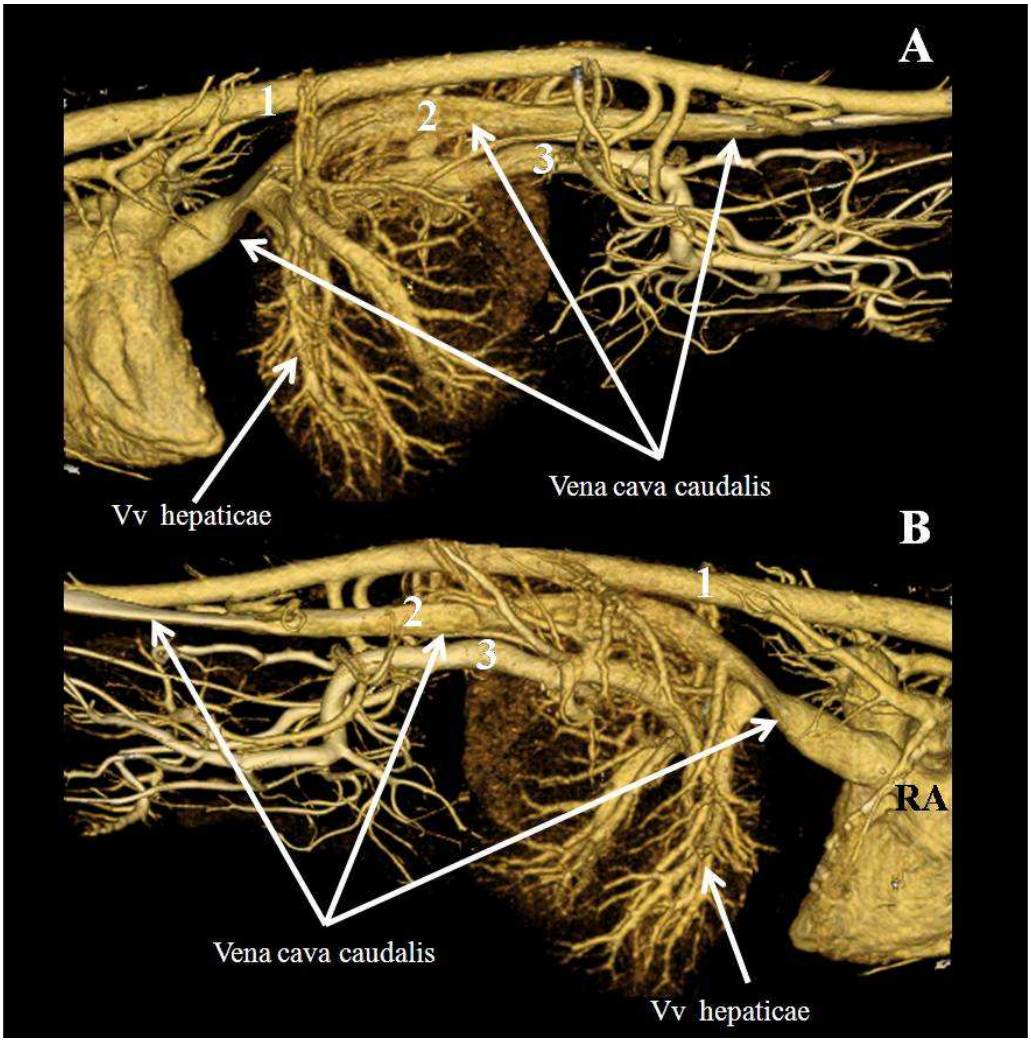

Fig. **36.** Volume Rendering images. **A.** Left lateral view. **B.** Right lateral view. 1. *Descending aorta* 2. *V. cava caudalis* 3.*V. portae.* RA: right atrium.

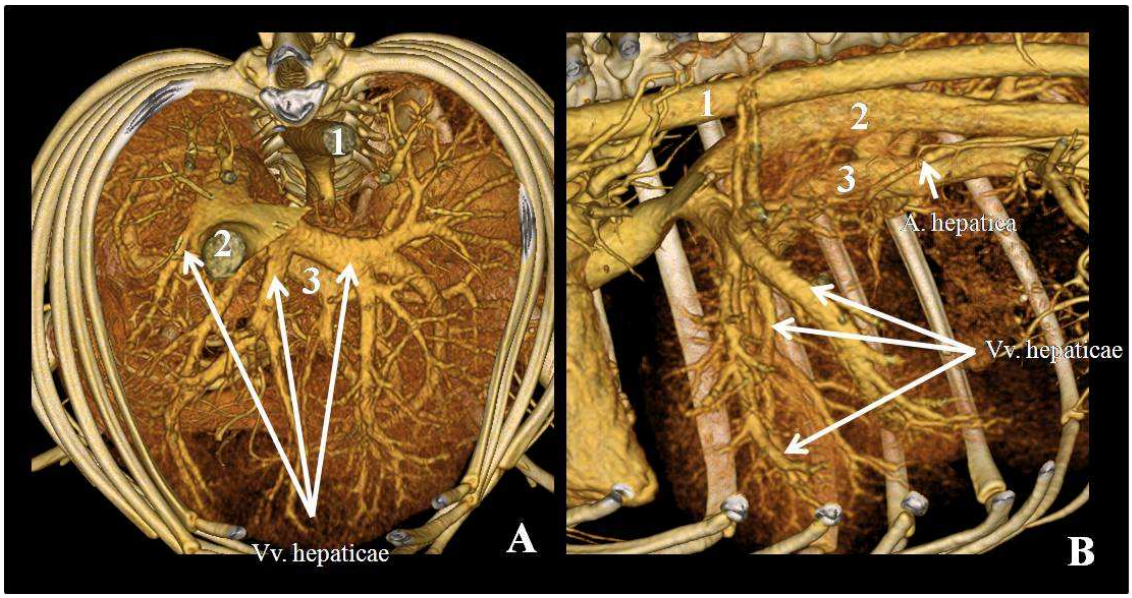

Fig. 37. Volume rendered images of the *Vv. hepaticae*. **A.** Cranial view. **B.** Left lateral view. 1. *A. thoracica* 2. *V. cava caudalis* 3. *V. portae*.

4.3 PORTAL SYSTEM

The *v. portae*, portal vein and its branches form the portal venous system which carries blood from abdominal viscera to the liver. It collects blood from the gastrointestinal tract (except the caudal segment of the rectum and the anal canal), spleen, and pancreas. Major tributaries of the venous portal system are: *vv. mesenterica cranialis et caudalis*, cranial and caudal mesenteric veins, draining most of the intestinal tract; *V. lienalis*, splenic vein, accompanying the corresponding artery; *v. gastrica sinistra*, which is a tributary of the splenic vein; *V. gastroduodenalis*, gastroduodenal vein; *v. gastrica dextra*, right gastric vein, *v. gastroepiploica*, and gastroepiploic vein.

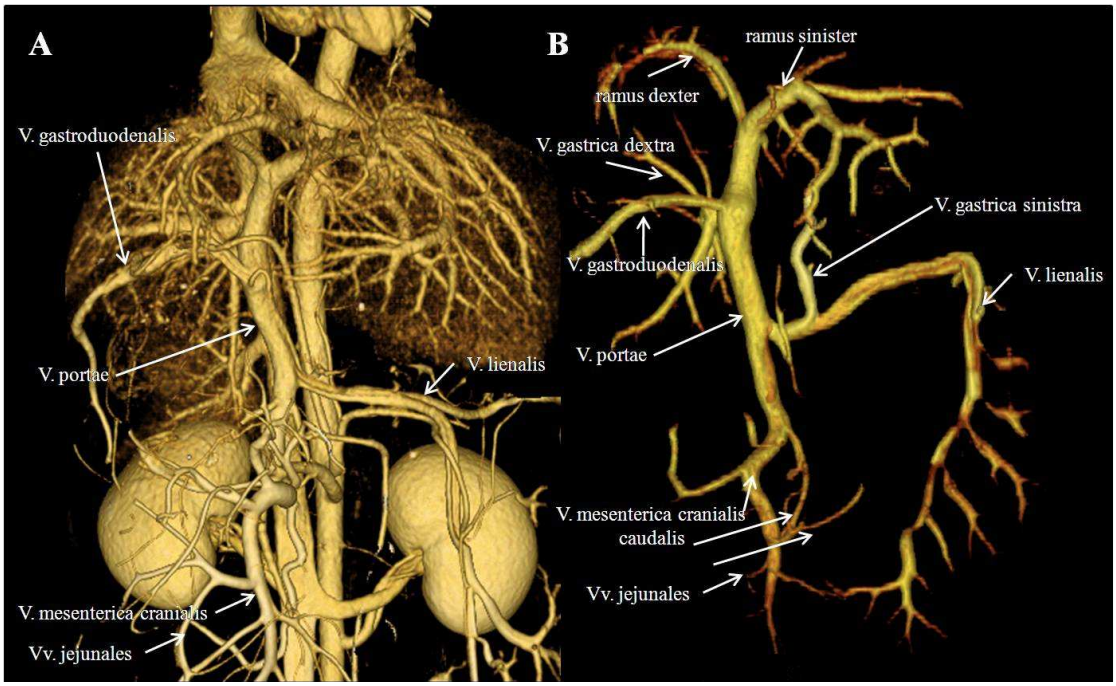

Fig. 38. A, B. Volume Rendering of the portal system. Ventral views.

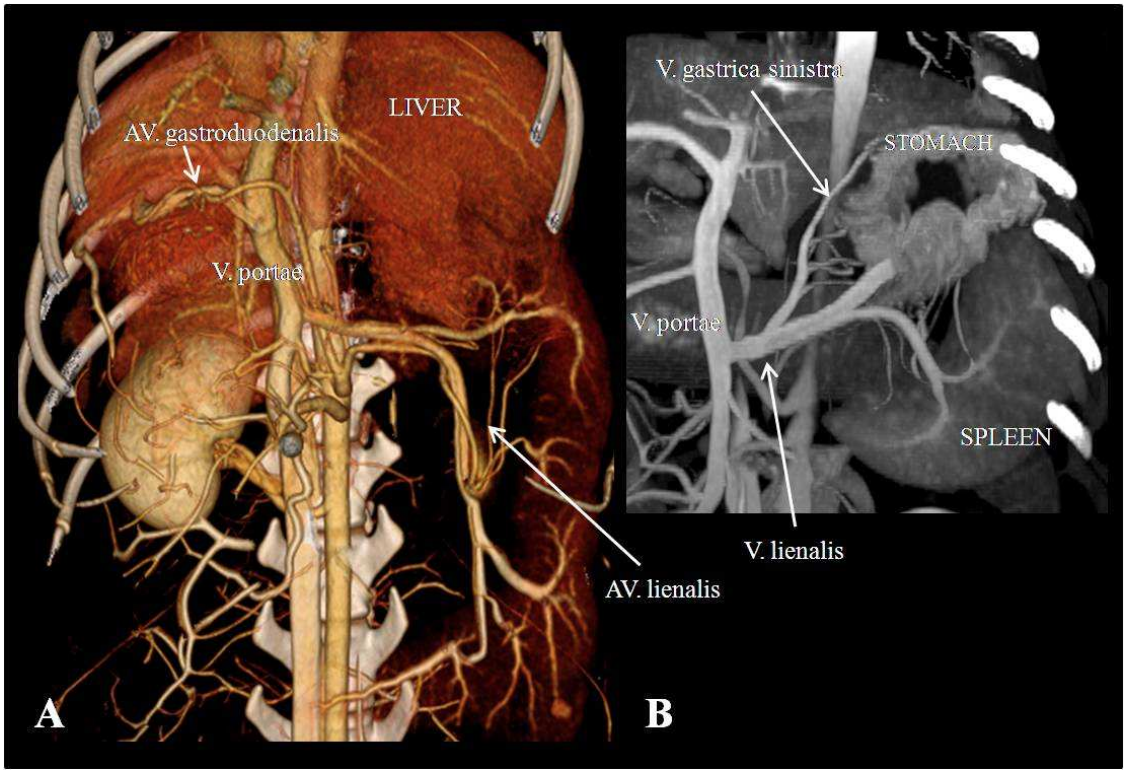

Fig. 39. A. Volume Rendering of the portal vein, ventral view. The left kidney has been removed for better visualization of the splenic vessels. **B**. Maximum Intensity Projection image.

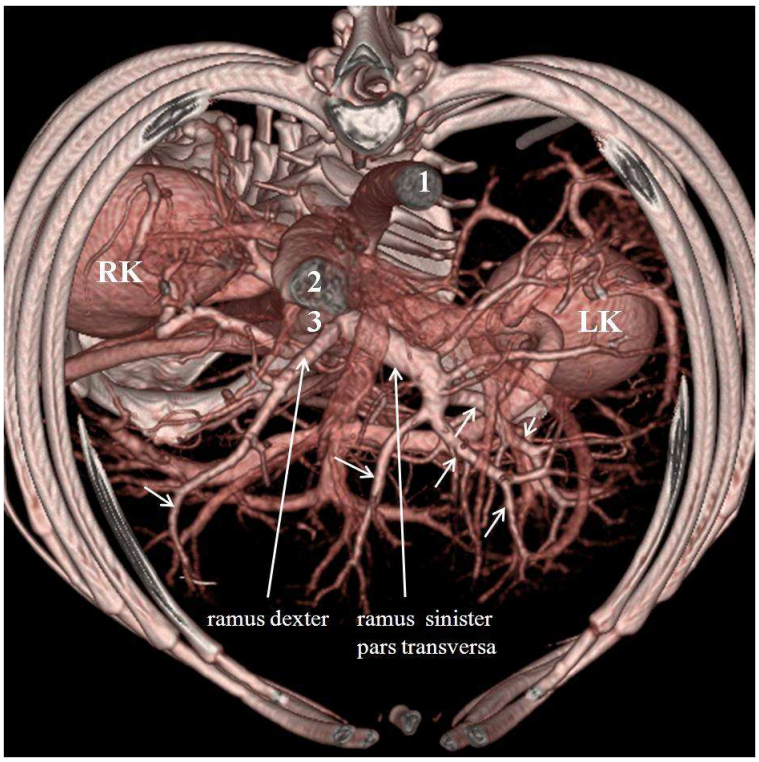

Fig. 40. Volume Rendering image, cranial view. 1. *A. thoracica*. 2. *V. cava caudalis*, post-hepatic segment. 3. *V. portae*. The two major intrahepatic branches of the portal vein are visible, as well as numerous small branches (arrows). RK: right kidney, LK: left kidney.

At the hepatic porta, the portal vein divides into the right and left portal vein branches. The right branch supplies the right division of the liver, including the right lateral lobe and the caudate process of the caudate lobe. The left branch of the portal vein supplies the central and left divisions of the liver, comprising the right medial, quadrate, left medial, and left lateral lobes. Small branches for the papillary process of the caudate lobe arise from the left branch.

CHAPTER 5

RESULTS *(part II)*

5.1 ANOMALIES OF THE AORTA AND ITS BRANCHES

Congenital anomalies involving the abdominal aorta were not found in this study. Congenital anomalies of branches of the abdominal aorta were detected in four dogs out of 1437 dogs that underwent abdominal multidetector row examination between January 2006 and October 2008 at San Marco Veterinary Clinic of Padua. These included two congenital communications between hepatic arteries and hepatic portal branches (arterioportal fistula), a connection between the left colic artery and left colic vein (arteriovenous fistula), and a dislocated lumbar artery. It arched and was situated at the right surface instead of at the left side of the caudal vena cava, causing stenosis of the caudal vena cava (Fig. 41).

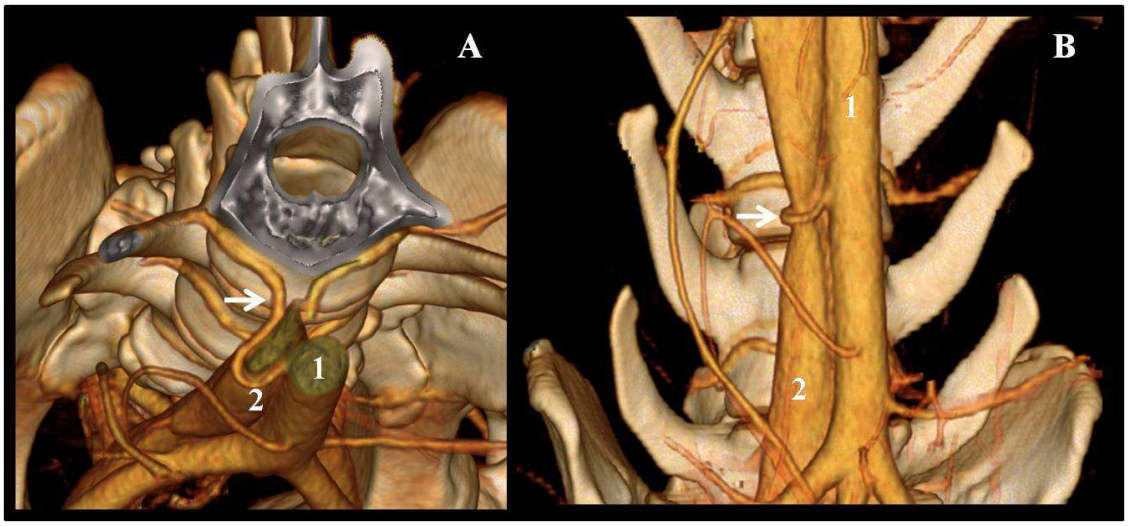

Fig. 41. Volume Rendering images of the lumbar segment of the abdominal aorta and the pre-renal segment of the caudal vena cava in a dog. Note the penultimate right lumbar artery that is situated at the right side of the caudal vena cava, causing stenosis of the vessel (arrow). 1. *Aorta abdominalis.* 2. *V. cava caudalis*.

5.2 ANOMALIES OF THE CAUDAL VENA CAVA

"Double caudal vena cava"

Twelve of 1437 dogs included in this study had the persistence of the left supracardinal vein. Represented breeds were: Poodle (*n*=4), Mongrel (*n*=3), West Highland White Terrier (*n*=2), Pinscher (*n*=1), Yorkshire Terrier (*n*=1), Shih-Tzu (*n*=1). Four were males and eight females. The median age was 70 months (from 16 to 158 months), the median body weight 4.6 kg (ranging from 2 to 9 kg).

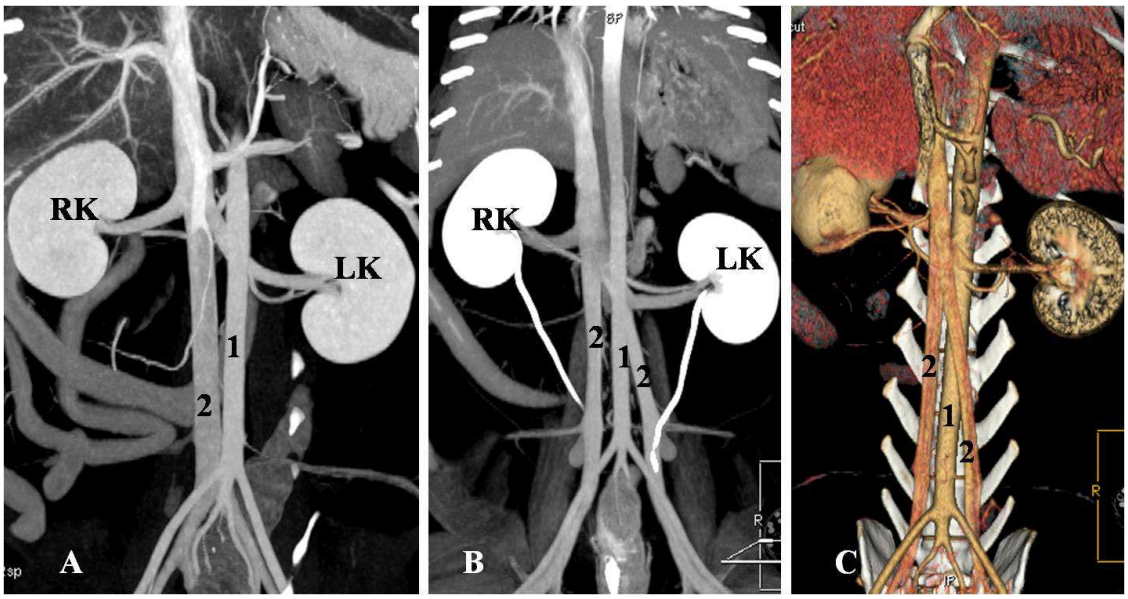

Fig. 42. A. Maximum Intensity Projection image in a 5-years-old, 8 Kg, male Mongrel dog with normal single caudal vena cava (2). **B.** Maximum Intensity Projection in a 11-years-old, 6 Kg, female Mongrel dog with "double vena cava" (2, 2). The left renal vein drains into the left-sides caudal vena cava. **C.** Volume rendered image in a 3-years-old, 3 Kg female, Yorkshire Terrier dog with duplication of the pre-renal segment of the caudal vena cava. The left renal vein drains into the caudal vena cava, just after the fusion of the two supracardinal veins. 1. *Aorta abdominalis*, 2. *V. cava caudalis*. RK: right kidney, LK: left kidney.

In two dogs, this anomaly was associated to anomalies of the portal system (portosystemic shunts).

"Azygous continuation of the caudal vena cava"

In the present study we found three dogs in which the caudal vena cava continued directly into the azygos veins. They were 2 males and 1 female of different breeds. The median age was 21 months, ranging from 2 to 148 months, and the median body weight was 16 kg, from 1 to 28 kg. In all cases, this anomaly was associated with other congenital anomalies. The first dog had *situs inversus abdominalis*, with the stomach and spleen on the right side, polysplenism, and azygous continuation. The portal trunk of this dog was situated on the left side. It was interrupted and there was a portosystemic shunt between the portal vein and the renal segment of the caudal vena cava (Fig. 43,44).

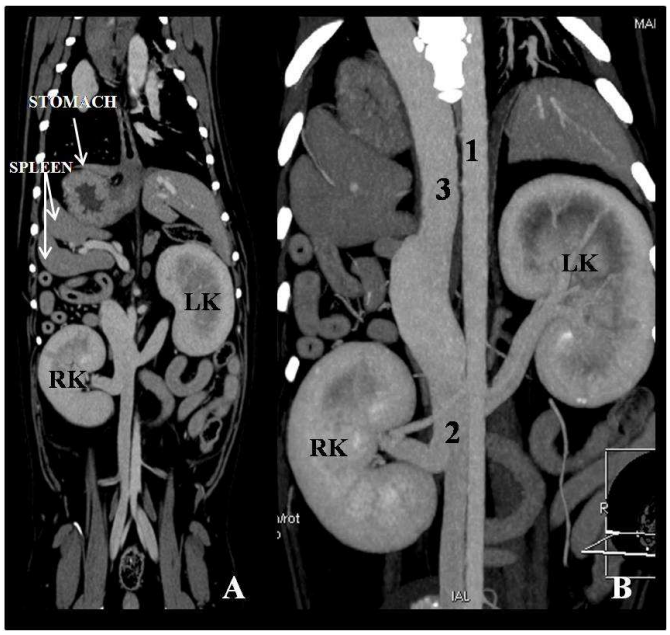

Fig. 43. Eleven-months-old, 28 Kg, male Mongrel dog with *situs inversus abdominalis*, portosystemic shunt, and azygos continuation of the caudal vena cava. **A.** Maximum Intensity Projection image showing the inversion of the abdominal viscera. Note the stomach and two spleens on the right side. The right kidney (RK) is located more caudally than the left kidney (LK). **B.** Maximum Intensity Projection showing the azygous continuation of the caudal vena cava. 1. *Aorta descendens* 2. *V. cava caudalis* 3. *V. azygous*.

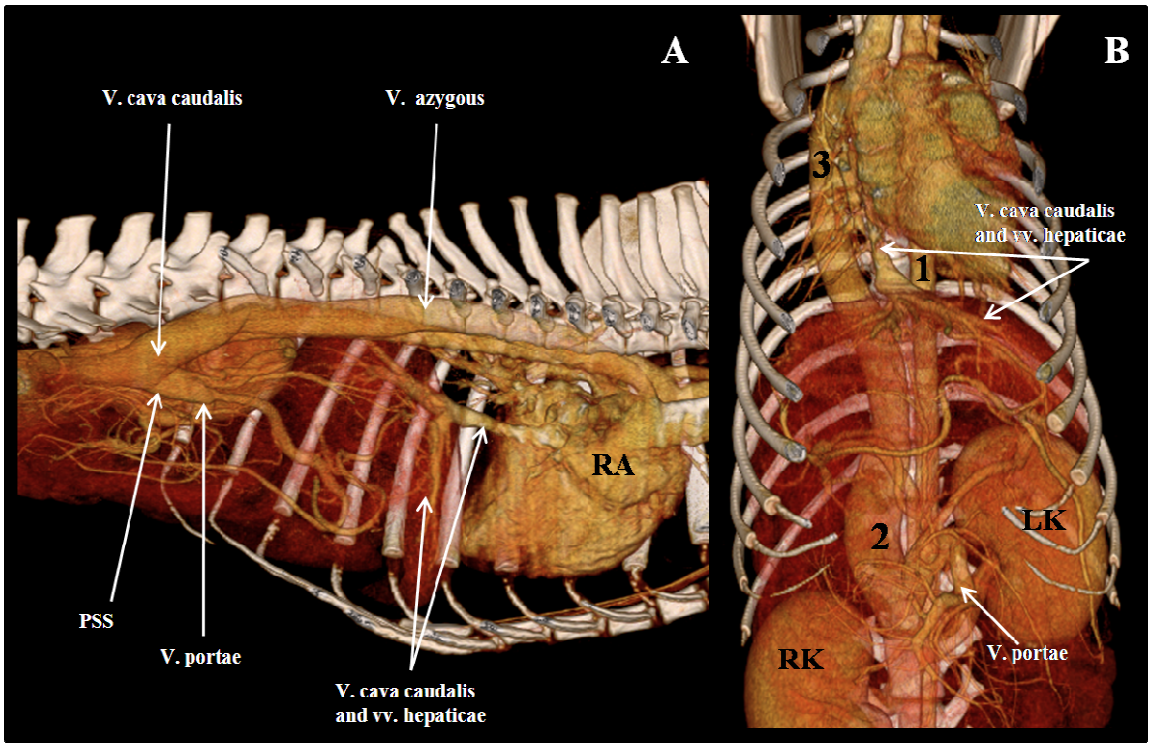

Fig. 44. Eleven-months-old, 28 Kg, male Mongrel dog. **A.** Volume rendered image, right lateral aspect**. B.** Volume rendered image, ventral aspect. Note that *v. portae* inserts into the pre-hepatic segment of the *v. cava caudalis* (PSS in A). The *v. cava caudalis* is enlarged. It deviates dorsally and joins the azygos vein. The enlarged azygos vein empties normally into the cranial vena cava which enters the right atrium (RA in A). The post-hepatic segment of the caudal vena cava and the *vv. hepaticae* are normally developed. 1. A*orta. thoracica* 2. *V. cava caudalis* 3. *V. azygous*.

The second dog had a congenital interruption of both the caudal vena cava and the portal vein, with a portosystemic shunt and azygous continuation (Fig. 45).

In the third dog the caudal vena cava coursed dorsal to the abdominal aorta, between the aorta and the spine. It was directly connected to the azygos vein, while its intrathoracic segment was very narrow and the. Additionally, the left gastric vein was shunted to the azygos vein (Fig. 46).

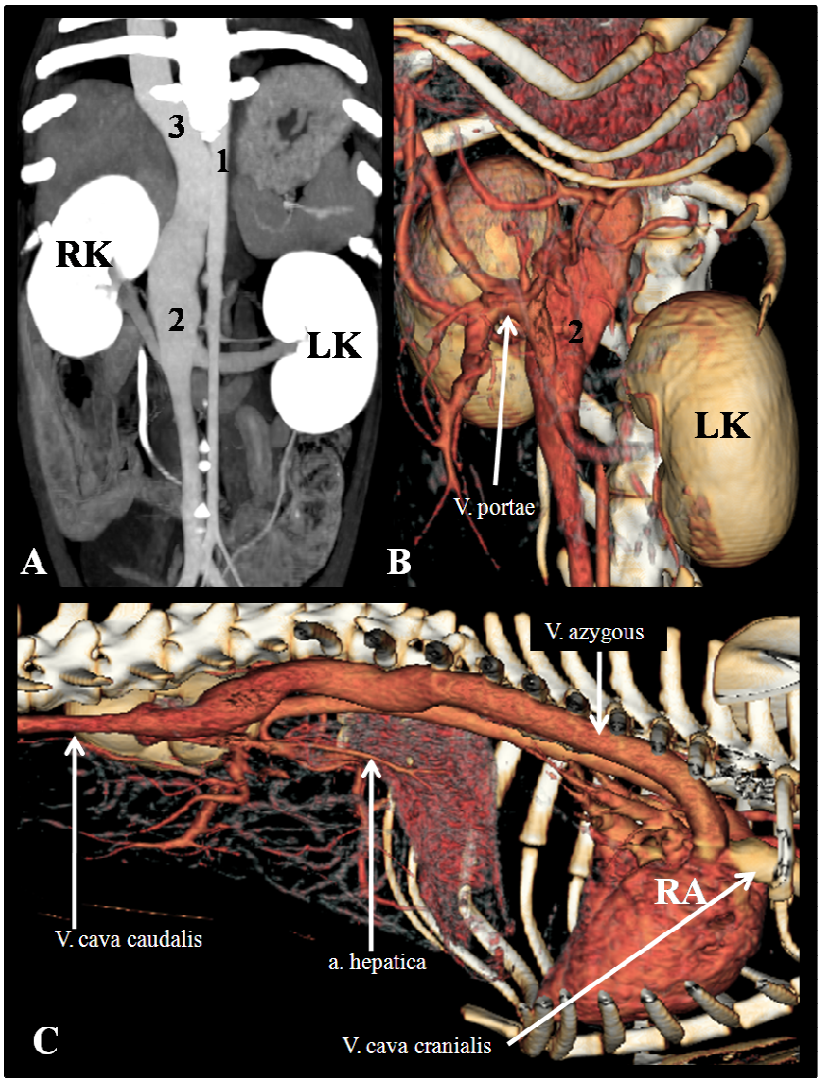

Fig. 45. Two-months old, 1kg, Jack Russel Terrier with congenital interruption of both the caudal vena cava and the portal vein, with azygos continuation of the caudal vena cava and portosystemic shunt between the portal vein and the pre-hepatic segment of the caudal vena cava. **A.** Maximum Intensity Projection showing the azygos continuation of the caudal vena cava. 1. *Aorta thoracica* 2. *V. cava caudalis* 3. *V. azygous*. **B.** Volume rendered image. Ventro-oblique aspect, showing the portal vein shunting into the pre-hepatic segment of the caudal vena cava. (2) **C.** Volume Rendered image, right lateral view. The pre-renal segment of the caudal vena cava is narrow. At the level of the kidneys (not visible) the caudal vena cava curves dorsally and joins the azygos vein. The enlarged azygos vein courses normally to the cranial vena cava and hence into right atrium. RK: right kidney, LK: left kidney. RA: right atrium.

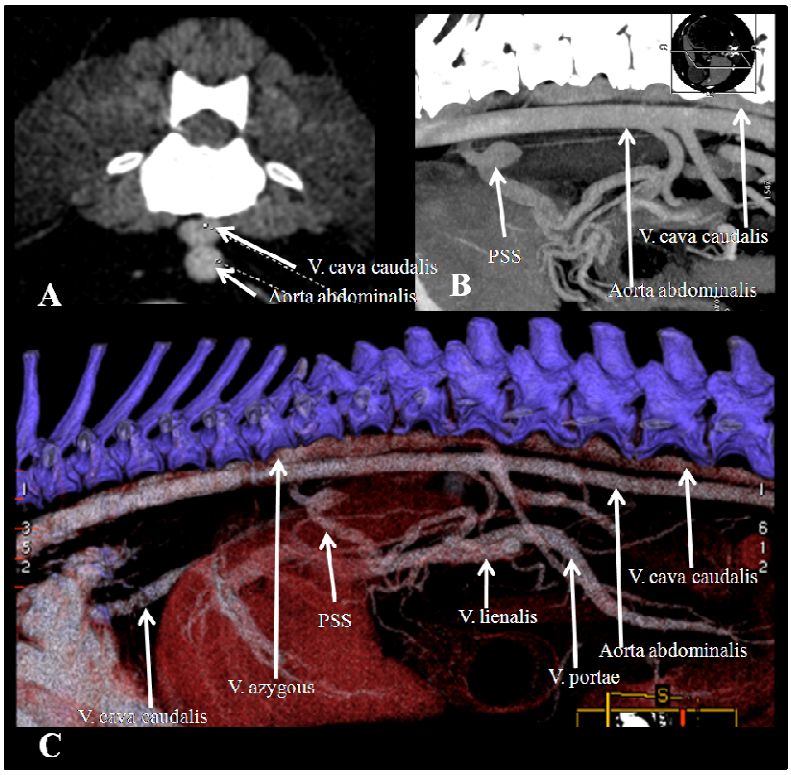

Fig. 46. Five-years-old, male Cocker Spaniel dog. **A.** 2D transverse view showing the *v. cava caudalis* coursing dorsal to the *aorta abdominalis*. **B.** Maximum Intensity Projection, sagittal view. Note the *v. cava caudalis* just ventral to the spine. The *Aorta abdominalis* courses ventral to the caudal vena cava. A tortuous shunting vessel (PSS) connects the left gastric vein (not visible) and the azygos vein. **C.** Volume rendered image. Left aspect. PSS, portosystemic shunt between the left gastric vein and the azygos vein. Note that the post-hepatic segment of the caudal vena cava is normally represented.

5.3 ANOMALIES OF THE PORTAL SYSTEM

Fourty-one dogs of the 1437 examined dogs had a congenital portosystemic shunt. *V. portae*, the portal vein, or one of its tributaries were connected to the caudal vena cava (n= 36) or to the azygos vein (n=5). Twenty-one dogs were males and twenty were females. The median age was 12 months (from 2 to 121 months), and the median body weight was 6 Kg (from 1 to 37), with several breeds represented.

5.3.1 PORTOAZYGOS SHUNT

Five dogs presented connections between one vessel of the portal system and the azygos vein:

- From *v. gastrica dextra* to *v. azygous* (Fig. 47)
- From *v. gastrica sinistra* to *v. azygous* (Fig. 48)
- From *v. lienalis* to *v. azygous* (Fig. 49)

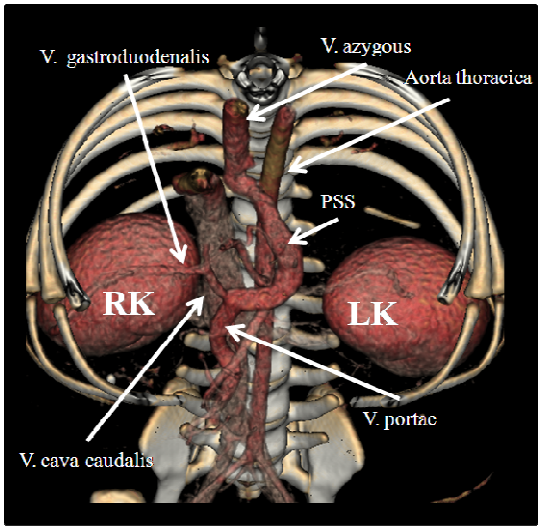

Fig. 47. Volume rendered image in 10 months-old, Mongrel, female dog. Cranial-oblique view. RK: right kidney, LK: left kidney. PSS, portosystemic shunt between the right gastric vein and the azygos vein.

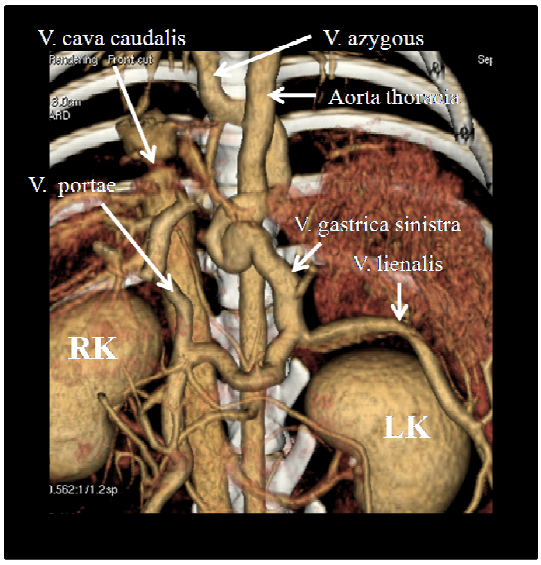

Fig. 48. Volume rendered image, ventral aspect, in a 4-months old, female, Pug dog. Note the enlarged and tortuous vessels from *v. gastrica sinistra* shunting with the azygos vein.

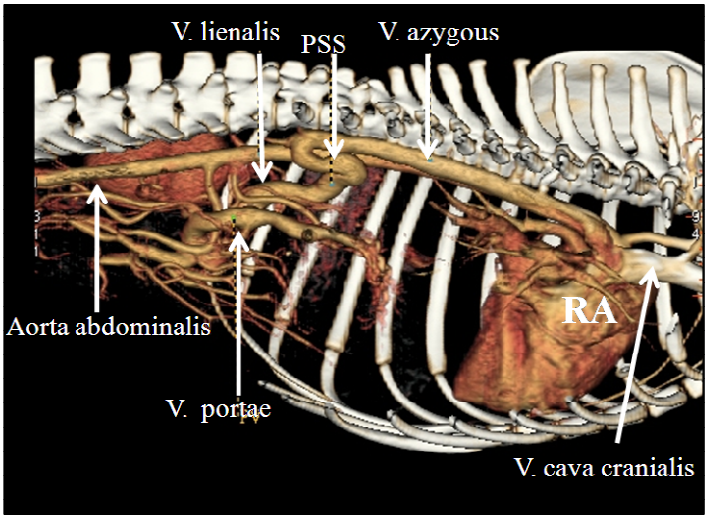

Fig. 49. Volume rendered image, right lateral aspect in a 2 months-old, male Pug dog. Note a large and tortuous vessel (PSS) arising from the *v. lienalis* that courses dorsally, describes some loops and then joints to the *v. azygous*. The enlarged azygous vein normally courses to the right atrium (RA).

5.3.2. PORTOCAVAL SHUNT

Thirty-six dogs had a communication between the *v. portae*, portal vein, or one tributary of it and the *v. cava caudalis*, caudal vena cava or to one of its tributaries. We present here some examples describing the origin, course, and termination of the shunting vessel.

- *V. porta*, portal vein -*v. cava caudalis*, caudal vena cava, fusion (Fig. 50).
- From *v. gastrica dextra* to the *v. cava caudalis*, pre-hepatic segment, with short or long shunting vessel (Fig. 51,52).
- From *v. gastrica dextra* to the *v. cava caudalis*, hepatic segment (Fig. 53).
- From *v. gastrica sinistra* to the *v. cava caudalis*, post-hepatic segment (Fig. 54, 55).
- From *ramus sinister* of the *v. portae* to *v. hepatica sinistra* (Fig. 56, 57).

- From *ramus sinister* of the *v. portae*, branches of the left portal branch for central hepatic segments, to the *v. cava caudalis*, caudal vena cava, hepatic segment (Fig. 58).

- From *ramus dexter* of the *v. portae* to the *v. cava caudalis*, caudal vena cava, hepatic segment (Fig. 59, 60).

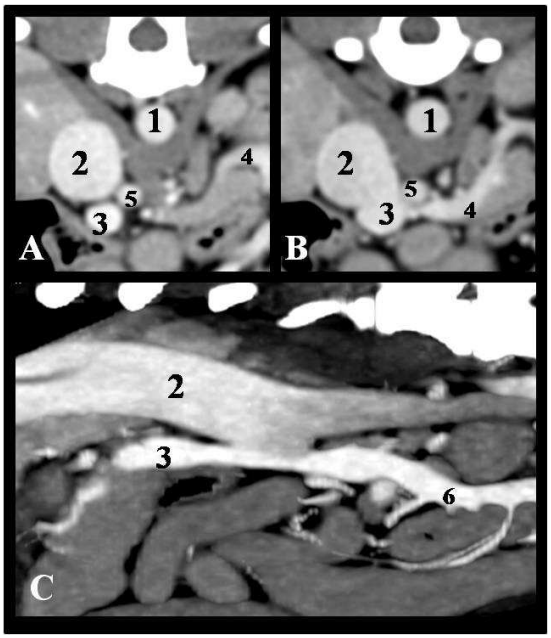

Fig. 50. Maximum Intensity Projection of the *v. portae*, portal vein, fusion with the v. cava caudalis, caudal vena cava, pre-hepatic segment. **A.** Transverse view at the level of T12. 1. *aorta thoracica* 2. *V. cava caudalis* 3. *V. portae* 4. *V. lienalis* 5. *A. hepatica* **B.** Transverse view, 1.2 mm caudal to the previous image. Note the fusion between the *v. cava caudalis* (2) and the *v. portae* (3). **C.** Left sagittal view showing the fusion between the *v. cava caudalis* (2) and *v. portae* (3). 6. *V. mesenterica cranialis*.

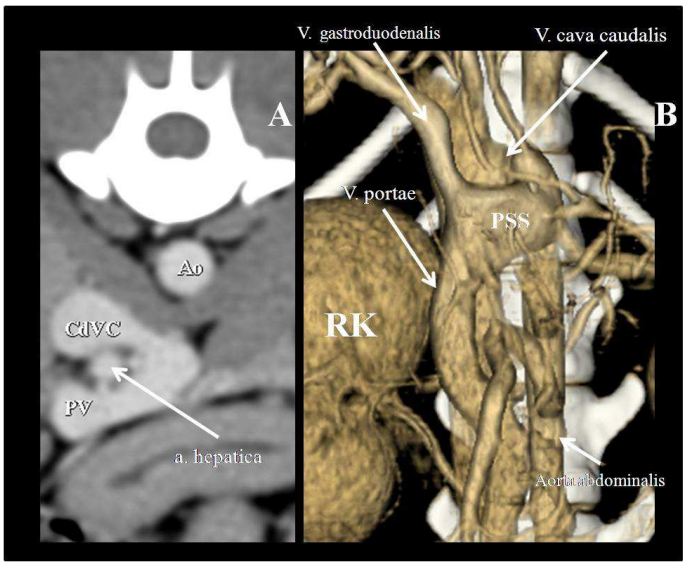

Fig. 51. A. Transverse view at the level of T12 in a 9-months-old, 5 Kg, female Beagle dog with portosystemic shun (PSS) between the *v. gastrica dextra* and the *v. cava caudalis*, pre-hepatic segment. **B.** Volume rendered ventral view of the previous dog.

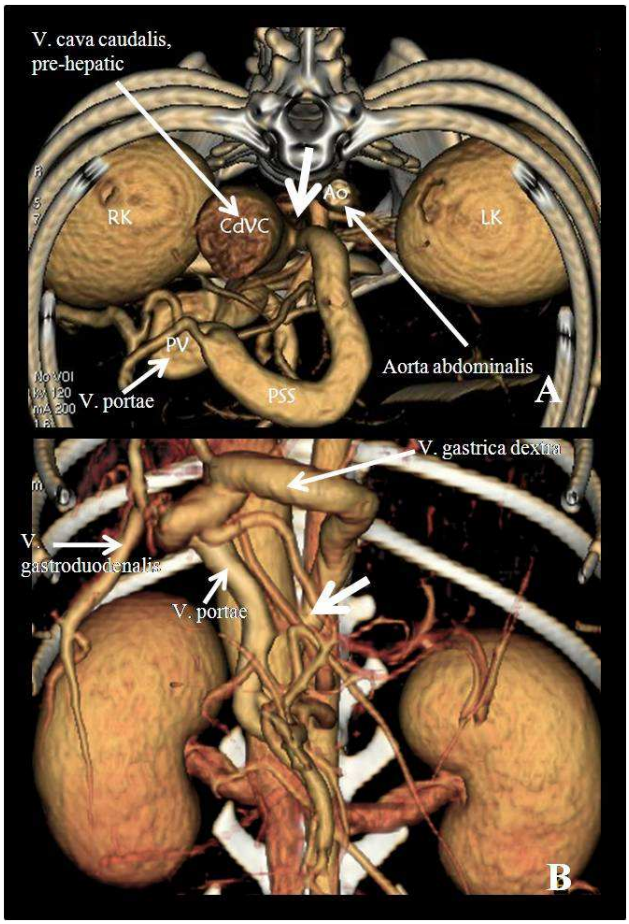

Fig. 52. Volume rendered images of a 5-years-old, male, Bolognese with portocaval shunt. **A.** Cranial view. Note the large shunting vessel (PSS) arising from the right aspect of the *v. portae* (PV) to the pre-hepatic segment of the *v. cava caudalis* (CdVC) (big arrow). RK: right kidney, LK: left kidney. **B.** Ventral view showing the course of the shunting vessel from the *v. portae* to the *v. cava caudalis*, left lateral aspect of the pre-hepatic segment (big arrow).

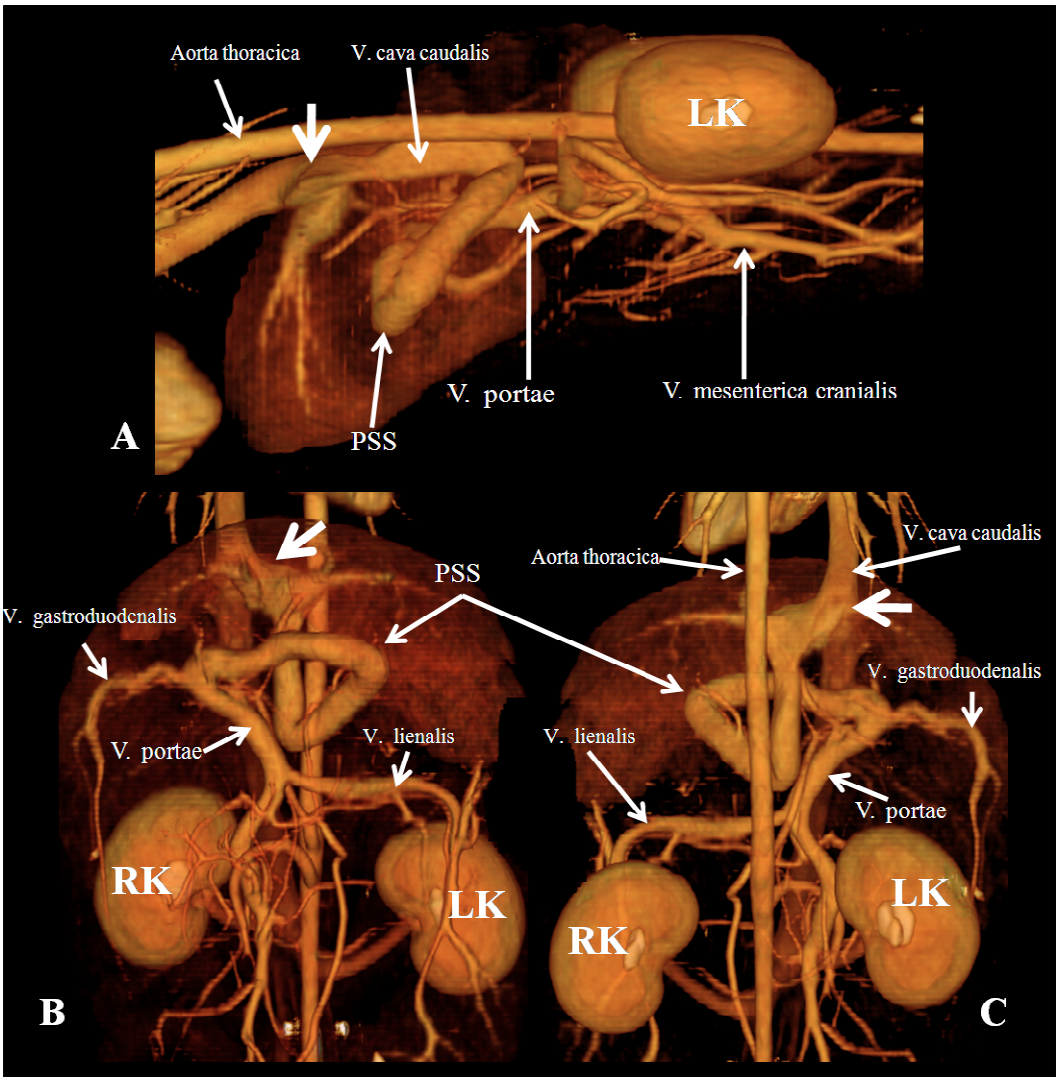

Fig. 53. Volume rendered images in a 1-year-old, male, Shih-Tzu with portacaval shunt. **A.** Right lateral view. **B.** Ventral view. **C.** Dorsal view. Note as the large shunting vessel (PSS) from right gastric vein courses in a caudal-dorsal direction; it suddenly curves cranially and courses just ventral to the aorta, to the right side, between the liver lobes. Then enter the liver and ends into the caudal vena cava, together with the left hepatic vein (big arrow). The shunting vessel has an extra-hepatic course and intra-hepatic end.

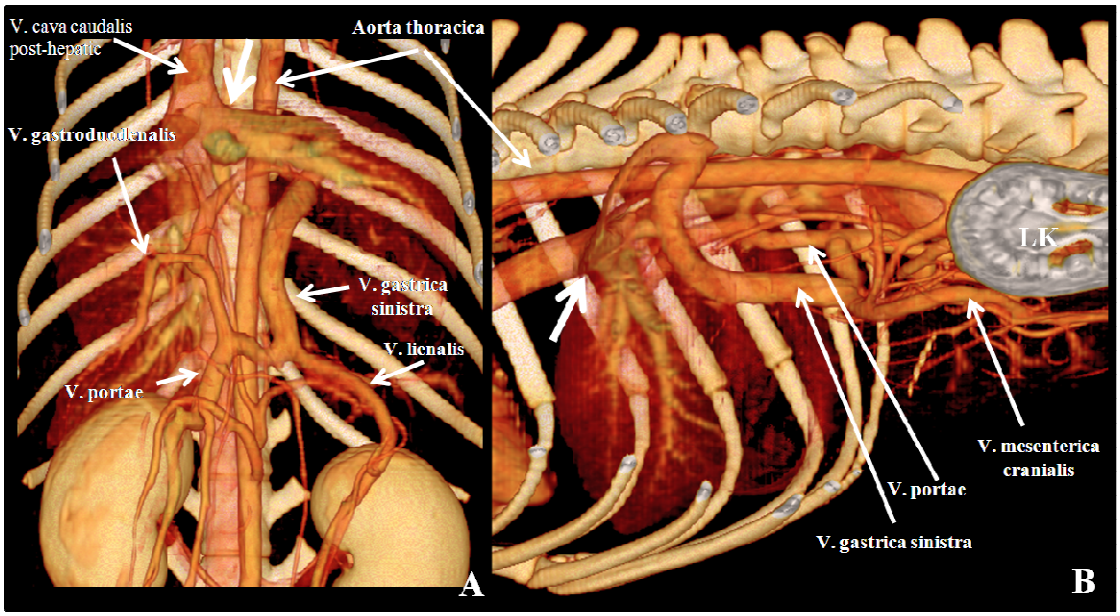

Fig. 54. Volume rendered image of a 2-years-old, male, Dachshund with portocaval shunt. **A.** Ventral view. Note a large shunting vessel from *v. gastrica sinistra* and the *v. cava caudalis*, post-hepatic segment (big arrow). **B.** Left lateral view. Note the large left gastric vein that courses cranially and dorsally, on the dorsal surface of the liver, and ends to the left lateral aspect of the initial tract of the *v. cava caudalis* post-hepatic segment. The course of the shunting vessel is completely extrahepatic (see also Fig. 55).

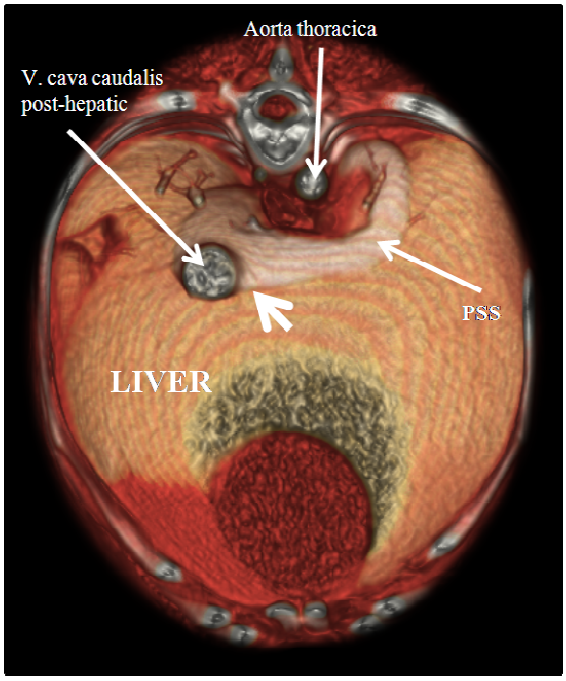

Fig. 55. Volume rendered image of the dog of Fig. 54. Cranial view at the dome of the diaphragm. Note the shunting vessel (PSS) that courses on the dorsal surface of the liver, to the left side, and enter the first tract of the *v. cava caudalis*, post-hepatic segment.

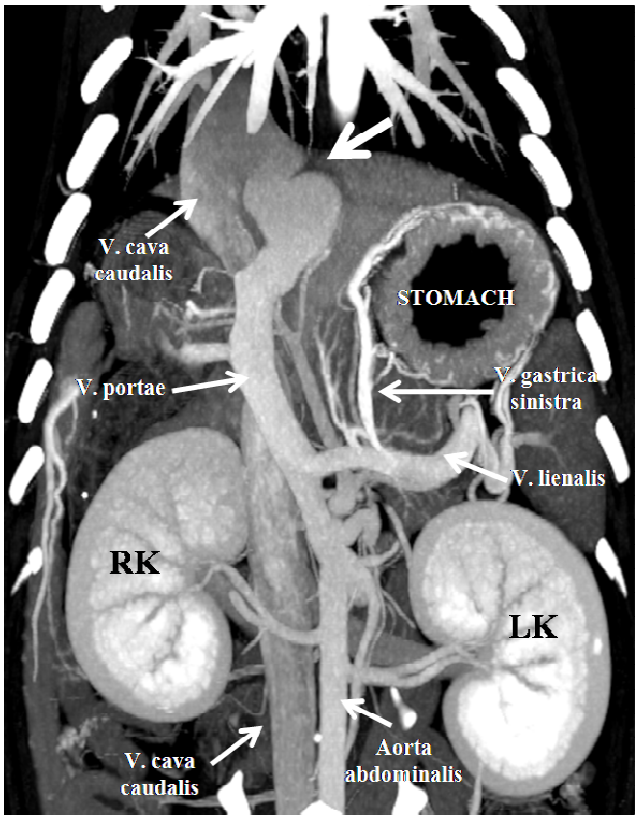

Fig. 56. Maximum Intensity Projection of a 1-year-old, female, Labrador Retriever with portocaval shunt. Ventral view. RK: right kidney, LK: left kidney. Note the large vessel that from *ramus sinister* of *v. portae*, left intrahepatic branch of the portal vein, shunting to *v. hepatica sinistra*, left hepatic vein (consistent with persistence of *ductus venosus*).

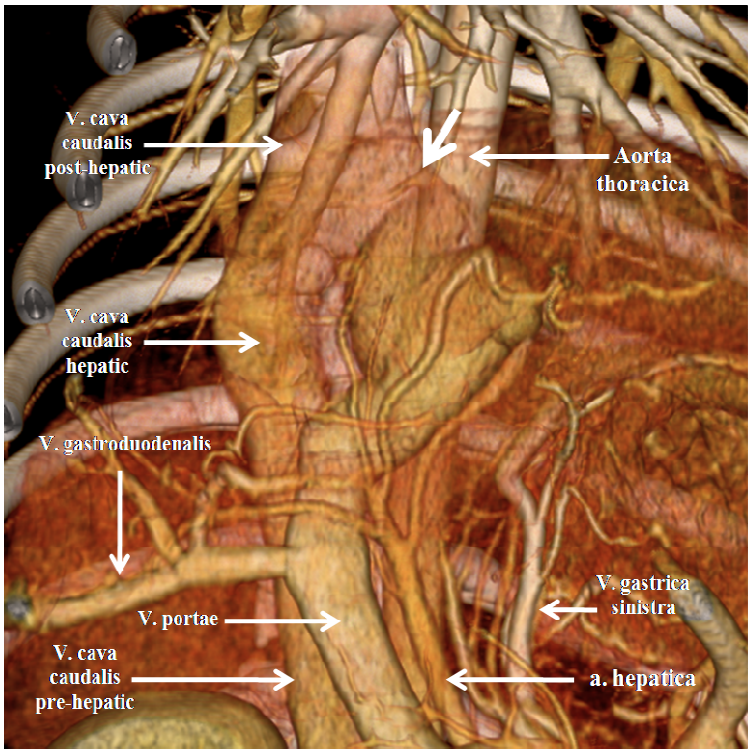

Fig. 57. Volume rendered image of the same dog of Fig. 56. Ventral view. The large *ramus sinister* of *v. portae* shunts into the left hepatic vein (big arrow). Note the aneurismal dilatation before shunting.

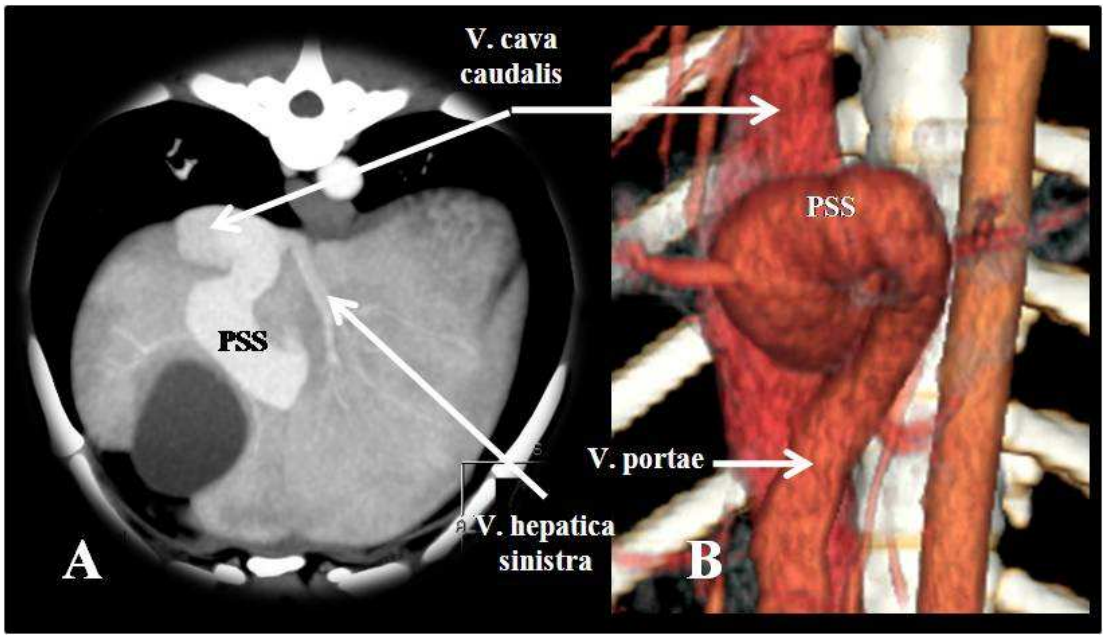

Fig. 58. One-year-old, 3 Kg, female, Mongrel dog with intrahepatic portocaval shunt. **A**. Maximum Intensity Projection transverse image. Note the large shunting vessel (PSS) reaching the caudal vena cava. **B.** Volume rendered image, ventral aspect, showing the shunting vessel (PSS) between a central branch of the left major branch of the *v. portae* and the *v. cava caudalis*. The portal branch is dilated at the point where it drains into the caudal vena cava.

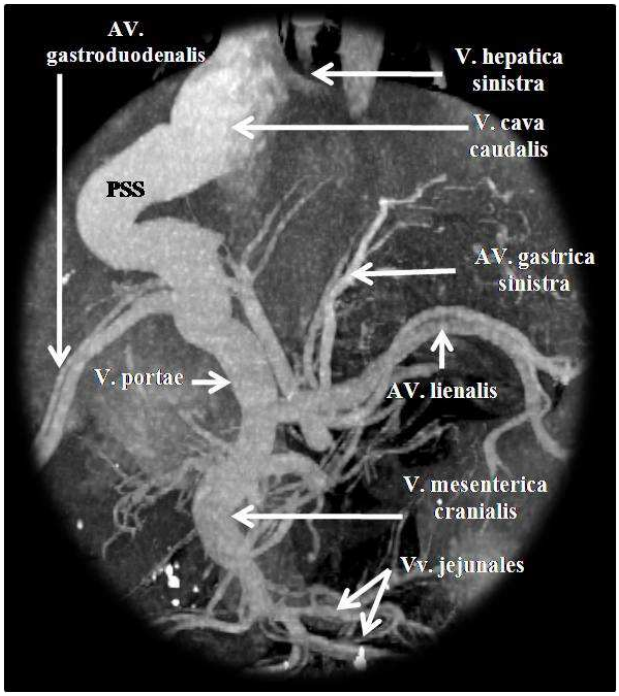

Fig. 59. Maximum Intensity Projection image of a 4-months-old, male, Bernese dog with a shunt between *ramus dexter* of *v. portae* and *v. cava caudalis*, intrahepatic segment (PSS).

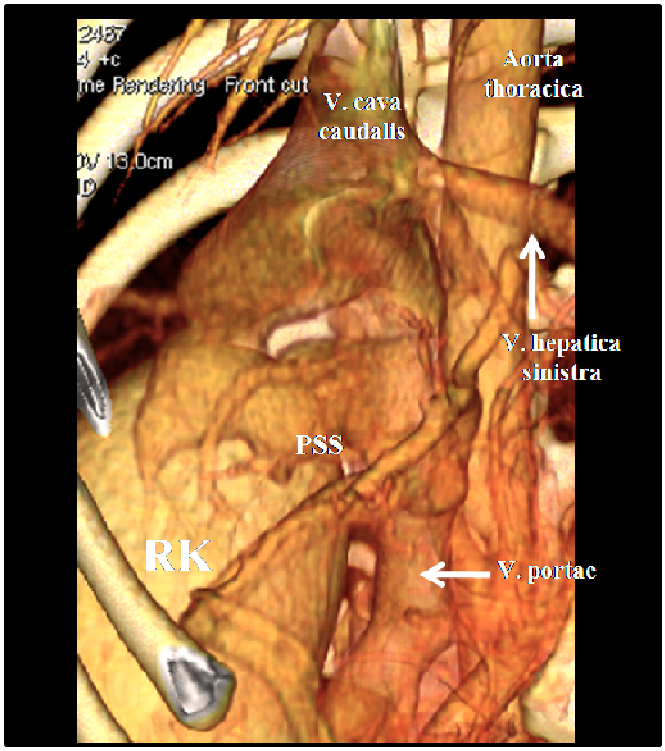

Fig. 60. Volume rendered image of a 10-months-old, 13 Kg, male, Mongrel dog with intrahepatic portocaval shunt. RK: right kidney. Note the large and strange shaped vessels (PSS) from *ramus dexter* of the *v. portae* to the *v. cava caudalis*.

CHAPTER 6

DISCUSSION

Third and fourth generation scanners and helical computed tomography (CT) have been described in veterinary medicine for studying normal canine cross-sectional anatomy of the abdomen. (FEENEY et al. 1991, SMALLWOOD et al. 1992, SMALLWOOD et al. 1993, TEIXEIRA et al. 2007). Recently, helical CT has been reported for normal canine portal and hepatic vasculature, and portosystemic shunt assessment (ZWINGENBERGER and SCHWARZ 2004, ZWINGENBERGER et al. 2005a). We first described the use of multidetector-row computed tomography (MDCT) combined with three-dimensional post-processing techniques for extrahepatic portosystemic shunt assessment in dog (BERTOLINI et al. 2006b). Multidetector row computed tomography represents a breakthrough in computed tomography technology, providing a substantial gain in performance in comparison to conventional and helical computed tomography. In the first part of this work we presented MDCT-images for describing the normal vascular abdominal anatomy in dogs, creating three-dimensional (3D) maps from original volumetric data sets.

The most immediate issue of the present study is that MDCT allows detailed *in vivo* imaging of the abdominal vasculature in dog. Normal vasculature, variants, and anomalies can be easily recognized. In clinical veterinary science training as well as in veterinary practice, an understanding of anatomy is essential. In traditional anatomy teaching, superficial anatomy is stressed, but little is taught about the actual three-dimensional (3D) position of structures, even though this is especially important in clinical practice. Understanding the 3D position of vessels *in vivo* is difficult, because this knowledge has been generally handed down by way of dissections or two-dimensional angiography. The results reported here (Chapter 4, Results, part I) prove that

MDCT can be an useful tool for educational support, using post-processed volume rendered images from living animals instead of specimens. Furthermore, MDCT angiography provides accurate mapping of individual venous and arterial variations, sometimes demonstrating vascular patterns not described in the textbooks of anatomy. Knowledge of individual variations is important for pre-operative imaging of the abdomen. MDCT can then provide additional detailed information in patients with radiographic or ultrasonography patterns of abdominal disorders.

Images included in this project are of patients that underwent multidetector row examination of the abdomen for clinical purposes. This means that detailed images can be routinely obtained choosing appropriate protocols and post-processing techniques. The goal of volumetric imaging with MDCT should be to acquire data sets with isotropic or near isotropic resolution whenever possible. Moreover, proper delivery of iodinated contrast medium is essential. In fact, most of the advantages of MDCT angiography can be nullified by improper contrast medium administration. The fast acquisition of data possible with MDCT has many benefits. It allows substantial anatomic coverage in few seconds obtaining separate arterial and venous phases, but, at the same time, it could be possible to completely miss or outrun the contrast bolus. The understanding of contrast medium kinetics in patients is then essential. The amount and concentration of the medium, rate of injection, and timing of injection are important variables for angiographic studies, as well as specific patient's factors such as the individual cardiac output (FISHMANN 2001, FLEISHMAN 2003, FLEISHMAN 2005, KISHIMOTO et al. 2008) This study includes patients from 1 to 84 kg , under general anesthesia, with extremely variable individual conditions. This made it difficult to obtained uniform

results. In the present study both angiographic and non-angiographic studies have been included. Angiographic studies provided excellent results, in terms of image quality, allowing fast and highly detailed vascular maps in post-processing. Results from non-angiographic studies are considered satisfactory as well, even if they were more time-consuming in post-processing for enhancing the vessels while discarding other structures, or just to remove the background noise. Acquiring the proper hardware data set is essential, but it is only the first step of the process for vascular mapping. Both Maximum Intensity Projection (MIP) and Volume Rendering (VR) were used here for generating comprehensive vascular images. Volume Rendering images always accurately displayed the vessels, especially on the arterial and portal phase-dominant images. VR also provides both the definition and the color display of the bone and parenchyma surrounding the vessels, which may contribute to a more comprehensive understanding of the anatomic relationships. In MIP images the 3D relationships among the structures in the display is not visible. However, MIP allows the visualization of smaller branches with less work than is required with VR. It is important to remember that volume rendering is an interactive technique. On the post-processing workstation we create a true 3D object that we can rotate and view from any angle. This facilitates the understanding and interpretation of the complicated vascular anatomy. However, full and accurate interpretation generally requires combining review of thin section 2D images (multiplanar reformatted images, MPR) with some type of volume techniques (MIP and/or VR).

The second part of our results (Chapter 5, Results, Part II) describes some congenital anomalies of the abdominal vessels. Over the course of this study, we did not identify any

anomalies of the abdominal aorta, nor have they been reported in veterinary literature. Several reports describe congenital abnormalities of the thoracic aorta, though there are no descriptions of congenital defects of the abdominal aorta in dog. In humans, congenital abdominal aorta aneurysm, hypoplasia of the descending aorta are rare anomalies described in infants (MEHALL et al.2001, TERRAMANI et al. 2002). Of four dogs with congenital abnormalities of the arterial system, two dogs had an intrahepatic congenital arterioportal fistula. CT is recognized as valuable tool for the diagnosis of this condition (MOORE and WHITING 1986, SZATMARI .et al. 2000, ZWINGERBERGER at al. 2005b).

Congenital anomalies of the caudal vena cava have been described in dog, and have been here reported as well. We observed the "double caudal vena cava" in 12 of 1437 dogs included in this study (0.83%). This result is consistent with other previous reports. The right-sided pre-renal segment of the caudal vena cava derives from the embryologic right supracardinal vein. The presence of a double vena cava in the pre-renal segment is believed to be a result of persistence also of the left supracardinal vein (REIS and TEPE 1956, LABORDA et al. 1996). In two cases this anomaly was associated to other venous anomalies of the abdominal vessels. Despite the small number of dogs with left supracardinal vein persistence reported here, it is interesting to note that they all were small size dog (< 10 kg), and four of these were Poodle dogs, suggesting a possible size or breed predisposition.

The segmental aplasia of the caudal vena cava is another anomaly described in this study, and in previous reports. This anomaly is supposed to be a failure of the anastomosis between the right subcardinal veins and the vitelline, causing an interruption of the

developing caudal vena cava. The communication between the prehepatic and hepatic segments of the caudal vena cava does not occur and the blood is then shunted to the aygous vein by way of a persisting right supracardinal vein (BARTHEZ et al. 1996, HUNT et al. 1998, HARDER et al. 2002). This anomaly is generally asymptomatic. However, in our cases it was always associated with portosystemic shunts. In one dog the azygous continuation was associated with the *situs inversus abdominalis*, with the stomach and multiple spleens situated at the right side (Fig. 43, 44). This association has been reported in humans as well as in dogs (ROGUIN et al. 1984, MATHEWS et al. 1999, LOHSE et al. 1978, HUNT et al. 1998).

Two dogs with an azygous continuation of the caudal vena cava had also the interruption of the portal vein and a portocaval shunt between the portal vein and the pre-hepatic part of the caudal vena cava. According to the supracardinal model, this part of the caudal vena cava is derived from the right subcardinal vein that in the embryo is programmed to anastomose with both the supracardinal vein and the cranial portion of the vitelline veins. Inappropriate anastomosis among these embryonic vessels can cause the interruption of caudal vena cava and/or portal vein and result in a portosystemic anastomosis. In normal adult dog there are no gross anatomical connections between the portal system and the caudal vena cava or its tributaries. Most extrahepatic shunts encountered over the course of this study, as well as by others, arise from gastric veins and end in the pre-hepatic segment of the caudal vena cava, suggesting a possible similar embryologic origin. In two cases, the shunting vessel arose from a tributary of the portal vein, viz. the right and the left gastric veins, and terminated in the hepatic and post-hepatic segments of the caudal vena cava, respectively (Fig. 51-53). These types of PSS have not been previously

described and are difficult to classify using the existing clinical criteria (intrahepatic or extrahepatic shunts).

To better understand the underlying developmental mechanisms and for planning the surgical approach, knowledge of the origin and course of the anomalous vessels is essential. In our preliminary study (BERTOLINI et al. 2006b), and in the present thesis, multidetector 16-row computed tomography angiography combined with post-processing techniques has proven to be extremely valuable in vascular normal anatomy and congenital anomalies assessment in dog.

CHAPTER 7

CONCLUSIONS

Multidector 16-row computed tomography was used for the first time in dogs.

In the present work some results have been described:

- Anesthesia protocol for dogs undergoing MDCT abdominal examination.

This protocol allowed safe and short general anesthesia, and brief subsequent apneas during the scans. None of dogs examined showed complications related to the anesthesia.

- Protocol for contrast enhanced MDCT examination in dogs.

The protocol described is routinely adopted when both parenchyma and vascular structures have to be evaluated, such as in oncology patients. It allows a good opacification of abdominal vessels, and can be used for morphological studies. However, post-processing for vascular mapping could be laborious.

- Protocol for MDCT-angiography using a bolus triggering technique

This protocol provides excellent results for angiographic studies in the arterio-portal phase. Post-processing offers more detailed vascular maps.

- Post-processing software techniques application in 3D vascular mapping

Multiplanar Reformatted Images (MIP), Maximum Intensity Projection (MIP), and Volume Rendering techniques are most useful tools for complicated vascular anatomy interpretation and depiction in dogs.

- Normal anatomy of abdominal vessels in dog as seen on MDCT

Volume rendered models can be an useful tool for educational support in anatomy training, and for assessment of vascular variations not previously described.

- Description of some congenital vascular anomalies not previously reported.

Knowledge of the course of anomalous vessels help in understanding possible underlying dvelopmental mechanisms, and is essential for pre-surgical planning.

LIST OF TERMS (alphabetical order)

Aa. arcuatae, arcuate arteries

Aa. iliacae externae, external iliac arteries

Aa. iliacae internae, internal iliac arteries

Aa. interlobares renis, interlobar renal arteries

Aa. lumbales, lumbar arteries

Aa. renales, renal arteries

Aa. jejunales, jejuna arteries

A. abdominalis cranialis, cranial abdominal artery

A. circumflexa ilium profunda, deep circumflex iliac artery

A. coeliaca, celiac artery

A. colica sinistra, left colic artery

A. adrenalis dextra, right adrenal artery

A. adrenalis sinistra, left adrenal artery

A. epigastrica caudalis superficialis, superficial epigastric artery

A. gastrica sinistra, left gastric artery

A. hepatica, hepatic artery

A. iliaca externa, external iliac artery

A. iliaca interna, internal iliac artery

A. intercostales dorsalis, intercostal artery

A. lienalis, splenic artery

A. mesenterica caudalis, caudal mesenteric artery

A. mesenterica cranialis, cranial mesenteric artery

A. phrenica caudalis, caudal phrenic artery

A. pudenda externa, external pudendal artery

A. renalis dextra, right renal artery

A. renalis sinistra, left renal artery

A. sacralis mediana, median sacral artery

A. testicularis, testicular artery

Aorta abdominalis, abdominal aorta

Aorta descendens, descending aorta

Aorta thoracica, thoracic aorta

Arcus aortae: aortic arch

AV profunda femoris, deep femoral artery and vein

Rami mammarii, mammary branches of the caudal superficial epigastric artery

Ramus dexter lateralis, right lateral branch of the hepatic artery

Ramus dexter medialis, right medial branch of the hepatic artery

Ramus dorsalis, dorsal branch of the dorsal intercostal artery

Ramus esophageus, esophageal branch of the left gastric artery

Ramus dexter, right branch

Ramus sinister, left branch

Ramus sinister medialis, left medial branch

Ramus sinister lateralis, left lateral branch

Ramus spinalis, spinal branch of the dorsal intercostal artery

V. azygous, azygos vein

Vena cava caudalis, caudal vena cava

V. iliaca communis, common iliac vein

Vena portae, portal vein

V. circumflexa ilium profunda, deep circumflex iliac vein

V. gastric dextra, right gastric vein

V. gastrica sinistra, left gastric vein

V. gastroduodenalis, gastroduodenal vein

V. gastroepiploica, gastroepiploic vein

V. hepatica dextra, right hepatic vein

V. hepatica media, medial hepatic vein

V. hepatica sinistra, left hepatic vein

V. iliaca communis, common iliac vein

V. lienalis, splenic vein

V. mesenterica caudalis, caudal mesenteric vein

V. mesenterica cranialis, cranial mesenteric vein

V. portae, portal vein

V. renalis dextra, right renal vein

V. renalis sinistra, left renal vein

V. ovarica sinistra, left ovarian vein

V. testicularis sinistra, left testicular vein

VV. hepaticae, hepatic veins

Vv. interlobares renis, renal intelobar veins

Vv. lumbales. lumbar veins

Vv. jejunales, jejunal veins

Vv. renales, renal veins

References

ABIDU-FIGUEIREDO M, DIAS GP, CERUTTI S, CARVALHO-DE-SOUZA B, MAIA RS, BABINSKI MA. Variations of celiac artery in dogs: anatomic study for experimental, surgical and radiological practice. Int J Morphol 2005;23:37-42

AURIEMMA E, VOORHOUT G, BARTHEZ PY. Determination of optimal window width and level for measurement of the canine pituitary gland height on computed tomographic images using a phantom. Vet Radiol Ultrasound 2007;48:113-117

BARONE R. Anatomia comparata dei mammiferi domestici. Vol. 5: Angiologia. Parte prima: cuore e arterie. Ed. Edagricole – Bologna 1993a Cap. II Arterie:97-125

BARONE R. Anatomia comparata dei mammiferi domestici. Vol. 5: Angiologia. Parte prima: cuore e arterie. Ed. Edagricole – Bologna 1993b Cap. V Arterie del tronco: 283-323

BARTHEZ PY, SIEMENS LM, KOBLIK PD. Azygous continuation of the caudal vena cava in a dog: radiographic and ultrasonographic findings. Vet Radiol Ultrasound 1996;37:354-356

BERRY CR. Physical principles of computed tomography and magnetic resonance imaging. In: Thrall, D.E. (Ed.), Textbook of Veterinary Diagnostic Radiology. W.B. Saunders Company, Philadelphia, 2002:28–35

BERTOLINI G, FURLANELLO T, DE LORENZI D, CALDIN M. Computed tomographic quantification of canine adrenal gland volume and attenuation. Vet Radiol Ultrasound 2006a;47:444-8

BERTOLINI G, ROLLA EC, ZOTTI A, CALDIN M. Three-dimensional multislice helical computed tomography techniques for canine extra-hepatic portosystemic shunt assessment. Vet Radiol Ultrasound 2006b;47:439-43

BERTOLINI G, FURLANELLO T, DRIGO M, CALDIN M. Computed tomographic adrenal gland quantification in canine ACTH-dependent hyperadrenocorticism. Vet Radiol Ultrasound 2008;49:449–453

BURTON CA, WHITE RN. The angiographic anatomy of the portal venous system in the neonatal dog. Res Vet Sci 1999;66:211-217

CÁCERES AV, ZWINGENBERGER AL, HARDAM E, LUCENA JM, SCHWARZ T. Helical computed tomographic angiography of the normal canine pancreas. Vet Radiol Ultrasound. 2006;47:270-278

CARDOSO L, GIL F, RAMÍREZ G, TEIXEIRA MA, AGUT A, RIVERO MA, ARENCIBIA A, VÁZQUEZ JM. Computed tomography (CT) of the lungs of the dog using a helical CT scanner, intravenous iodine contrast medium and different CT windows. Anat Histol Embryol 2007;36:328-31

CHRISTENSEN GC. Circulation of blood through the canine kidney. Am J Vet Res 1952;13:236-245

CITTADINI G, CITTADINI G. "La tomografia computerizzata" cap. V in Cittadini G. Diagnostica per immagini e radioterapia" 2002 V ed. ECIG, Genova, Italia, pp. 69-78

CORNILLIE P, SIMOENS P. Prenatal development of the caudal vena cava in mammals: review of the different theories with special reference to the dog. Anat Histol Embryol 2005;34:364-372

CORNILLIE P, VAN DEN BROECK W, SIMOENS P. Three-dimensional reconstruction of the remodeling of the systemic vasculature in early pig embryos. Microsc Res Tech 2008b;7:105-111

CORNILLIE P, VAN DEN BROECK W, SIMOENS P. Origin of the infrarenal part of the caudal vena cava in the pig. Anat Histol Embryol. 2008a;37:387-393

COTMOIS A, GORCZYCA W, GRASSINO A. Anatomy of diaphragmatic circulation. J Appl Physiol 1987;62:238-244

CRAWFORD CR, KING KF. Computed tomography scanning with simultaneous patient translation. Med Phys 1990; 17:967-982

DROST WT, MATTOON JS, SAMII VF, WEISBRODE SE, HOSHAW-WOODARD SL. Computed tomographic densitometry of normal feline thyroid glands. Vet Radiol Ultrasound 2004;45:112-116

ECHANDI RL, MORANDI F, DANIEL WT, PAQUETTE JL, DANIEL GB. Comparison of transplenic multidetector CT portography to multidetector CT-angiography in normal dogs. Vet Radiol Ultrasound. 2007;48:38-44

ENGE I, FLATMARK A. Selective coeliac and hepatic artery angiography in normal dogs. Scan J of Gastroent 1972;7:361-368

EVANS HE. The heart and arteries. Chapt. 11 in: Miller's Anatomy of the Dog (H. E.Evans ed.), Philadelphia: W. B. Saunders Company, 1993:586-681

EVANS HE. The veins. Chapt. 12 in: Miller's Anatomy of the Dog (H. E.Evans ed.), Philadelphia: W. B. Saunders Company, 1993:682–716

FASOULIOTIS SJ, ACHIRON R, KIVILEVITCH Z, YAGEL S. The human fetal venous system: normal embryologic, anatomic, and physiologic characteristics and developmental abnormalities. J Ultrasound Med 2002;21:1145-115

FEENEY DA, FLETCHER TF, HARDY RM. Atlas of correlative imaging anatomy of the normal dog ultrasound and computed tomography. 1991 W.B. Saunders ed., Philadelphia.

FISHMAN EK. CT Angiography: clinical applications in the abdomen. Radiographics 2001;21:S3–S16

FISHMAN EK, NEY DR, HEATH DG, CORL FM, HORTON KM, JOHNSON PT. Volume Rendering versus Maximum Intensity Projection in CT angiography: what works best, when, and why. Radiographics 2006;26:905-922

FLEISCHMANN D. Use of high concentration contrast media in multiple-detector-row CT: principles and rationale. Eur Radiol 2003;13:14–20

FLEISCHMANN D. How to design injection protocols for multiple detector-row CT angiography (MDCTA). Eur Radiol 2005;15S:E60-65

FLOHR TG, SHALLER S, STIERSTORFER K, BRUDER H, OHNERSORGE BM., SHOEPF UI. Multi-detector row CT systems and image reconstruction techniques. Radiology, 2005;235:756-773

FRANK, P., MAHAFFEY, M., EGGER, C., CORNELL, K.K. Helical computed tomographic portography in ten normal dogs and ten dogs with a portosystemic shunt. Vet Radiol Ultrasound 2003;44:392–400

GOMEZ JA, LAWSON L, KOROBKIN M, MOSS AA. Selective abdominal angiography in the dog. J. Am Vet Radiol Soc 1973;14: 72-80

GUIMARÃES FILHO HA, DA COSTA LL, ARAÚJO JÚNIOR E, NARDOZZA LM, NOWAK PM, MORON AF, MATTAR R, PIRES CR. Placenta: angiogenesis and vascular assessment through three-dimensional power Doppler ultrasonography. Arch Gynecol Obstet 2008;277:195-200

HARDER MA, FOWLER D, PHARR JW, TYRON KA, SHMON C. Segmental aplasia of the caudal vena cava in a dog. Can Vet J 200;43:365-368

HAMMERSTINGL R, VOGL TJ. Abdominal MDCT: protocols and contrast considerations. Eur Radiol 2005;15:E78–90

HITTMAIR K, FLEISCHMANN D. Accuracy of predicting and controlling time-dependent aortic enhancement from a test bolus injection. J Comput Assist Tomogr 2001;25:287–294

HOFSTAETTER C, PLATH H, HANSMANN M. Prenatal diagnosis of abnormalities of the fetal venous system. Ultrasound Obstet Gynecol 2000;15:231-241

HOUNSFIELD G.N. Computerized transverse axial scanning (tomography). 1. Description of system. British Journal of Radiology 1973;46:1016-1022

HUNT GB, BELLENGER CR, BORG R, YOUMANS KR, TISDALL PL, MALIK R. Congenital interruption of the portal vein and caudal vena cava in dogs: six case reports and a review of the literature. Vet Surg 1998;2:203-215

HUNTINGTON GS, MCCLURE CFW. The development of the veins in the domestic cat (Felis domestica) with especial reference, (1) to the share taken by the supracardinal veins in the developmentof the postcava and azygos veins and (2) to the interpretation of the variant conditions of the postcava and its tributaries as found in the adult. Anat Rec 1920:20:1-30

ISHIOKA K, OKUMURA M, SAGAWA M, NAKADOMO F, KIMURA K, SAITO M. Computed tomographic assessment of body fat in beagles. Vet Radiol Ultrasound. 2005;46:49-53

ISOGAI S, LAWSON ND, TORREALDAY S, HORIGUCHI M, WEINSTEIN BM. Angiogenic network formation in the developing vertebrate trunk. Development 2003;130:5281-5290

JOHNSON PT, FISHMAN EK. IV contrast selection for MDCT: current thoughts and practice. Am J Roentgenol 2006;186:406–415

KALENDER W, SEISSLER W, KLOTZ E, VOCK P. Spiral volumetric CT with single-breath-hold technique, continuous transport and continuous scanner rotation. Radiology, 1990;176:181-183

KALENDER WA, POLACIN A, SUES C. A comparison of conventional and spiral CT: an experimental study on the detection of spherical lesions. J Comput Assist Tomogr 1994;18: 167–176

KALENDER W. Thin-section-three-dimensional spiral CT: is isotropic imaging possible? Radiology, 1995;197:578-580

KALENDER WA. Computed Tomography – Fundamentals, System Technology, Image Quality, Applications, second ed. Publicis Corporate Publishing, Erlangen. 2005:17–97

KALRA MK, SAIN S. Standardized Nomenclature and Description of CT Scanning Techniques. Radiology 2006;241:657-66

KISHIMOTO M, YAMADA K, TSUNEDA R, SHIMIZU J, IWASAKI T, MIYAKE Y. Effect of contrast media formulation on computed tomography angiographic contrast enhancement. Vet Radiol Ultrasound 2008;49:233-237

LABORDA L, GIMENO M, DOMINGUEZ L, GIL J. Anomalous caudal vena cava

in the dog. Vet Record 1996:20-21

LAWSON ND, SCHEER N, PHAM VN, KIM CH, CHITNIS AB, CAMPOS-ORTEGA JA, WEINSTEIN BM. Notch signaling is required for arterial-venous differentiation during embryonic vascular development. Development 2001;128 3675-3683

LELL MM, ANDERS K, UDER M, KLOTZ E, DITT H, VEGA-HIGUERA F, BOSKAMP T, BAUTZ WA, TOMANDI BF. New technique in CT angiography. Radiographics 2006;1:S45-62

LOHSE CL, SELCER RR, SUTER PF. Hepatoencephalopathy associated with situs inversus of abdominal organs and vascular anomalies in a dog. J Am Vet Med Assoc 1976;168:681-688

MACCHI V, PARENTI A, DE CARO R. Pivotal role of the sub-supracardinal anastomosis in the development and course of the left renal vein. Clin Anat 2003;16:358-361

MARTIN ML, TAY KH, FLAK B, FRY PD, DOYLE DL, TAYLOR DC, HSIANG YN, MACHAN LS. Multidetector CT angiography of the aortoiliac system and lower extremities: a prospective comparison with digital subtraction angiography. Am J Roentgenol 2003;180:1085-1091

MATHEWS R, SMITH PA, FISHMANN EK, MARSHALL FF. Anomalies of the inferior vena cava and renal veins: embryologic and surgical considerations. Urology 1999;53:873-880

MCCLURE CFW, BUTLER E.G. The development of the vena cava inferior in man. Am J Anat 1925;35:331-384

MCGRATH KE, KONISKI AD, MALIK J, PALIS J. Circulation is established in a stepwise pattern in the mammalian embryo. Blood 2003;101:1669-1676

MEHALL JR, SALTZMANN DA, CHANDLER JC, KIDD JN, WELLS T, SMITH SD. Congenital abdominal aortic aneurysm in the infant: a case report and review of the literature. J Pediatr Surg 2001;36:657-658

MINNITI S, VISENTINI S, PROCACCI C. Congenital anomalies of the venae cavae: embryological origin, imaging features and report of three new variants. Eur Radiol 2002;12:2040-2055

MOORE PF, WHITING PG. Hepatic lesions associated with intrahepatic arterioportal fistulae in dogs. Vet Pathol. 1986;23:57-65

NOMINA ANATOMICA VETERINARIA (NAV) World Association of Veterinary Anatomists. Available at: http://www.wava-amav.org/Downloads/nav_2005.pdf

NOMINA EMBRYOLOGICA VETERINARIA, World Association of Veterinary Anatomists. Available at: http://www.wava-amav.org/Downloads/nev_2006.pdf.

OLERTH S. SHARF G. Computed tomography in small animals – Basic principles and state of the art applications. Vet J. 2007;173:254-71

PASSARIELLO R. “La tomografia computerizzata” cap. 28 in: Passariello R. Radiologia - Elementi di tecnologia, 2005 IV Ed. Idelson-Gnocchi, Napoli, Italia, pp. 333-64

PAYNE JT, MARTIN RA, CONSTANTINESCUE GM. The anatomy and embryology of portosystemic shunts in dogs and cats. Seminars in veterinary medicine and surgery (small animal) 1990;5:76-82

PROKOP M. General principles of MDCT. Eur J Radiol 2003;45:S4-S10

PROKOP M. New challenges in MDCT. Eur Radiol Suppl 2005;15: E35-E45

PROKOP M. “Principi di TC, TC spirale e TC multistrato” cap 1 in: Prokop M, Galanski M. Tomografia computerizzata - spirale e multistrato. 2006 Ed. Masson, Milano, Italia, pp. 2-46

REIS RH, ESENTHER G. Variations in the pattern of renal vessels and their relation to the type of posterior vena cava in man. Am J Anat 1959;104:295-318

REIS RH, TEPE P. Variation in the pattern of renal vessels and their relation to the type of posterior vena cava in the dog (Canis familiaris). Am J Anat 1956:99:1-15

RIECK AF, REIS RH. Variations in the pattern of renal vessels and their relation to the type of posterior vena cava in the cat (Felis domestica). Am J Anat 1953;93:457-474

RISAU W, FLAMME I. Vasculogenesis. Annu Rev Cell Dev Biol 1995;11:73–91

RISAU W. Mechanisms of angiogenesis. Nature 1997;386:671-674

RIVERO MA, VÁZQUEZ JM, GIL F, RAMÍREZ JA, VILAR JM, DE MIGUEL A, ARENCIBIA A. CT-soft tissue window of the cranial abdomen in clinically normal dogs:

an anatomical description using macroscopic cross-sections with vascular injection. Anat Histol Embryol 2008;17 [Epub ahead of print]

ROGUIN N, HAMMERMAN H, KORMAN S, RISS E. Angiography of azygos continuation of inferior vena cava in situs ambiguus with left isomerism (polysplenia syndrome). Pediatr Radiol 1984;14:109-112

ROSENBLUM JD, BOYLE CM, SCHWART LB. The mesenteric circulation, anatomy and physiology. Surg Clin North Am 1997;77:289-306

ROSSANT J, HOWARD L. Signaling pathways in vascular development. Annu Rev Cell Dev Biol 2002;18:541-573

SAKAMOTO S, KIURA Y, SHIBUKAWA M, OHBA S, ARITA K, KURISU K. Subtracted 3D CT angiography for evaluation of internal carotid artery aneurysms: comparison with conventional digital subtraction angiography. Am J Neuroradiol 2006;27:1332-1337

SIMOENS P, DE VOS N.R. Arteriae, arteries. In: SCHALLER O. (Editor): Illustrated Veterinary Anatomical Nomenclature. 2edn. Georg Thieme Verlag 2007a:242-337

SIMOENS P, DE VOS N.R. Venae, veins. In: SCHALLER O. (Editor): Illustrated Veterinary Anatomical Nomenclature. 2edn. Georg Thieme Verlag 2007b:338-401

HABEL R, SACK. W. Organa urinaria, urinary organs, apparatus urogenitalis, urogenital apparatus, splanchnologia, splanchnology. In: SCHALLER O. (Editor): Illustrated Veterinary Anatomical Nomenclature. 2edn. Georg Thieme Verlag 2007c:194-197

SHIVELY MJ. Origin and branching of renal arteries in the dog. J Am Vet Med Assoc 1978;173: 986-989

SCHMIDT S, C. L. LOHSE CL, AND P. F. SUTER. Branching patterns of the hepatic artery in the dog: arteriographic and anatomic study. Am J Vet Res 1980;41:1090–1097

SCHMIDT S, SUTER PF. Angiography of the hepatic and portal venous system in the dog and cat: an investigation method. Vet Radiol 1980;21:57-77

SINGH AP, SINGH GR, SHARMA DN, NIGAM JN, BHARGAVA AK. Arteriographic anatomy of the abdominal aorta in the goat, dog, pig, and rabbit. Vet Radiol 1982;23:279-281

SMALLWOOD JE, GEORGE TF. Anatomic atlas for computed tomography in mesaticephalic dog: caudal abdomen and pelvis. Vet Radiol Ultrasound 1992;33:143-167

SMALLWOOD JE, GEORGE TF. Anatomic atlas for computed tomography in mesaticephalic dog: thorax and cranial abdomen. Vet Radiol Ultrasound 1993;34:65-84

SUTER PF. Portal vein anomalies in the dog: their angiographic diagnosis. Am J Vet Radiol 1975;16:84-97

SZATMARI V, NEMETH T, KOTAI I, VOROS K, SOTONYI P. Doppler ultrasonographic diagnosis and anatomy of congenital intrahepatic arterioportal fistula in a puppy. Vet Radiol Ultrasound 2000;41:284-286

TAEYMANS O, SCHWARZ T, DUCHATEAU L, BARBERET V, GIELEN I, HASKINS M, VAN BREE H, SAUNDERS JH. Computed tomographic features of the normal canine thyroid gland. Vet Radiol Ultrasound 2008;49:13-19

TATEISHI K, KISHIMOTO M, SHIMIZU J, YAMADA K. A Comparison Between Injection Speed and Iodine Delivery Rate in Contrast-Enhanced Computed Tomography (CT) for Normal Beagles. J Vet Med Sci 2008;70:1027-1030

TEIXEIRA M, GIL F, VASQUEZ JM, CARDOSO L, ARENCIBIA A, RAMIREZ-ZARZOSA G. AGUT A. Helical computed tomography anatomy of the canine abdomen. Vet J 2007;174:133-138

TERRAMANI TT, SALIM A, HOOD DB, ROWE VL, WEAVER FA. Hypoplasia of the descending thoracic and abdominal aorta: a report of two cases and review of the literature. J Vasc Surg 2002;36:844-888

TIDWELL AS. Updates in CT and MRI, Part I. Advanced imaging concepts: A pictorial glossary of CT and MRI technology, in Clinical Techniques in Small Animal Practice 1999;14:65-111

TISDALL PLC, HUNT B, BORG RP, MALIK R. Anatomy of the Ductus Venosus in Neonatal Dogs (Canis familiaris). Anat Histol Embryol 1997;26:35-38

TROMBLEE TC, JONES JC, BAHR AM, SHIRES PK, AREF S. Effect of computed tomography display window and image plane on diagnostic certainty for characteristics of dysplastic elbow joints in dogs. Am J Vet Res. 2007;68:858-871

URSˇICˇ M, RAVNIK D, HRIBERNIK M,. PECˇAR J, BUTINAR J, FAZARINC G. Gross anatomy of the portal vein and hepatic artery ramifications in dogs: corrosion cast study. Anat Histol Embryol 2007;36:83–87 **(Check the spelling of the names Ursic and Pecar)**

VETERINARY CT/MR Society Letter, Letter from the Annual Meeting of the American College of Veterinary Radiology. Vet Radiol Ultrasound 1996;37:40

VITUMS A. Portal vein in the dog. Zbl Vet Med 1959;6:723–741

WANG G, VANNIER MW. Maximum volume coverage in spiral computed tomography scanning. Acad Radiol 1996;3:423–428

WEINSTEIN BM. What Guides Early Embryonic Blood Vessel Formation? Developmental dynamics 1999;215:2–11

YAMADA K, TANIURA T, TANABE S, YAMAGUCHI M, AZEMOTO S, WISNER ER. The use of multi–detector row computed tomography (MDCT) as an alternative to specimen preparation for anatomical instruction. J Vet Med Education 2007;34:143-150

YANCOPOULOS GD, DAVIS S, GALE NW, RUDGE JS, WIEGAND SJ, HOLASH J. Vascular-specific growth factors and blood vessel formation. Nature 2000;407:242–248

ZWINGENBERGER AL, SCHWARZ T. Dual-phase CT angiography of the normal canine portal and hepatic vasculature. Vet Radiol Ultrasound. 2004;45:117-124

ZWINGENBERGER AL, MCLEAR RC, WEISSE C. Diagnosis of arterioportal fistulae in four dogs using computed tomographic angiography. Vet Radiol Ultrasound 2005b;46:472-7

ZWINGENBERGER AL, SCHWARZ T, SAUNDERS HM. Helical computed tomographic angiography of canine portosystemic shunts. Vet Radiol Ultrasound 2005a;46:27-32